Analysis of Semi-Rigid Connections Subject to Fire Loads in a Steel Framework

by

Kuan Ming Gary Chen

A thesis
presented to the University of Waterloo
in fulfillment of the
thesis requirement for the degree of
Master of Applied Science
in
Mechanical Engineering

Waterloo, Ontario, Canada, 2010

Author's Declaration

I hereby declare that I am the sole author of this thesis. This is a true copy of the thesis, including any required final revisions, as accepted by my examiners.

I understand that my thesis may be made electronically available to the public.

Abstract

The purpose of this study is to develop an approach that considers fire as a load in the design of structures. Recent studies of the full-scale fire tests in Cardington, UK and the World Trade Centre collapse have shown that the behaviour of steel structures in fire when assembled into a frame differs from that measured or predicted by fire testing of individual structural elements, revealing the importance of accounting for realistic fire loads in the design of structures and the potential inadequacy of fire testing individual elements as employed by current building codes. Yet, there has been limited basic research and development to allow consideration of fire as a load in the analysis and design of structures. In response to this much needed work, this thesis develops an approach to include fire as a load in the analysis of a 2-bay by 2-storey structure when a semi-rigid connection is exposed to thermal loads typical of those that might be encountered during a real fire.

The structural fire analysis is principally based on incorporating moment-rotation-temperature data for the connection, as found in archival literature, into a structural analysis software package developed at the University of Waterloo. The software employs a modified Displacement Method for analyzing structures, which involves the computation of stiffness reduction factors that represent the deterioration of strength of the structural elements as they are subjected to various loads. By modifying the moment-rotation-temperature data for a semi-rigid connection into a form recognized by the software, a fire load is simulated by incrementally elevating the temperature of the affected steel connection. In this way, a fragility analysis of the entire structure under fire load is conducted.

A series of example calculations are presented for cases in which the semi-rigid connection is exposed to increasing temperatures of 20°C, 200°C, 400°C and 600°C. The analysis showed that as the connection is heated, it is weakened, and the steel structure undergoes a redistribution of moments from the heated connection to other non-heated elements within the framework, which is essentially a form of fire-resistance of the assembled structure that unassembled members in isolation do not have. The study also demonstrated that the experimental moment-rotation-temperature data reported in archival literature can be incorporated into the structural analysis, and that additional force-deformation data obtained from further experimental work or through finite-element analyses would allow the study to be extended to analyze the effects of fire loading on other structural elements of an assembled framework. To demonstrate the link between the predicted structural response at different temperatures and the development of a compartment fire, a fire modelling analysis is also performed.

Acknowledgements

The author expresses his profound gratitude to Professor Elizabeth J. Weckman (P.Eng.) and Professor Donald E. Grierson (P.Eng.) for their teaching and guidance during his study; most importantly, their relentless effort to review each and every draft of this document. They gave constructive criticism, taught the physics of fire and structure, and brought the author to the state of the art thinking needed to fulfill the candidacy for a Master of Applied Science.

The author gives his deep appreciation to Dr. Yuxin Liu (P.Eng.) for his tireless assistance in understanding the theory and the operation of the SODA software.

The author is indebted to the principals of GHL Consultants Ltd: Mr. David Graham (P.Eng.), Mr. Andrew Harmsworth (P.Eng.) and Mr. Teddy Lai (M.A.I.B.C.) for their support of this academic endeavor; in particular, the author is grateful to Andrew for his mentorship of professional engineering practice.

A special thanks goes to Ms Yin-Ting Chang, who with her family generously provided warm hospitality to the author during his stays in Waterloo.

Finally, this work is dedicated to the author's grandparents who have inspired him to pursue graduate studies; motivated him to ask questions and learn more about the world we live in, even when we think we knew very much about it already.

Table of Contents

List of Figures

List of Tables

Chapter 1
Introduction

Fire is a natural phenomenon that can bring adverse effects on building structures. In steel structures, a reduction in mechanical properties takes place at elevated temperatures, which can lead to effects ranging from local deformation to collapse of the entire building. Therefore, structures are required by building codes to attain a certain level of fire-resistance in order to remain serviceable during the fire to allow occupants to escape and emergency responders to conduct rescue and firefighting operations. The current practice of structural fire safety design is divided into two broad approaches: a) the prescriptive-approach based on providing fire protection, usually via thermal insulation, to achieve a fire-resistance rating, determined based on standard fire testing of individual structural members; and b) the performance-based approach based on demonstrating an acceptable level of performance of the proposed structure through the use of models that represent the behavior of real fires and structures at elevated temperatures.

Traditionally, building codes have taken the prescriptive-based approach towards regulating the design of fire safety systems in buildings, including the protection of structures for fire. As a result of the regulatory framework, structures are designed without an explicit concern for the thermal effects of fire and thermal insulation as fire protection are specified without an explicit concern for the design of the structure. Prescriptive-based fire protection employs standard fire tests to evaluate fire-resistance rating of structural members in a laboratory furnace when the fire protection is applied. While this approach provides a systematic means of evaluating and comparing performance of various fire protection systems, which has been arguably successful based on relatively few structural failures due to fire in recent history, there has been an increasing interest to shift design practice to a more performance-based approach as prescriptive solutions often lead to overly conservative use of fire protection material and strategies. More importantly, there is a realization that the prescriptive-based approach lacks a complete treatment of the physical behaviour of compartment fires and/or the structures when they are exposed to elevated temperatures. On the fire front, the prescriptive-based approach uses the standard time-temperature history described in test standards that originated from early fire tests that do not represent the temperature history of real fires and predate much of the current understanding of fire dynamics in an enclosed compartment. Structurally, the standard fire test evaluates the fire-resistance of individual members and not of an assembled framework (ULC 2004 and ASTM 2008); as such, the intrinsic behavior of the overall structural frame when a part of it is

exposed to fire is not captured. Moreover, the deterioration of the structural capacity as the fire progresses is not considered as part of the fire test; instead, the fire test determines the fire rating of a component based on the time when that structural member reaches a predetermined critical temperature. For example, the critical temperature used in fire tests of structural steel members is 538°C (ULC 2004), the temperature when structural steel loses approximately 50% of its strength (Fike 2009 and Kodur 2009). Clearly, the prescriptive-based approach, while it has worked successfully, lacks a real-world consideration of structural behavior in fire on both the fire and the structural fronts. To this end, recent studies from the full-scale fire tests conducted in Cardington, UK (BS 1998) and from the World Trade Centre Collapse on September 11, 2001 (NIST 2005) have confirmed the importance of analyzing fire performance of the entire structure as an assembled framework and the need to consider fire explicitly as a load in the performance-based design of building structures (Bukowski 2001).

Performance-based fire safety design is a design methodology based on demonstrating an acceptable level of fire performance with respect to a pre-determined set of objective and functional (SFPE 2004). In Canada, the National Building Code of Canada 2005 (NRCC 2005) was released in a new objective-based format with stated objective and functional requirements. While the objective-based code is new, performance-based design has been practiced under the 'equivalency clauses' available in past editions of the NBCC. Since the 1950s, significant advances in fire science and the availability of analytical fire and smoke flow models, such as parametric, zone and field models based on computational fluid dynamics (CFD) principles, have provided engineers specializing in the practice of fire protection the tools to perform performance-based design of structures subject to fire. In these, fire models aimed at representing hot gas layer development and smoke movement in real fires were used in lieu of fire testing to the standard fire curve specified in CAN/ULC-S101. However, performance-based practice has remained limited in terms of the specification of fire induced thermal exposures to structures; there has been relatively little development of combined models for fire and structural performance. The behaviour of structural materials such as steel, concrete and timber at elevated temperatures are well documented in fire protection engineering literature (SFPE 2002). There are also some procedures described to calculate fire-resistance based on limit states design criteria, which takes into account the reduction of mechanical properties at elevated temperatures (Buchanan 2001). However, these are limited to the analysis of individual structural members, such as a single beam or a column; there is yet little work aimed at considering fire as a design load in the integrated analysis of a full structural framework.

1.1 Research Objective and Scope

The objective of this research is to develop a procedure that utilizes available data for steel properties at elevated temperatures in a steel frame analysis. The goal is to present an approach for including thermal effects of fire as stresses in the analysis of a steel framework and demonstrate how a fire load acting on an individual structural member in a steel frame has a propagated effect on other structural members, including those not immediately connected to the member exposed to fire.

Chapter 2 presents a review of the current practice of structural fire protection engineering. Fire models based on the standard time-temperature curve, parametric models, zone models and CFD models are discussed and the fire-resistance evaluation procedure using the critical temperature and limit states criteria for an individual structural member is summarized. Chapter 3 presents the theory behind the structural software used in this study, and the procedure used for implementing the fire load into the computer-based analysis. Chapter 4 provides example calculations to illustrate a structural frame analysis that includes the fire loading. Finally, Chapter 5 outlines conclusions and recommendation for future work.

Chapter 2
Fundamentals of Structural Fire Analysis

In order to design fire protection strategies for structures – whether this is through a prescriptive design approach of providing thermal insulation, or through an analytical approach of directly accounting for the fire load in the design calculations – a fundamental analysis of appropriate fire scenarios must be undertaken to specify how energy from the fuel loading within the structure is translated into thermal energy via a fire. This, in turn, provides the temperature or heat flux data needed to properly define the impact of the fire on the structure. Temperatures attained during fire in a building are dependent on a number of physical and chemical processes. At the molecular level, mixing governs the stoichiometric relationship between the fuel and oxygen which drives the combustion reactions and thermal energy produced by the fire. Heat transfer governs the transport of thermal energy within the compartment to the exposed structure; and heat-driven fluid motion determines the bulk movement of the fire plume and smoke within the compartment. Although many aspects of the basic science that define a compartment fire are well understood, it has been, and remains, difficult to scientifically describe fire behaviour at the highest level of detail. This is due to the complex nature and interactions of the physical and chemical processes involved, as well as unknown factors in the building environment that are unique to each fire occurrence. To avoid the difficulties associated with such detailed representation of the physics, models that generalize fire phenomena at the macroscopic level have been developed for scientific research and design purposes. There is currently no standard practice or regulation that dictates a preference for use of one type of fire model over another for the purposes of structural or building fire safety analysis, although standard time-temperature curves have often been specified in prescriptive building codes (NRCC 2005; NFPA 2009). In scientific research and performance-based analysis or design, the most appropriate 'design' fire model must be determined for the application at hand (Bukowski 2001; Hurley 2005). In this chapter, the fundamentals of enclosure fire phenomena are presented, followed by three generally accepted methods of modeling compartment fires with respect to assessing fire loads for structural design. The compartment temperatures determined from any one of the models is used for specification of the necessary fire protection systems for the structure. In the following sections of this chapter, Section 2.1 discusses the basics of compartment fire phenomena; Section 2.2 presents the standard time-temperature curve used in fire resistance testing and prescriptive building

code applications; Section 2.3 presents slightly more complex parametric models for post-flashover fire compartments; Section 2.4 presents even more sophisticated models for fire growth based on zone modelling and computational fluid dynamics principles; and finally, Section 2.5 provides an overview of current structural protection and design practices for fire.

2.1 Fundamentals of Fire Phenomena

Fire is the exothermic reaction of fuel with oxygen that takes place at a critical temperature, which releases heat as one of the products (NFPA 1997; Drysdale 1998). Fire begins when there is sufficient ignition energy to initiate the combustion reaction. The ignition energy may be attributed to mechanical, chemical, electrical or thermal sources; for example, friction from mechanical movements; excessive heat from chemical reactions; electrical energy from lightning or static discharge; or thermal energy from a local heat source. The combustion reaction takes place in the gas phase, where gaseous fuel molecules react with gaseous oxygen, releasing chemical byproducts and thermal energy in the form of heat. For solid and liquid fuels, the input ignition energy initially vapourizes the fuel molecules to the gas phase via decomposition and evapouration processes, allowing the combustion reaction to begin. As burning progresses, thermal energy released from ongoing combustion reactions continues to vapourize fuel, which results in sustained reaction provided there remains sufficient fuel and oxygen.

The gaseous fuel may react with oxygen in two regimes; namely, a) premixed burning, in which the fuel is intimately mixed with oxygen before burning, or b) diffusion burning, in which the fuel and oxygen are initially separated but burn in the region where they mix (NFPA, 1997). Structural fires are characterized predominantly by diffusion burning since the fuel is gradually vapourized from the source, then consumed as it diffuses across the flame envelope and reacts with oxygen. Due to the complexity of modeling the details of these vapour diffusion and reaction processes, fire sizes are generally defined using a macroscopic characteristic such as the heat release rate (HRR). One expression for HRR is given by (Drysdale 1998):

$$Q = \chi \dot{m}'' A_f \Delta H_c \tag{2.1}$$

where Q is the HRR (kW), A_f is the area of the fire (m^2), ΔH_c is the heat of combustion (kJ/kg), χ is a factor (<1.0) included to account for all physical processes leading to incomplete combustion , and $\dot{m}''$ is the mass burning rate (kg/m^2s) of the fuel given by:

$$\dot{m}'' = \frac{\dot{Q}_F'' - \dot{Q}_L''}{L_v} \tag{2.2}$$

where $\dot{Q}_F''$ is the heat flux supplied by the flame (kW/m^2), $\dot{Q}_L''$ is the heat losses from the fuel surface (kW/m^2), and L_v is the latent heat of vapourization or the heat required to excite the fuel to the gas phase (kJ/kg). The calculated HRR then defines the thermal energy that is generated by the fire and is available to interact, via combined fluid mechanic and heat transfer processes, with the surrounding compartments and structures. Due to their importance in structural fire analysis, these processes are outlined in more detail below.

On the fluid mechanics side, as the fuel burns, energy is released into the environment as hot fire gases (products of combustion), which are less dense than the surrounding air. Buoyancy driven by the difference in densities between the fire gases and cold ambient air results in the formation of a column of upward moving, accelerating gases called the fire plume. Figure 2.1 depicts a typical fire plume in a room or "fire compartment" in a building. The buoyant plume is the source of momentum that drives fluid movement in the fire compartment, which in turn governs the transport of thermal energy within the compartment. The plume is best characterized as a turbulent flow (NFPA 1997; Drysdale 1998; Versteeg 2007). At the smallest scale, the turbulence of the fire plume is unpredictable due to rapid variation of pressure and velocity in time and space as a result of the large temperature difference driven by the rapid release of thermal energy from the fire into the compartment. However, the bulk movement of the fire plume is relatively predictable and is greatly affected by the interior layout and the ventilation conditions in the compartment. As the rising plume reaches the ceiling in an enclosed compartment, it will be deflected to travel horizontally as shown in Figure 2.1. The horizontal flow, commonly known as the ceiling jet, corresponds to the visible smoke layer near the ceiling during the early stages of a fire. As the hot gases travel along the ceiling, they cool and become denser, leading to a thickening of the smoke layer below the ceiling. When the ceiling jet reaches the walls of a compartment, it is deflected again to turn downward and will flow along the end walls until reaching the floor. Alternatively, when the ceiling jet encounters an opening in the compartment boundaries, it exits the compartment and carries smoke and hot gases into the adjacent, connected spaces or the exterior environment. The movement of the ceiling jet out of the fire compartment is balanced by incoming streams of fresh air from the adjacent compartment or the exterior environment, which provides fresh air to the compartment and the fire. As the hot fire plume rises and forms the ceiling jet, the surrounding fresh air is "pulled" or entrained into the fire plume,

resulting in gradual cooling of the plume gases as well as more oxygen being supplied to the fuel for combustion. This in turn draws more fresh air from the adjacent compartments or the exterior environment as the hot fire gases exit the compartment at the openings. The supply of fresh air sustains the combustion during the early stages of a compartment fire. However, as the fire grows, there will be a point when the generation of hot fire gases outpaces the fluid exchange with the exterior environment at openings, or when the adjacent compartment is also filled with the products of combustion. At this point, due to the limited supply of fresh air (and therefore oxygen), the fire heat release rate will be controlled by the amount of available air. Heat transfer processes are occurring at the same time as the fluid mechanics driven by the fire in a compartment. These provide heat-feedback to the fire, resulting in greater temperature gradients in the compartment, enhancing the buoyancy effects, and ultimately leading to more turbulent movement of gases.

In terms of heat transfer to the compartment or structure, the hot plume and the smoke layer emit thermal energy to their environment by conduction, convection and radiation heat transfer processes. Conduction occurs at walls, ceilings and any solid construction such as interior partitions and structural beams and columns, where the thermal energy stored in the hot smoke is transferred into the solid structure. Conduction through the walls and ceiling releases energy to the exterior environment; therefore, the thermal properties of the compartment construction will affect the degree of heat loss and, indirectly, the severity of the fire effects. Convection is a form of heat transfer where the thermal energy is transported by the movement of fluids as constituted by the hot smoke layer and the fire plume as they propagate within the compartment. During the early stages of a fire, as the hot smoke layer fills up the compartment, energy is carried from the fire source to other parts of the compartment by convection. Finally, radiation is a type of heat transfer where the thermal energy is transported by electromagnetic waves from the hot fire gases (plume and smoke layer) to cooler surfaces. As the thermal energy is released from the fire and enters the compartment by radiation and convection (and some of the energy lost by conduction through the compartment enclosure), it begins to impact various objects within a compartment. In terms of the building structure, unprotected beams, columns and any other load-bearing members may begin to change physical and chemical properties as a result of their increase in temperature. On the other hand, the energy released may ignite more fuel, effectively increasing the A_f term in Eq. (2.1), which characterizes the situation of a growing and spreading fire. In an enclosed compartment, such as a room or suite in a building, such uncontrolled generation of thermal energy from the fire will eventually reach a critical level, when there is sufficiently high energy in the compartment such that all fuel contents will ignite and combust

simultaneously, changing the fire rapidly from a localized event into one involving the entire compartment through a phenomenon known as flashover (Babrauskas 1976; Drysdale 1998; Buchanan 2001). After reaching flashover, the fire is said to be at the fully-developed stage, which endures for a period of time depending on the availability of fuel and oxygen. At some point, as the fuel load begins to decrease, the thermal energy released will decrease and the fire will enter a decay period, and eventually will burn out when the fuel or the oxidizer has been consumed or other requirements for combustion are no longer satisfied. Figure 2.2 shows a plot of the fire heat release rate versus time curve that shows the four stages of a typical fire under well ventilated conditions: incubation phase, growth phase, steady-state burning phase, and the decay phase. From a structural design perspective, while the structure definitely heats during the early stage of the fire, the temperatures attained during post-flashover burning and the cooling effects during the decay period have the most profound impact on the total structural response to a given fire scenario (SFPE 2004).

Theoretically, it is possible to carefully account for every aspect of the burning process and therefore allow a) the HRR to be calculated using Eq. (2.1) and (2.2) and b) the subsequent fluid mechanics and heat transfer processes to be determined for a simplified compartment geometry. However, in practice, even this level of macroscopic analysis is not possible due to other complexities in building fires. Key factors related to the burning and the subsequent heat transfer processes can differ in any and all building fire scenarios, including the countless number of chemical compounds that constitute fuel in a building; the arrangement of fuels from room to room and building to building even for the same occupancy type; and rapid changes in oxygen concentration in the compartment as a fire progresses. Any of these factors impact the HRR of a fire. Undefinable variations in any of the foregoing preclude generalized analysis using the above equations. Further, as a given fire develops, heat-driven fluid motion leads to effects reaching far beyond the compartment of fire origin. This has led scientists and engineers to circumvent explicit treatments of fire phenomenon and to turn, instead, to describing fire events via models developed based on observation and measurements from experiments. Even advanced computational fluid dynamics models that solve the governing equations of fluid motion and energy conservation from first principles to differing extents rely on the use of empirical sub-models to simplify the fire chemistry and fire-induced phenomenon in compartments, particularly those which are not easily solved at the smallest scales.

In the following sections, three common types of fire models that are being used by scientists and engineers to simplify the analysis of compartment fires are presented, and their advantages and

limitations in the context of structural design for fire are discussed. The standard time-temperature approach is used in prescriptive building codes, where the fire model is used to evaluate the thermal protection of a structural member for a so called fire-resistance rating, which is a standardized measure of the fire endurance of the protected member. Fire models based on empirical correlations or derived from first principles of mass and energy conservation, namely, the zone and computational fluid dynamics models, are used in performance-based design. As discussed in earlier parts of the thesis, the standard time temperature test approach evaluates the integrity of a structure based on the time or on a thermal criterion, assuming that if it can be shown that the structure will not reach a certain critical temperature, the protected structure designed for ambient conditions would remain sound during the course of a fire (Kodur 2009). This is in contrast with the performance-based approach, where the fire model only provides a thermal condition, which then needs to be incorporated into the design of a structure.

2.2 The Standard Time-Temperature Curve: the Prescriptive Approach

The standard time-temperature curve is a basic empirical model that specifies a relation for the temperature to which an element is exposed as a function of time after ignition. The standard time-temperature curve is unique from other fire models in that it is the fire curve specified by the building code (NRCC 2005). Therefore, from a regulatory perspective, the curve represents the "fire load" that is assumed in the design of all building elements. Most industrialized countries utilize a standard fire curve in their prescriptive building code; for example, ASTM E119 in the United States Life safety Code (NFPA 2009) and CAN/ULC-S101 in Canada's National Building Code (NRCC 2005). Figure 2.3 includes plots of the standard time-temperature curves used in major industrialized nations (ASCE 1992). The time-temperature curves are not presented as full curves in the test standards, rather as a set of data points of temperatures that must be reached at certain times during a test, given it is not possible to follow precisely the curve in an actual test. However, for convenience, the specified data points have been fitted and described by equations by designers and scientists. For example, the CAN/ULC-S101 and ASTM E119 curve, which are identical, is given by (Kodur 2009):

$$T = T_0 + 750\left(1 - 3.795e^{\sqrt{t}}\right) + 170.4\sqrt{t} \tag{2.3}$$

where T_0 is the ambient temperature (C) and t is time (s). The ISO 834 is given by (Kodur 2009):

$$T = T_0 + 345\log_{10}(8t + 1) \tag{2.4}$$

With the exception of the Japanese fire curve for times longer than 2 hours of fire exposure, most of the standard curves are sufficiently similar that, in practice, all the standard curves are generally considered as a "standard time-temperature curve". The standard fire test, then, exposes a particular structural member to a design fire described by the standard time-temperature curve in a furnace, and an hourly fire-resistance rating (FRR) is assigned to the structural member if it has passed the test exposure criteria for a certain length of time. The pass/fail criterion is based on maintaining structural integrity, if the test specimen is loaded, or maintaining the temperature of the structure below a certain critical temperature, if the test specimen is not loaded. For example, in ASTM E119, steel columns do not necessarily need to be loaded; it is assumed that provided the steel temperature does not reach 538°C (ASTM 2008), the temperature at which ASTM A32 steel loses approximately 50% of its strength (NFPA 1997), the column will continue to be serviceable. In Canada and the United States, certified laboratories such as Underwriters Laboratory, Underwriters Laboratory of Canada, and Intertek carry out standard fire tests and annually publish a directory of designs (floors, columns, beams and walls) that have passed and received certain fire-resistance ratings. This, in turn, allows practitioners to select structures and authorities having jurisdiction to verify the fire performance of each element of a structure used in a particular design.

While the prescriptive-based building code system of using the time-temperature fire curve permits a convenient and standardized way to test, evaluate and compare the performance of different building elements in fire, from a design and science perspective the near century-old standard curve and the associated prescriptive system behind the use of the standard fire curve are questionable. In light of new research and the increasing societal acceptance of performance-based fire safety design (Ellingwood 2008; Kodur 2009), two fundamental aspects of the prescriptive approach are being questioned. The first is how realistic is the standard time-temperature curve in terms of representing real fire exposures? The second is how appropriate is it to rely on a protection-based approach to address structural performance in fire? To begin to answer these questions, it must be recognized that the standard fire curve was first published in the United States in 1917 (Babrauskas 1976; Kodur 2009). The curve was developed as an idealization of time-temperature relations fit to data obtained in number of non-standardized fire tests that were conducted in the late 1800s and early 1900s (Babrauskas 1976). However, since these early tests were performed prior to development of much of the current scientific understanding of fire behaviour, the tests did not mimic real fire behaviour in enclosed compartments in buildings. They were designed to sustain 'high' temperature exposure on an element for a duration of time sufficient to satisfy the experimenters that the specimen had

achieved a certain fire endurance. As such, the tests were conducted in a furnace where fuel was supplied periodically during the test to maintain an increasing temperature as the temperature in the furnace began to drop. This is in great contrast to the time-temperature relation for real fires which generally includes an incubation period, a rapid growth period to flashover, a steady-state burning phase and a decay phase as depicted in Figure 2.2 and shown with the standard curve in Figure 2.4. The behavior of real fires is largely dependent on the fuel load density (type and amount of fuel) and the ventilation conditions in the fire compartment, which dictates the ratio of fuel and oxygen and thereby determines the rate of combustion. Clearly, the standard time-temperature curve is not a realistic representation of the time-temperature development in real fires.

Traditionally, it has been argued, and perhaps it was the intent of the authors of the standard curve in 1917 although no such documentation can be found, that the standard curve is meant to be a conservative representation of a vast number of possible fire scenarios that may occur in a building. Indeed, depending on the ventilation conditions and fuel arrangement, not all fires will grow to flashover; not all fires will have the same burning duration; and even identical fires may not produce the same time-temperature history. Therefore, the original intention of the standard time-temperature curve in 1917 appears to be sound, particularly in the absence of the fire science needed to more accurately understand and predict fire behaviour. However, research in the last century has greatly advanced scientific understanding of enclosure fire dynamics. At the same time, the use of a standard fire curve with an ever-increasing temperature in modern building design often leads to conflicts with other important design objectives such as sustainability or housing cost, as the standard fire approach often leads to overly conservative requirements for fire protection that may become costly (Kodur 2009). Further, simply assuming a standard time-temperature relation without analyzing the conditions in a fire compartment, as well as the underlying fire dynamics and heat transfer processes, does not constitute a comprehensive scientific approach to fire modeling. In this regard, performance-based approaches that assess the time-temperature history of realistic fire scenarios within a structure and design that structure to resist more precisely the thermal effect of real fire would seem to be a more prudent practice.

Beyond the time-temperature relation itself, the application of a standard fire curve leads to the larger question of the universal appropriateness of the overall prescriptive fire protection practice that is currently and predominantly in place. Without designing a structure to withstand the range of possible thermal effects of fire – whether one elects a standard fire curve or other fire models that

better represent the thermal loads from real fires – and instead simply relying on fire protection via insulation materials, concern arises as to whether the fire protection will remain reliable during the lifetime of a building. Use of membrane protection (e.g. gypsum and plaster wallboard) relies on the integrity of the membranes and their ability to remain in place during a fire, but these membranes are at risk of being damaged, being penetrated by new electrical and mechanical services, or even mistakenly being replaced by non-fire resistive membranes during renovation (Chen and Harmsworth 2008). Intumescent paint requires activation of chemical substances during a fire in order to "foam up"; there are significant unknowns with respect to long term durability of such paint, particularly when the paint is subjected to adverse weather conditions (Buchanan 2001; UL 2009). The use of spray fire-resistive material (SFRM) has been a popular and less costly alternative to intumescent paint for steel structures. However, there are also long term durability considerations as these materials do not adhere well to the steel structure. The investigation of the World Trade Centre collapse has identified that the lack of maintenance of the SFRM on the steel structures and the detachment of the SFRM due to the plane impact were main contributing causes of the building failure when the structural steels were exposed to high temperatures without protection (NIST 2005).

It is certain that the utilization of the standard time-temperature curve as the fire model and the reliance on thermal protection strategies based on thermal loads specified by this model to address structural performance in fire is inappropriate and in certain circumstances, unsafe. While prescriptive fire protection practice has provided a useful, fairly conservative and standardized approach to evaluate fire resistance for the past century, as society moves towards accepting performance-based fire engineering, a more scientific methodology of analyzing the fire and including the effects of the fire directly into a structural design is needed. In this regard, parametric or even more complex computer-based models that are founded on first principles should be utilized to more accurately represent the effect of a given fire load and to form the basis of a structural analysis for design purposes. Because the topic of fire modeling and structural design as currently practiced in performance-based design are two broad topics, Sections 2.3 and 2.4 will first present the fire models for fire analysis; Section 2.5 will discuss current approaches in structural design that include account for fire loads.

2.3 Parametric Models

Parametric models are empirical models that take into consideration some of the characteristics of the fire and the fire compartment in representing fire exposure to a structure as a function of time after ignition. The impact of fuel load densities and ventilation characteristics on the progression of a fire in a compartment, as well as the accompanying heat transfer processes, were studied extensively during the 1970's in attempts to understand the effect of complex fire compartment interactions on fire development and to include additional physical considerations into the fire models used for structural design and analysis (Drysdale 1998). During this period, a number of parametric fire models were developed to describe the overall development of the fire in a compartment, each capturing a combination of different aspects of the physics. These fall into two broad categories: a) time dependent models for the evolution of fire heat release rate during the early stages of fire growth, based on consideration of fuel characteristics (Drysdale 1998); and b) steady-state models for prediction of fire heat release rate or compartment temperature in a post-flashover compartment fire based on compartment size, fuel load, a ventilation factor, F, generally defined as $A\sqrt{H}/A_t$, and the thermal properties of compartment walls and ceilings (Drysdale 1998). Each of these models is discussed below.

2.3.1 Fire Growth Models

During the early stages of a fire, the fire is localized; however, the behaviour can be quite unpredictable depending on the ignition source, the fuel and the fuel arrangement. As depicted in Figure 2.2, pre-flashover fires can exhibit long incubation or smouldering periods, during which little energy is released and much smoke is generated. Alternately, immediately after ignition, the fire can enter a relatively fast growth phase with clearly visible flame and stratification of smoke and hot gases from floor to ceiling of the compartment. Despite these variations, it has been found that, in its earliest stages, the growth of a fire very often can be modeled by a parabolic relation known as the t-squared fire growth model, which is given by (NFPA 92B 2008 Kodur 2009):

$$Q = \alpha\left(t - t_0\right)^2 \tag{2.5}$$

where Q is the HRR (kW), t is time (s), t_0 is the incubation period (s), and α is a constant that is arbitrarily defined based on the time required for the fire to reach 1000 BTU/s (1055kW). Different values of α are assigned to account for different fuel loads and fuel types within a compartment. For

example, a cellulose-based solid fuel fire is generally characterized as a "fast" fire - one that reaches 1055 kW in 150 s, giving $\alpha = 1055/150^2 = 0.0469$. Data from full scale room fire tests or even smaller-scale fire performance tests of common furniture items can be used to derive α for other types of fires.

The key physical assumption underlying prescription of a pre-determined HRR time curve to the fire growth is that the fire in the compartment is increasing in size under well-ventilated, fuel-controlled conditions, whereby there is always sufficient ventilation to feed enough oxygen to the fire to sustain combustion of the fuel at its maximum rate. Except for well sealed compartments or compartments with very little ventilation, this assumption is generally valid until flashover, after which depletion of oxygen in the compartment can cause the fire to progress to a ventilation-controlled condition, in which the HRR of the fire is determined by the availability of oxygen, generally modeled using a ventilation factor. At this stage, the fire will no longer grow. Instead it enters a phase of steady burning, termed the post-flashover phase, in which the HRR or the temperature can remain relatively constant and is governed primarily by the availability of air (oxygen). Following this phase, of course, the fire will eventually decay due to complete consumption of fuel, as depicted in Figure 2.2. From a structural design perspective, pre-flashover fires do not generally pose a risk to structures as most building materials have a degree of inherent fire resistance at mildly elevated temperatures (Hurley 2005). Therefore, in structural design for fire, emphasis has been placed on specification of the maximum temperature that might be attained during post-flashover burning. Notwithstanding this, a definition of pre-flashover fires in structural fire engineering design is still important. It allows for a complete assessment of the history and time of exposure of the structure to fire (from ignition to decay) and thus allows either the accumulated level of structural damage to be assessed or the time to structural collapse to be determined; the latter facilitates all important calculations of the time available for safe evacuation and emergency response operations.

2.3.2 Models for Post-Flashover Compartments

A number of parametric models have been developed to predict the behaviour of post-flashover fires in compartments as applied to structural fire safety calculations. These models are formulated through correlation of results from sets of experiments and are based on the assumption of a well-stirred mixture, or uniform temperature, throughout the compartment as has been generally observed in post

flashover fire compartments (Babrauskas 1976). Parametric models account for a range of compartment characteristics, including compartment size, ventilation conditions, fuel load density, and thermal properties of the ceiling and walls. By including these factors as independent variables, parametric models provide a more physical representation of fire behaviour than standard time-temperature curves, whilst offering a relatively simpler means of estimating the average compartment temperature than sophisticated zone or computational fluid dynamics models.

The formulation of parametric models began with the observation that the HRR of a fire in a compartment correlated with the ventilation conditions in that compartment. Kawagoe first determined that, under ventilation-controlled conditions, the HRR of a compartment fire is related to a ventilation factor according to the relation (Feasey 2002):

$$Q = 0.09 A_W H^{1/2} \Delta h_c \tag{2.6}$$

where A_w is the area of the ventilation opening (m^2), H is the height of the ventilation opening (m), Δh_c is the effective heat of combustion (kJ/kg) and the expression $A_W \sqrt{H}$ is defined as the ventilation factor. Later studies by Harmathy extended these ideas and found that the boundary between ventilation-controlled and fuel-controlled fires is not definitive; however, the transition can be estimated using the area of fuel involved in the fire and the ventilation conditions in the fire compartment as (Drysdale 1998):

$$\frac{\rho g^{1/2} A_w H^{1/2}}{A_f} < 0.235 \qquad \text{(ventilation-controlled)} \tag{2.7}$$

$$\frac{\rho g^{1/2} A_w H^{1/2}}{A_f} > 0.290 \qquad \text{(fuel-controlled)} \tag{2.8}$$

where ρ is the density of air (kg/m^3), g is the acceleration due to gravity ($9.81 m/s^2$), and A_f is the area of the fuel. Babrauskas, McCaffrey, Thomas and Law proposed similar methods based on the ventilation factor for calculating the onset of flashover when a fire begins to burn under ventilation-controlled conditions (SFPE 2002; Kodur 2009). Using Eqs. (2.6) and (2.7) as a rule of thumb, the HRR of a fire can be estimated by Eq. (2.6) when the fire is ventilation-controlled and by the t-square fire growth curve of Eq. (2.5) when it is fuel-controlled. Once a model or value for the HRR of fire has been specified, the overall compartment temperature can be estimated by performing an energy

balance on the hot compartment gas to account for heat transfer due to convection, conduction and radiation (Drysdale 1998; Feasey 2002):

$$Q = Q_L + Q_R + Q_W \tag{2.9}$$

Where Q is the HRR, Q_L is heat transfer due to convection, Q_R is heat transfer due to radiation, and Q_W is heat transfer due to conduction through walls, ceilings and floors as shown in Figure 2.5. Because convection, conduction and radiation heat transfer can all be expressed as functions of temperature, given a known fire heat release rate, the post-flashover compartment temperature can be determined by solving Eq. (2.9) implicitly using numerical techniques. Several main categories of parametric fire models are discussed in the following sections.

2.3.2.1 Swedish Curves (1970)

Magnusson developed one of the earliest parametric models in 1970 using the energy balance given in Eq. (2.9) (Drysdale 1998; Feasey 2002). Using Kawagoe's expression in Eq. (2.5) as the fire burning rate, Magnusson was able to show that compartment gas temperatures estimated using Eq. (2.9) were in reasonable agreement with experimental data obtained from fire tests, which are plotted against the model curve in Figure 2.6 (Feasey 2002). The solid line represents results from the experimental data while the dashed line is the calculated compartment temperature, based on the measured rate of burning, $\dot{m}$, to give heat release rate, Q, as a function of time (shown in Figure 2.6 inset). Scientifically, this finding was significant in that it resulted in a relatively robust and simple method to estimate compartment temperature using factors that bear physical meaning to a given compartment fire scenario. The work of Magnusson gained significant recognition and eventually led to the development of a series of parametric time-temperature curves adopted in the Eurocode BSEN1991-1-2 as shown in Figure 2.7 (Drysdale 1998). These fire curves are often referred to as the "Swedish fire curves" based on their origin. However, the use of these Swedish curves has certain limitations as a result of the range of experiments that were used in their development. This includes limitations on compartment size to a maximum floor area of 500m^2, maximum compartment height of 4m, no ventilation through the ceiling, cellulose-based solid fuels only, and thermal inertia, $\sqrt{k\rho c_p}$, between 100 and 2200 J/m^{2}s$^{1/2}$K for all walls and ceilings in the compartment. While the Swedish curves are applicable for most building conditions, other parametric fire curves that have a lesser degree of constraint have been developed and have been shown to provide reasonable representations of real fires. These are outlined below.

2.3.2.2 Work of Babrauskas and Williamson (1978)

The Swedish curves are based on a burning rate (HRR) calculated using Eq. (2.5), which assumes ventilation controlled burning throughout the entire post-flashover fire being modelled. However, it is possible that in a real scenario, the fire may enter the fuel-controlled regime, such that the use of the Swedish curves may result in a overestimation (albeit conservative estimate) of the actual fire severity in terms of potential damage to building structures. In order to address this issue, Babrauskas developed a more sophisticated model that required a check to determine if the fire was in the mode of fuel-controlled or ventilation-controlled burning at every time step in a compartment temperature calculation. He proposed, instead of Kawagoe's method for the calculation for Q in Eq. (2.9), the calculation be based on (Drysdale 1998; Babrauskas and Williamson 1978):

$$Q = \dot{m}\Delta h_c \tag{2.10}$$

for fuel-controlled burning, or

$$Q = \dot{m}_{air}\frac{\Delta h_c}{r} \tag{2.11}$$

for ventilation-controlled burning, where m_{air} = rate of air inflow (kg/s) and r = stoichiometric ratio of air to fuel in the combustion reaction. The work of Babrauskas illustrates the level of detail that can be included in a parametric model to account for the different burning regimes of post-flashover compartment fires. At the same time, however, it can be argued that such detail may be premature given that fundamentally, parametric models are already a significant simplification of the actual compartment fire behaviour.

2.3.2.3 Work of Lie (1974)

While the early work based on the energy balance approach (Eq. (2.9)) has led to the establishment of parametric models, the determination of temperature-time curves using these models requires relatively lengthy computation. In 1974, Lie suggested a different approach. Recognizing that the objective of parametric models was to determine compartment temperatures for structural fire safety calculations, Lie developed a model without considering the energy balance in the compartment, but instead based solely on fitting a series of time-temperature curves developed by Magnusson (Drysdale 1998). Lie proposed the following expression for compartment gas temperatures in a post-flashover fire compartment (Lie 1974; Drysdale 1998):

$$T = 250(10F)^{0.1/F^{0.3}} \exp\left(-F^2 t\right)\left\{3\left(1-e^{-0.6t}\right)-\left(1-e^{-3t}\right)+4\left(1-e^{-12t}\right)\right\}+C\left(\frac{600}{F}\right)^{0.5} \tag{2.12}$$

where $F = A_w\sqrt{H}/A_t$ is the ventilation factor, t is the time after flashover (hours), A_w is the area of the ventilation opening (m^2), A_t is the fire compartment's interior surface area (m^2) and C is a constant ranging between 0 and 1 for heavy ($\rho \geq 1600$ kg/m^3) and light ($\rho \leq 1600$ kg/m^3) fuels, respectively. The maximum temperature, T_{max}, calculated using Eq. (2.12) is attained at time $t = \tau$, where

$$\tau = \frac{M_f}{330F} \tag{2.13}$$

where M_f is the fuel load per unit of internal surface area (kg/m^2). After the compartment attains the maximum temperature, compartment temperature is assumed to cool following a linear relationship given by:

$$T = -600\left(\frac{t}{\tau}-1\right)+T_\tau \tag{2.14}$$

Lie's method presented a very simple method by which to calculate temperature, and one that did not require the use of numerical techniques since the temperature term, T, is explicitly expressed. At the same time, Lie's model takes into account the fuel load density and the ventilation factor in a given compartment when determining the length of time for which the fire will burn and the maximum temperature that will be reached in the compartment.

The foregoing sections discussed a select number of parametric models that were developed in the 1970s. Other parametric models based on the similar ventilation factor, $AH^{1/2}/A_T$ have also been proposed, including methods of Law (SFPE 2002) and Tanaka (SFPE 2002). These parametric models are commonly used to calculate compartment temperatures for performance-based structural fire protection designs and are documented in the SFPE Fire Protection Handbook (SFPE 2002). However, all of these earlier parametric models assume a linear decay phase, which is arguably not an accurate representation of real compartment fire behaviour as the fuel burns out. Therefore, some more recent parametric fire models have been developed to specifically include all phases of fire development including account of the nonlinear time-temperature relation that characterizes the cooling phase of a compartment fire.

2.3.2.4 Ma's Model

In 2000, Ma and Mäkeläinen proposed a parametric model for small and medium compartment fires based on a study of 25 complete time-temperature curves from different experimental compartment fire data from around the world (Ma and Mäkeläinen 2000). Ma's relation for compartment gas temperature as a function of time is given by:

$$\frac{T - T_0}{T_{\max} - T_0} = \left(\frac{t}{t_{\max}} \exp\left(1 - \frac{t}{t_{\max}}\right) \right)^{\delta} \tag{2.15}$$

where T_0 is the ambient temperature (C), t is time (s), $t_{\max}$ is the time when the maximum gas temperature is reached (s), δ is the shape factor that accounts for fire growth and decay, and $T_{\max}$ is the maximum compartment temperature given by:

$$T_{\max} = 1240 - 11\eta \tag{2.16}$$

if ventilation-controlled, or

$$T_{\max} = \sqrt{\eta / \eta_{cr}}\, T_{\max,cr} \tag{2.17}$$

if fuel-controlled, where $\eta = A_t / A_w \sqrt{H}$ is the inverse of the ventilation factor, $\eta_{cr} = 14.34 / \left(\kappa \varphi M_f\right)$, where κ is the ratio of floor area A_f to total interior surface area A_t of the compartment, φ = the surface area ratio of fuel (m^2/kg), and M_f is the fuel load density per unit floor area (kg/m^2). The total burning period of the fire is given by:

$$\tau = \frac{G_0}{R} \tag{2.18}$$

where G_0 is the total fire load in equivalent of wood (kg), and R is given by:

$$R = 10.8\left(1 - \exp\left(-0.036\eta\right)\right) A_w \sqrt{HW / D} \tag{2.19}$$

if ventilation-controlled, or

$$R = 0.372 \varphi G_0 \tag{2.20}$$

if fuel-controlled, where D is the depth of the compartment, R is the burning rate, and W is the width of the compartment. The time to reach maximum compartment temperature is approximated by:

$$t_{\max} = 0.63\tau \tag{2.21}$$

Ma reported that with $\delta = 0.8$, the proposed fire curve showed the most reasonable agreement with the time-temperature data that his group examined. Ma's model is fundamentally similar to earlier parametric models in that the ventilation factor and the fuel load density are factored into the equations used to define the burning regime and fire duration; but with the enhancement that the parameter δ was introduced to account for the behaviour of the fire in the decay phase. Although the use of δ is supported by a reasonably well fitted curve as shown in Figure 2.8, the parameter δ is simply a result of a curve-fitting exercise and lacks physical connection to the parameters that have been known to affect the behavior of post-flashover compartment fires. As such, when fire test data is not available for a specific compartment fire scenario, the selection of δ may be difficult to justify.

2.3.2.5 BFD Fire Model

In 2002, Barnett proposed a new empirical model for estimation of compartment fire temperatures called the "BFD curve". This parametric model, which accounts for all phases of fire development, was specifically aimed at including a more physically-based approach for modelling the cooling phase of a fire (Barnett 2002). In analyzing results from the Cardington Large Scale Tests, Barnett observed that the experiments were carried on well into the cooling phase of the compartment fire, which continued to have an effect on the steel structure. In attempts to describe the time-temperature relationship from the Cardington tests, Barnett proposed the BFD curve, an equation of the form:

$$T = T_a + T_{\max} e^{-z} \tag{2.22}$$

where T is the compartment temperature at time t, T_a is the ambient temperature (°C), $T_{\max}$ is the maximum compartment temperature, and z is given by:

$$z = \frac{\left(\ln t - \ln t_{\max}\right)^2}{s_c} \tag{2.23}$$

where t is the time from ignition of fire (min), $t_{\max}$ is the time at which $T_{\max}$ occurs (min), and s_c, a dimensionless number, is the shape constant for the temperature-time curve. Barnett performed a comprehensive study of time-temperature curves from past fire tests and found that s_c was related to the pyrolysis coefficient, which was related to the ventilation factor. The shape constant could be determined by:

$$s_c = \frac{1}{4A_w\sqrt{H}/A_t + 0.1} \tag{2.24}$$

for uninsulated fire compartments and by

$$s_c = \frac{1}{9.25A_w\sqrt{H}/A_t + 0.21} \tag{2.25}$$

for insulated fire compartments. The BFD curve proposed by Barnett is significant in that it is a parametric model that correlates well with experimental data from a wide range of test configurations and, at the same time, is capable of representing the entire burning history of a compartment fire allowing prediction of temperatures from pre-flashover to post-flashover, as well as during the cooling phase.

2.3.3 Remarks on Parametric Models

Parametric models provide estimates of the time-temperature history of compartment fires with a considerable level of sophistication included to account for the physics of compartment fire. In comparison to standard time-temperature curves, parametric models provide considerably more accurate, and more scientifically based, representations of real fire behavior applicable to a wide range of compartment geometries, ventilation conditions and construction materials. In this respect, they should allow more accurate determination of the thermal load from the fire to the structure, enabling better analysis of the response of a building structure to a given fire scenario.

Because the application of parametric fire models is only currently permitted under the setting of building code "equivalents", the special clause under which prescriptive codes permit a performance-based approach to satisfy fire safety requirements, and because the practice of structural fire safety is still based on the standard fire test, it is of interest to compare the results from parametric curves with those from the standard curve. Therefore, various studies have looked at how to indirectly relate the results from a standard time-temperature curve to those from parametric curves. One common method is through one of a number of time-equivalence methods based upon correlating the thermal exposure between the two fire models (Babrauskas 1974; Drysdale 1998; Kodur 2009). The most frequently used method is based on computing the area underneath the HRR-time curve, which is the energy released by the fire. In 2006, however, Barnett made a more direct comparison of these curves when he correlated his BFD curve to the equations for the standard time-temperature curves. Through

curve-fitting, the parameters in the BFD curve, Eq. (2.22), were adjusted to fit the standard time-temperature curves leading to evaluation of the constant, s_c, which is a function of the ventilation factor for the standard curves. This indirectly provided valuable insight into the ventilation conditions that would be necessary in a fire compartment to produce a time-temperature history such as that described by the standard curves. Although not explored further by Barnett, an examination of the values for s_c would confirm that no compartment fire could physically result in the time-temperature history represented by the standard curve, based on the BFD model. As an example, Barnett found that the ASTM E119 time-temperature curve is best fit using a value of s_c = 58. Assuming, for example, an insulated fire compartment, it follows that using Eq. (2.25) the ventilation factor would have to be:

$$s_c = 58 = \frac{1}{9.25 A_w \sqrt{H} / A_t + 0.21} \quad \Rightarrow \quad \frac{A_w \sqrt{H}}{A_t} = -0.02084 \tag{2.26}$$

meaning that either A_w or A_t would have to be negative. A negative result would also be obtained for the case of a non-insulated fire compartment. Since neither A_w or A_t, the area of ventilation or the total interior area less the window area, respectively, can be negative, this simplified analysis suggests that it is physically impossible to achieve the standard time-temperature curves during real fires in compartments. In support of this idea, other studies of both the Cardington Full Scale Fire Tests and the events of the World Trade Center collapse have clearly shown that real fires are not well described by standard time-temperature curves and that structures will respond differently in real compartment fires than would be determined using the standard temperature exposures specified in a fire test furnace (Barnett 2002; Kodur 2009). In this light, perhaps the scientific relevance of trying to establish any further connection between parametric models and the standard time-temperature curve should be brought into question. On the other hand, in the current practice of fire protection engineering, answers to such questions are often very important as building code compliance currently is evaluated on the basis of the standard time-temperature exposure, whether this is through a fire-resistance test or an analysis to justify an alternative solution or equivalency.

Overall, parametric models can be used to represent many aspects of the behaviour of real fires in compartments, as supported by their agreement with the experimental data (Hurley 2005). There are two key shortcomings of parametric models, however, that should be stated. First, time dependent parametric models for early fire growth provide no information on the history of the fire beyond the initial growth phase. Real structural fires do not necessarily exhibit the smooth growth assumed by

the t-squared model. Initial fuel arrangement, fuel properties and ventilation conditions around the time of ignition also play a significant role in early fire development. Even when the fire has entered the "steady" growth phase normally associated with post flashover fires, changes in ventilation conditions due, for example, to failure of glass windows or occupants opening doors during escape, will greatly alter the fire heat release rate. Real fires most often undergo alternating stages of fuel controlled and ventilation controlled burning prior to reaching a fully developed steady state burning phase (Drysdale 1998; Weckman 2008). Parametric models are not capable of predicting the true features of the dynamic environment driven by the fire in a compartment or the dynamic response of the fire to that environment. However, this shortcoming is not generally thought to be significant because pre-flashover fires do not generally pose a threat to the structure itself unless the fire origin is in close proximity to the structure (Hurley 2005). A second, and perhaps more profound, shortcoming of parametric models is their lack of consideration of the temperature distribution that in reality develops within a fire compartment. The most fundamental assumption of parametric models is that the temperatures in post-flashover fire compartments are uniform throughout the compartment at any given time step, which, in turn, means that all elements of the structure are exposed to a uniform temperature field. This assumption may be valid for small fire compartments, but must be examined further for the case of larger compartments, where the temperature gradient developed within the compartment during the fire is more significant. This aspect of the parametric model is important in the design of structures for fire in that it will greatly affect the number of structural columns and beams that need to be assumed to be exposed to fire. To truly account for temperature distribution and stratification within a compartment, more sophisticated zone and computational fluid dynamics models that determine the heat transfer and smoke flow processes based on first principles are needed. Such models form the topic for the next section.

2.4 Zone and CFD Models

The availability of personal computers and their advancement, particularly during the last decade, have led to the development and use of computer-based fire models to provide more physics-based modeling of compartment fires (Olenick 2003). Utilizing the computer's ability to repeatedly and reliably solve mathematical equations based on a given set of instructions, computer models incorporate numerical methods to solve the complex equations that govern the various fire induced physical and chemical processes. This approach is distinct from the parametric models and the standard time-temperature curve model, which are models correlated against experimental

observations. Instead, computer models are employed to directly solve simplified forms of the equations that govern the fire physics and chemistry, so they should provide a greater degree of accuracy in terms of predicting the reality of fire. Because of this, use of a computer fire model should provide a significant benefit in modern performance-based design and scientific research, when the conventional approaches of fire testing or simplified fire modeling are costly or inappropriate. For example, researchers can often eliminate the need for certain fire tests based on predictions using computational fluid dynamics models, allowing them to instead focus their resources on a selected number of carefully targeted fire experiments. Performance-based designs based on fire modeling results are yielding new fire protection strategies and methodologies that are different from, but superior to, those indicated using a prescriptive building code approach. There are currently two broad groups of computer fire models: the zone models, which are physically based fire models of intermediate complexity, and computational fluid dynamics (CFD) models, which incorporate a full physics based treatment of the fluid mechanics and energy exchange in a compartment fire. These form the subject of the next two sections.

2.4.1 Zone Fire Model

Zone models are the most basic computer fire models. They involve application of the principles of mass and energy conservation over one, two or more control volumes (or zones) used to represent various areas within a fire compartment. In zone modelling, macroscopic transport of mass and energy between control volumes and between volumes and the exterior are considered, while small scale processes within a control volume are not considered since the temperature of each individual volume is considered uniform (well-mixed assumption). While overall balances ensure global conservation of mass and energy in the compartment, the exchange of momentum and energy between volumes and to the exterior are represented by various source terms and sub-models based on empirical correlations. Therefore, zone-models can be viewed as models of intermediate complexity which incorporate some key aspects of the fire physics, with a “quasi-rigorous” treatment of other phenomena that govern the detailed behaviour of compartment fires.

The most basic zone model is the one zone model, which assumes one uniform control volume to represent the entire fire compartment as illustrated in Figure 2.9 (Bailey 2009). Because of this assumption, one zone fire models are only suitable for modelling post-flashover fire compartments, similar to parametric models. Despite the more advanced, physics-based approach taken in one-zone models, they are in fact seldom used in practice as they do not present a significant advantage over

parametric models. However, to capitalize on its inherent advantages and expand the zone modelling technique to account for all stages of compartment fire development, more advanced, and more popular, two-zone models have been formulated. These are again founded on mass and energy conservation but distinguish between the "hot upper" and the "cool lower" zones seen during pre-flashover and decay-phases of a compartment fire as shown in Figure 2.10. As the fire evolves into the fully-developed, post-flashover stage, consideration for mixing between these two control volumes inherently built into the two-zone model allows for transition of the model to the case of well-ventilated, post-flashover fires. Therefore, two-zone models are able to represent the full scenario, including the stratified fire compartment observed prior to flashover.

The two zone model concept was first considered by Thomas in the 1970s (Fu 2000). In the subsequent decade, a significant amount of work went into refining the model and validating model predictions. Friedman provided a comprehensive survey of computer models indicating that 31 zone models were developed and available in 1992 (Friedman 1992). Olenick provided an updated survey in 2003 showing that the number of zone models had increased to 48 (Olenick 2003). Amongst these, the zone model developed by the National Institute of Standards and Technology (NIST) called CFAST has been the most widely used and accepted (Remesh, 2006). Despite the wide range of zone models available, the founding principles of each are the same – with minor differences in the numerical techniques employed to solve the governing equations and/or in the selection of sub-models used to model the source terms and exchange processes. The software manuals for a particular zone model should contain all pertinent details of the formulation of that model; however, Quintiere in 1989 also presented a comprehensive summary of a generic zone model formulation for compartment fires (Quintiere, 1989) which is considered here. The mass conservation equation for a zone within the compartment is given by:

$$\frac{d\dot{m}}{dt} + \sum_i \dot{m}_i = 0 \tag{2.27}$$

where $\sum \dot{m}_i$ is the net rate of mass flow into the control volume and $d\dot{m}/dt$ is the rate of change of mass in the control volume with respect to time. Since mass equals the product of density and volume (i.e., $m = \rho V$), Eq. (2.27) can be written as

$$\frac{d\dot{m}}{dt} + \sum_i \dot{m}_i = 0 = A\frac{d}{dt}\left(\rho z_{upper}\right) + \sum_i \dot{m}_i \tag{2.28}$$

for the upper zone and

$$\frac{d\dot{m}}{dt} + \sum_i \dot{m}_i = 0 = A\frac{d}{dt}\left\{\rho\left(h - z_{upper}\right)\right\} + \sum_i \dot{m}_i \tag{2.29}$$

for the lower zone, where A is the floor area of the fire compartment (m^2), z_{upper} is the height of upper control volume (m), and h is the height of the compartment (m) which gives $z_{lower} = h - z_{upper}$. Therefore, in solving Eq. (2.28) and (2.29), the height of the two control volumes can be calculated with respect to time.

Secondly, the conservation of energy is given by:

$$\frac{d\dot{E}}{dt} + \sum_i \dot{E}_i = 0 \tag{2.30}$$

where $\sum \dot{E}_i$ is the net rate of energy flow into the control volume and $d\dot{E}/dt$ is the rate of change of energy in the control volume with respect to time. Using the first law of thermodynamics, defining enthalpy $H = E + PV$, Eq. (2.30) for constant pressure, P, can be rewritten as:

$$\frac{dE}{dt} + P\frac{dV}{dt} + \sum_i \dot{H}_i + \sum_i Q_i = 0 \tag{2.31}$$

where $\sum \dot{H}_i$ is the net rate of enthalpy gain in the control volume due to mass flow across the volume boundaries, and $\sum Q_i$ is the net rate of heat gain in the control volume due to heat transfer or combustion. Since $E = \dot{m}c_v T$ and $H = \dot{m}c_p T$, it follows that the energy balance for the upper and the lower control volumes, with constant thermophysical properties, can be written as:

$$\frac{dE}{dt} + \sum_i E_i = 0 = Ac_v\frac{d}{dt}\left\{\rho T_{upper}\left(z_{upper}\right)\right\} + c_p\sum_i T_i\dot{m}_i + \dot{Q} \tag{2.32}$$

where c_v and c_p are the heat capacities of the gas at constant volume (J/K) and constant pressure respectively, T_{upper} is the temperature of the fluid in the upper control volume (K), and T_i is the temperature in the stream of mass, $\dot{m}_i$, entering or leaving the control volume. Similarly, one can write the expression for the lower layer, noting that $z_{lower} = h - z_{upper}$:

$$\frac{dE}{dt} + \sum_i E_i = 0 = Ac_v\frac{d}{dt}\left\{\rho T_{lower}\left(h - z_{upper}\right)\right\} + c_p\sum_i T_i\dot{m}_i \tag{2.33}$$

In the mass and energy conservation equations, $\rho = P/RT_{upper}$ for the upper control volume and $\rho = P/RT_{lower}$ for the lower control volume as given by the ideal gas law, since P is constant (atmospheric pressure) for both control volumes. Accordingly, there are four ordinary differential equations, Eqs (2.28), (2.29), (2.32), (2.33) for mass and energy conservation for the upper and total control volumes, and four unknowns, P, T_{upper}, T_{lower} and z_{upper}, which can theoretically be solved. The chief foundation of zone models is a first principles analysis of mass and energy conservation. However, within the governing equations are source terms; namely: $\sum \dot{m}_i$, $\sum \dot{H}_i$ and $\sum Q_i$ which represent the various interactions that occur between the fire, the compartment and the surroundings, such as mass transfer, combustion, conduction, convection and radiation heat transfer; these are not modeled using first principles. Instead, they are obtained from sub-models which are based on empirical correlations. It is the choice of these sub-models which also distinguishes one zone model from another, and the validity of these sub-models has a great influence on the overall accuracy of the zone model predictions.

Various studies have been carried out to compare zone model predictions to experimental compartment fire test data. Based on comparison with experimental data for fires of 2MW to 7MW in a room of 21m^3, Peacock showed that the CFAST zone model provided reasonable predictions of compartment temperature history, though he noted that the CFAST predictions were slightly higher than the actual measurements (Peacock, 1993). Dembsey compared CFAST results against twenty full-scale compartment fires ranging from pre-flashover to post-flashover stages and concluded that while CFAST predicted the compartment temperature history well, the temperatures were overestimated on average by about 100C in comparison to the experimental data (Dembsey, 1995). Dembsey attributed this finding to inaccuracies in how the model accounted for the heat loss by conduction through the compartment enclosures. Based on these findings, it can be argued that CFAST is a reasonable zone model software package for fire safety design in that it provides designers an order of magnitude estimate of the compartment temperature history while the trend toward over-estimation of the upper layer temperatures would err on the side of conservatism. Nonetheless, CFAST and zone models in general are not suitable for providing physical or chemical details of compartment fire development at scales finer than the one or two large control volumes assumed to exist within the compartment. In addition, Babrauskas pointed to the following limitations with zone models in modeling the detail of compartment fire growth (Babrauskas, 1996):

- No flame spread calculations

- No heat release rate calculations
- No fire chemistry
- No smoke chemistry
- Absence of realistic mixing between zones

It should be noted that these limitations relate to fire chemistry, fire spread and smoke management, so are not generally of as much concern in structural fire safety where compartment temperature is of chief interest. Therefore, in terms of compartment temperature prediction capability for engineering design purposes, results from two zone fire model predictions of the scenarios are usually considered acceptable.

Because of the success of two-zone models in providing reasonable predictions through simple formulations that require relatively little computer power, there has been limited additional development of two-zone models in recent years. Zone models have became an accepted practice in determining the time-temperature relation for current performance-based fire protection practice.

In modeling compartment fires, multi-zone modeling techniques present a clear advantage over basic parametric models or the standard time-temperature curve in terms of integrating appropriate physical fire phenomena into the model, while offering a reasonable compartment fire temperature prediction without demanding the significantly higher computer overhead needed by CFD models. This level of sophistication is suitable for many fire engineering applications. However, where further detailed simulation of enclosure fire dynamics is required, such as in forensic fire investigation work, detailed fire analysis, or scientific research, computational fluid dynamics models can be employed to integrate greater amounts of physics directly into the model.

2.4.2 CFD Fire Model

The most advanced fire models currently available are based on direct solution of the governing equations of energy, mass and momentum over a finite number of control volumes using computational fluid dynamics. CFD models have been used for some time to examine the movement of fluid and transport of mass and energy in various engineering and scientific applications. In fire engineering, CFD models are currently used to examine aspects of compartment fire behaviour such as the spread of fire, the movement of smoke, or predicting activation times of fire detectors. Although well-within their capability, CFD fire models are generally not employed for calculating

post-flashover compartment temperatures for structural fire protection design. The reason is that the maximum compartment temperatures can more easily be estimated using less sophisticated parametric models or zone-models. However, in the context of providing a more accurate representation of the temperature fields developed in a compartment fire, CFD models are by far the most scientific way of representing enclosure fire dynamics. For completeness, therefore, they are discussed briefly in this section.

The starting point for a computational fluid dynamics based analysis of fire behaviour is the conservation equations of fluid motion; namely: a) the continuity equation for mass conservation; b) the Navier-Stokes equations for momentum conservation; and c) the energy equation for energy conservation, which are respectively (Versteeg 2007):

$$\nabla \cdot \rho \vec{v} + \frac{\partial \rho}{\partial t} = 0 \tag{2.33}$$

$$\rho\left(\frac{\partial \vec{v}}{\partial t} + \vec{v} \cdot \nabla \vec{v}\right) + \nabla p - \mu \nabla^2 \vec{v} - \rho g = 0 \tag{2.34}$$

$$\frac{\partial(\rho i)}{\partial t} + \nabla \cdot \rho i \vec{v} + p \nabla \cdot \vec{v} - \nabla k T - \Phi - S_i = 0 \tag{2.35}$$

In essence, the CFD approach is to specify a finite number of control volumes (or grids) that define the computational domain, then discretize the foregoing equations and employ numerical techniques to solve for the unknowns ρ, T and v for each control volume. The results, assembled across all control volumes, provide the detailed distribution of the variables within the computational domain at a given time. This allows the modeler to study the results of a model in great detail, with a resolution defined by the size of the control volumes. In modern CFD packages, post-processing software is available to allow users to visualize the model results in time frames, permitting a more visualized approach by which to assess a physical phenomenon. Because it is not possible to solve the coupled conservation equations analytically, the governing equations are first simplified to represent only the key physics for the problem at hand and the remaining terms are approximated (discretized) using Taylor series expansions, then solved numerically. Depending on the CFD application, then, both the formulations and the numerical solution methods for the governing equations may be different. The exact derivation of the CFD equations for fire modeling, or any fluid mechanics application, is complex and specific to a particular application. Since this information readily exists in the literature

and is not the core subject of this thesis; it is not reproduced further here. Instead, it is important to note that in formulating a tractable solution to the governing conservation equations, certain key physical phenomena must be represented using submodels. One such aspect that is key to fire modelling is the treatment of turbulence in the momentum equations for fire-driven flows. Due to their importance in CFD modeling of fires, the two main approaches to turbulence modeling are described briefly below.

Fire-driven flows are unique from a fluid dynamic perspective since large temperature, and therefore density, differentials between the fire gases and the bulk fluids in the fire compartment, result in large buoyancy effects closely linked to large and rapidly changing velocity magnitudes and directions over time. To calculate these effects through direct solution of even a simplified form of the Navier-Stokes equations above is beyond the capabilities of even the most powerful computers today (SFPE 2002). In order to address this, a turbulence submodel must be used. There are two commonly used types of turbulence submodel in CFD modeling of fires: one is based on Reynolds averaging of the Navier-Stokes equations, which is commonly known as the "RANS" model; the other is using large eddy simulation, which is commonly referred to as "LES simulation". In the RANS model, terms in the time-averaged Navier-Stokes equations that account for turbulent fluctuations in the flow are solved using sub-models; the most common being the k-ε model (other models include Spalart-Allmaras model, Algebraic stress model and Reynolds stress model) (Versteeg 2007). The issue with employing RANS models for fire applications, however, is that the velocity is averaged over time so that any large-scale motions which drive mixing and entrainment in the hot gases of the fire plume and the ceiling jet may be lost. Because of this, an alternative, and arguably more popular, approach based on LES simulation has been developed. In this method, the large eddies which would represent the bulk movement of the fluid (for example the plume and the ceiling jet) are modeled via direct numerical solution of the Navier-Stokes equations, while the smaller scale motions are filtered from the solution, which are either ignored completely or represented using a sub-model based on empirical correlations (SFPE 2002; Versteeg 2007). The LES modeling approach can be regarded as an intermediate treatment of the turbulence; the Navier-Stokes equations are not directly solved, as would be the case in direct numerical simulation (DNS), but some aspects of the predictions can be significantly improved over those found using a RANS approach.

There is little debate that computational fluid dynamics models represent the most advanced and physics-based modeling approach for detailed prediction of the interior environment developed in a compartment during a fire. However at the present time, their significant advantage in the practical sense is mainly with respect to improved modeling of the fluid mechanics of fire and smoke movement for fire safety evaluations. While this is significant, it must be recognized that even in CFD models some important sub-processes, such as combustion and radiation heat transfer, are often still calculated using empirical sub-models. The accuracy of prediction, like that of any fire model discussed in this chapter, is limited by the simplifications, sub-models and assumptions employed to formulate the overall model that represents the compartment fire. Consequently, CFD modeling is used primarily in pre-flashover compartment fire modeling, when the detailed modeling of smoke movement as induced by buoyant effects of fire is crucial to occupant life safety. In terms of structural fire protection, however, which is traditionally a concern in post-flashover fire compartments (Hurley 2005), CFD modeling is not commonly used. Not only does it require significant time and effort to set up the parameters for, and to calculate, a full fire scenario to post flashover conditions, but a user must also examine the sensitivity of the results to the size of control volume, time step and input parameters for the compartment. Instead, it is most often assumed that by the post flashover stage, the compartment temperature will be uniform, so predictions made using parametric and zone models are deemed reasonably appropriate. In special instances where the costs and effort are justified or necessary – such as forensic investigation work or fire design of unique or unusual structures where experimental re-creation of a real fire event is not possible – or in scientific research, CFD fire models should be used due to their ability to predict fire scenarios with added realism over other fire modeling approaches, and at a comparatively lower cost than would be incurred in setting up full-scale fire reconstructions or experiments.

There has been very limited published work pertaining to verification of the predictions from CFD fire models, particularly as related to structural fire protection applications (Zou 2005). The most popular CFD fire model is probably the Fire Dynamics Simulator, created and maintained by the National Institute of Standards and Technology (NIST) in the USA. The overall predictive capability of FDS has been verified internally at NIST (NIST 2009). Although not formally documented in archival literature, some aspects of the most recent release, Version 5.0 of FDS, principally for smoke management and compartment temperature predictions, have been confirmed publicly through an online discussion forum that includes users from academic, governmental and private institutions (NIST 2009). In the published literature, Zou compared FDS modeling results with data from full-

scale experiments involving flashover fires in a small 2.4 m by 2.4 m by 3.6 m room fire test compartment and found that FDS results agree reasonably well with experimental data, with the temperature near the ceiling agreeing to within 10% (Zou, 2005). Perhaps the most significant verification work published in literature is that of Pope (Pope, 2006) where he compared the compartment temperature history measured from the full-scale fire tests at Cardington, UK against predictions by the BFD parametric model, the Swedish curve parametric model, and FDS. Pope's study found that on average, the BFD parametric model offered a more consistent and accurate representation of the compartment temperature than did FDS. For instance, using the BFD curve, the error in maximum predicted gas temperatures varied between 0.9% to 5.4% of the maximum compartment temperatures measured in the Cardington tests, while errors in temperature predicted using the Swedish curves was between 1.0% to 15% and using FDS with $(0.2\ m)^3$ grid size between 3.4% to 21.1% and with $(0.4\ m)^3$ grids between 10.9% to 32.9%. It should be possible to improve the accuracy of the FDS simulation by further increasing the number of grids or improving the models used for heat transfer into the structural elements; however, the computational time would significantly increase as well. In contrast, the BFD curve provided the most accurate prediction of the Cardington fire test compartment temperatures without the use of a computer. In this way, Pope's study seems to support the notion that for the purpose of post-flashover fire compartment calculations, CFD offered little, if any, advantage in comparison to the BFD parametric model. One must be careful in comparing results from different families of fire model, however, as it can also be argued that CFD output data are point measurements and should not be directly compared to parametric models, which estimate time and spatially averaged compartment temperatures (Moinddin, 2008).

Recognizing the benefit of CFD modeling for providing detailed fire analysis and the disadvantage of the associated time and cost constraints, some recent research has focused on finding an intermediate modeling approach between zone and CFD modeling. For example, Chen proposed a multi-layer extension to the two zone model for predicting fire behavior in a room and developed a 20 zone formulation aimed at improving the prediction of temperature stratification during pre-flashover compartment fire growth (Chen 2005). Reasonable agreement between the model prediction and the experimental data was shown, with significantly better resolution of the temperature profile than achieved with two-zone models, while at the same time requiring substantially less computational power than for a CFD model. In a different approach, Hua proposed a hybrid CFD-zone model where the fire and fire compartment are modeled in detail using computational fluid dynamics principles and

connected compartments are then modeled using two-zone models (Hua 2005). While indicating some potential, these hybrid approaches still require significant work to address the issue of interfacing results between the CFD and zone models.

2.4.3 Remarks on Fire Modeling

In designing structures to resist the thermal effects of fire – whether this is in the form of specifying thermal insulation or by directly accounting for the thermal effects of a fire in the structural design – the selection of an appropriate fire model is critical and essentially defines the 'fire loading' that will be incorporated into the design. The use of the standard time-temperature curve, while convenient, is inappropriate in performance-based design in that it does not account for many real effects of a fire. On the other hand, advanced CFD modeling provides a close-to-reality treatment of the enclosure fire dynamics and fluid mechanics by solving the governing equations of the physics. However, such practice is often cost-prohibitive and unless present day computer power advances many fold, it will not be an appropriate design tool for day-to-day practice. In this light, it is apparent that parametric models and zone models offer a happy medium - a scientific way of representing the thermal environment in real fires while not being constrained by the computing overhead of CFD models or the over-simplification of the standard time-temperature curve. Early parametric models and one-zone fire models appear to be sound for prescriptive fire protection practice in that they are able to predict the maximum compartment temperature based on the uniform temperature assumption valid in a post-flashover fire compartment. However, in advancing the practice of structural fire engineering by looking at fire as a time-varying 'load' on a structural frame, advanced parametric models such as the BFD fire curve and two-zone fire models are more appropriate, and provide a parallel level of sophistication in the fire analysis as that which is used in the structural mechanics analysis. These models offer a reasonable degree of accuracy in predicting the overall growth, steady-state and decay phases of a compartment fire that would allow a structural analysis to account for the thermal effects in all aspects. Even if there is no interest in designing the structure to withstand a specified fire load, but instead that the prescriptive practice of specifying appropriate fire protection via thermal insulation is desired, these fire models would still offer a more performance-based approach to the structural fire engineering problem, although the "performance-based" aspect of the design would only be limited to the fire analysis.

For the research work presented in this thesis, the BFD parametric fire model (Section 2.3.2.5) has been selected for estimation of fire temperature on a structure as it is thought that this model presents

a robust means of representing the time-temperature relation of real fires such as that of the Cardington fire test, and does not require the computer setup of zone models. Further, as one purpose of this thesis is to illustrate the incorporation of fire as a design load in structural design, it was considered that the computationally simpler BFD model is appropriate in this regard, although there may be equally good reasons for using a two-zone fire model such as CFAST in a practical design situation.

Prior to entering the discussion in Chapter 3, the last section of Chapter 2 presents a short review of the current state of structural design for fire which, while providing a powerful design tool, at the present time is rarely used in performance-based engineering practice.

2.5 Limit States Design of Structures for Fire

The current prescriptive approach to address the impact of fire on a structure involves providing fire protection to the structure almost exclusively via thermal insulation. The evaluation of structural performance in fire is then based on a time criterion, known as the fire-resistance rating, which is based on the survival time of the structure when exposed to the standard time-temperature fire curve. Although a performance-based approach to structural fire protection has been practiced through the use of fire models to represent real fires, it has nonetheless taken a "protection" based approach in that the design of the structure for fire still relies 100% on providing appropriate insulation without explicitly accounting for the actual integrity of the structure. In true performance-based design, structures are engineered by explicitly accounting for the effects of fire on the strength and integrity of the structure under design. That is, similar to design for earthquake or wind resistance, the acceptability of a design is established by demonstrating that the structure has adequate strength and integrity to withstand the fire effects throughout the period of fire exposure. In keeping with current limit states design practice, the thermal effects of fire can be accounted for by ensuring that the ultimate limit state criterion is maintained during fire events (Buchanan 2001; Ellingwood 2005), i.e.:

$$U_{fire} \leq \Phi_{fire} R_{fire} \tag{2.36}$$

where U_{fire} is the ultimate applied loading on the structure in the presence of fire, R_{fire} is the load resistance capacity of the structure during the fire, and Φ_{fire} is the specified strength reduction factor for fire. Limit states design is a more rational approach to design of structures than the conventional working stress method in that the design loading and the design structural strength are both factored

up to a specified limit level, below which it is considered unlikely failure would occur due to any variability in actual loading and strength. In limit states design, the Φ factor is used to represent the uncertainty in the strength of a structural member due to the variability in quality of the manufacturing process. However, it is thought that the probability is low for a structural member to not be at its design strength at the time of a structurally significant fire and, therefore, it is appropriate to take $\Phi_{fire} = 1$, i.e., no strength reduction (Buchanan 2001; Kodur 2009). Therefore, designing a structure subject to fire so as to satisfy Eq. (2.36) involves determining that the ultimate loading on the structure, U_{fire}, is not greater than the limit-states resistance capacity of the structure, R_{fire} during the fire.

2.5.1 Load Combination for Fire

In limit states design, the applied load, U, is a combination of a number of different load types, including the self-weight of the structure, the weight of occupancy (occupants and furniture and equipment), as well as external effects such as snow, wind and even seismic activity (Buchanan 2001). Because these loads can vary greatly in time and in space throughout the course of a building's lifetime, structural design based on the limit states principle determines an appropriate load combination factor to represent the probability of a given event occurring. Fire with the potential to cause structural damage is generally considered a rare event in comparison to events that lead to significant live, snow, wind or earthquake loads (Ellingwood 2005). A proposed load combination appropriate for fire conditions that is based on limiting the probability of structurally significant fire to less than 10^{-6}/yr is as follows (Ellingwood 2005; AISC 2005):

$$U_{fire} = 1.2D + T + 0.5L + 0.2S \tag{2.37}$$

where D is the dead load (N), T is the load induced by fire actions (N), L is the live load (N), and S is the snow load (N). This compares to the suggested acceptable limit state probabilities of 10^{-5}/yr to 10^{-4}/yr for gravity loads (Ellingwood 2001). The National Research Council of Canada, which publishes the National Building Code of Canada, also suggests a similar load combination for determining a fire-resistance rating based on the standard fire test, which is based on earlier work of Ellingwood (NRCC 2005):

$$U_{fire} = D + T + \left(\alpha L + 0.25S\right) \tag{2.38}$$

where $\alpha = 1.0$ for storage areas, equipment areas and service rooms and $\alpha = 0.5$ for other occupancies to recognize that occupants move during a fire. Equations (2.37) and (2.38) reflect the view that in the rare occurrence of a structurally significant fire, it is unlikely that excessive live and snow loads would occur at the same time; therefore, it is appropriate to use factors ≤ 1 for these loads. But what is truly unique about these equations is the inclusion of a thermal load, *T*, that accounts for the loads due to fire actions, which has not been greatly considered in the past.

The thermal load is primarily attributed to the thermal expansion of the structural members, which may result in a thrust force if the members are restrained (CAN/ULC-S101 2004; Kodur 2009). In fire-resistance testing, the *T* load is indirectly considered if a structure is thermally restrained (i.e., capable of resisting *T*) in that a higher fire-resistance rating is assigned, whereas a lower fire-resistance rating is assigned if the same structure is not thermally restrained (CAN/ULC-S101 2004; Gewain 2001). Although the test standards such as ASTM E119 and CAN/ULC-S101 provide a list of qualitative ways for assessing whether a structure is thermally restrained, there is currently no simple method of quantitatively determining thermal restraint. That said, National Research Council of Canada notes that *T* can be taken equal to zero for statically determinate structures or for structures that have sufficient ductility to allow the redistribution of temperature forces before collapse (NRCC 2005). It has been suggested by AISC that *T* must be determined on the basis of an appropriate design fire – namely, using the standard fire model, parametric models or computer-based models to represent the post-flashover fire compartment temperatures (AISC 2005). But again, the question of how to actually compute *T* at the determined temperature remains unanswered in both the archival literature and in design documents available today.

Despite provisions for performance-based design that are available in building codes and even the release of full performance- and objective-based building codes, the basic science for structures subject to fire has not progressed much; current practice remains stagnant on the concept of fire-resistance testing and the associated component-qualifying approach established in 1917 – i.e., structural performance is basically assessed on a member-by-member basis, with concern only for the time it takes for a certain member in the structure to attain a certain temperature, without assessing the integrity of the structure as a whole during the fire. Consequently, structural design for fire has essentially been confined to statically determinate structures such as a simply-supported beam, such that *T* may be ignored; or alternatively, has been conducted by making qualitative assessments to ascertain the presence of thermal restraint. A true performance-based analysis requires the

satisfaction of Eq. (2.36) for an entire structural frame, which is generally statically indeterminate (i.e., structurally redundant). Despite the slow progress, some research work has been done to investigate the performance of entire structures subject to fire. This includes the full-scale fire test of an eight storey steel structure exposed to natural fire in Cardington, UK (BS 1998), and the extensive computational investigation of the World Trade Centre collapse (NIST 2005). These works have illustrated that if necessary, sophisticated computer fire and structural models using CFD and finite element methods are available today to assess the performance of structures subject to fire. That is, with available time and funding, it is possible now to provide a comprehensive analysis of a structure under fire loading. However, it yet remains to develop more simplified approaches to the analysis and design of structures subject to fire that can be used for day-to-day engineering practice. To this end, this thesis proposes to develop a method for assessing the thermal effects of fire in structural steel frameworks. The frame analysis software and definition of fire load for inclusion in the software form the basis for the discussion in Chapter 3.

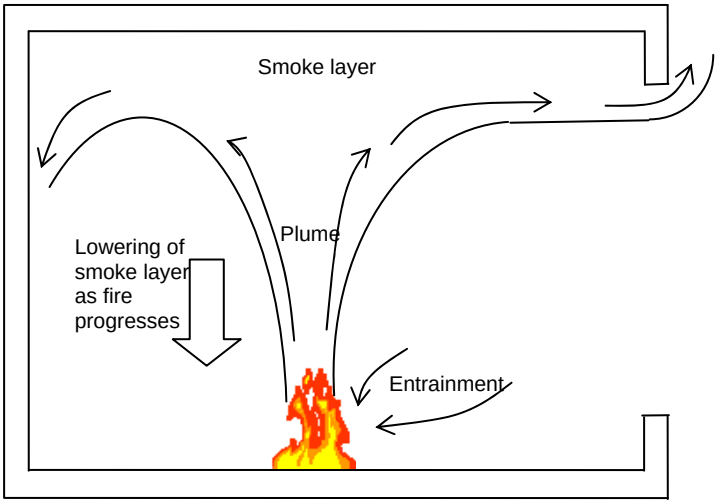

Figure 2.1: Illustration of a typical pre-flashover compartment fire.

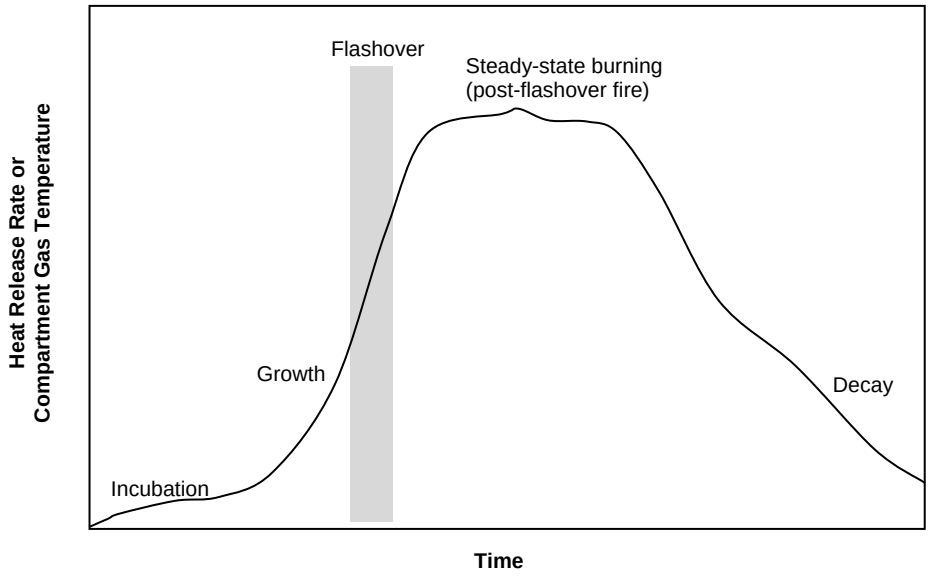

Figure 2.2: A typical plot of the HRR / temperature versus time curve showing the course of development of a natural compartment fire.

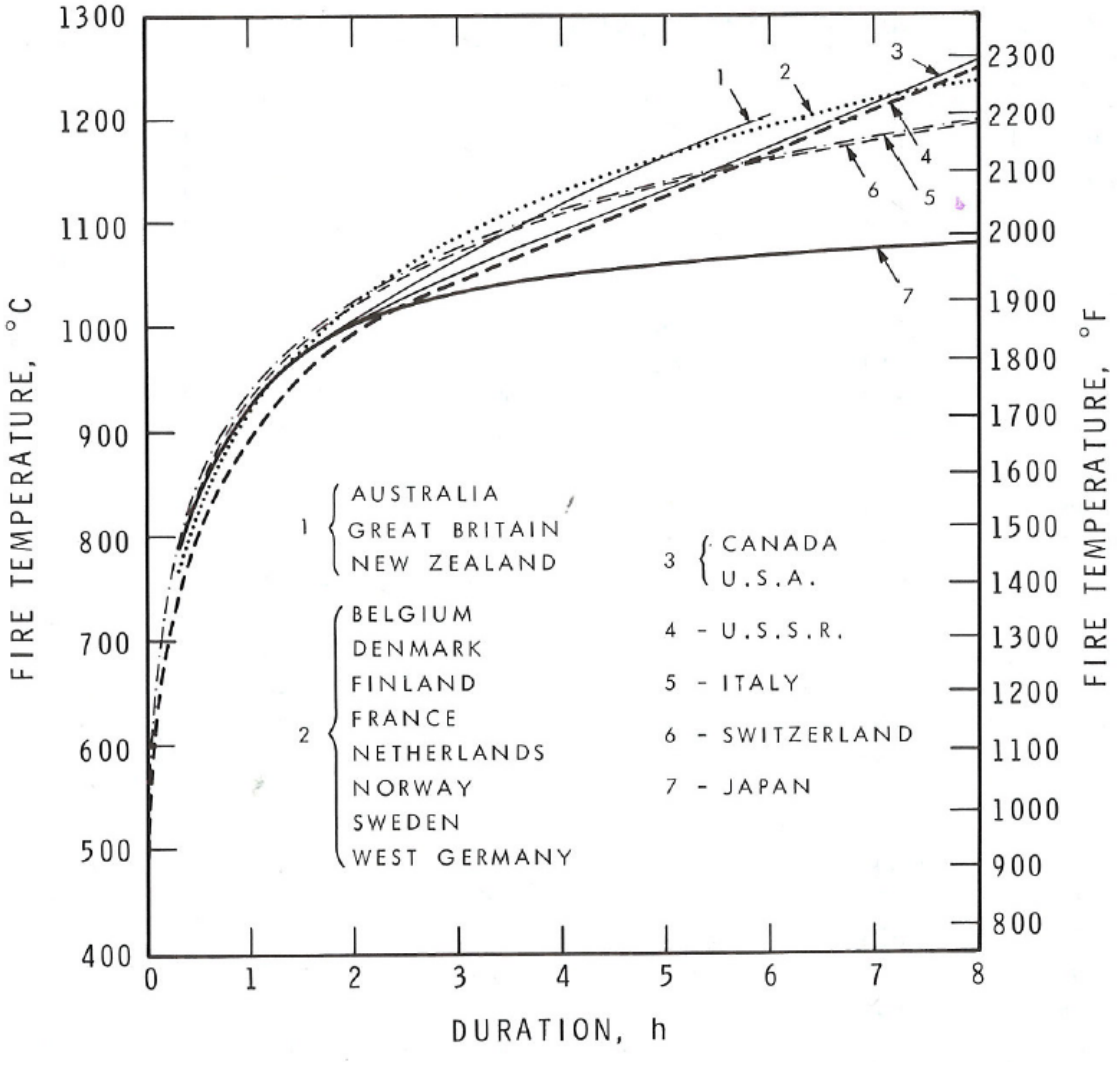

Figure 2.3: Plot of the standard time-temperature curves used in major industrial nations (ASCE 1992).

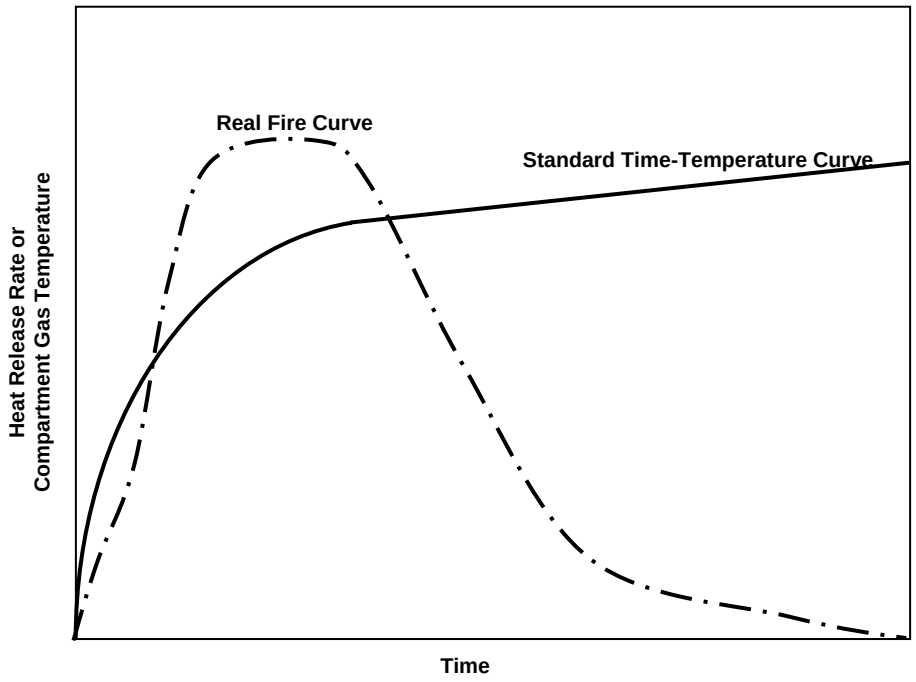

Figure 2.4: Plot of the standard time-temperature curves against real fire behavior.

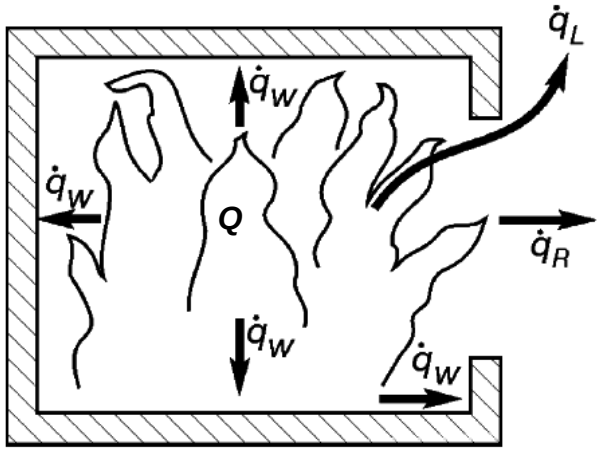

Figure 2.5: Schematic illustration of the energy balance in a fire compartment (Feasey 2002).

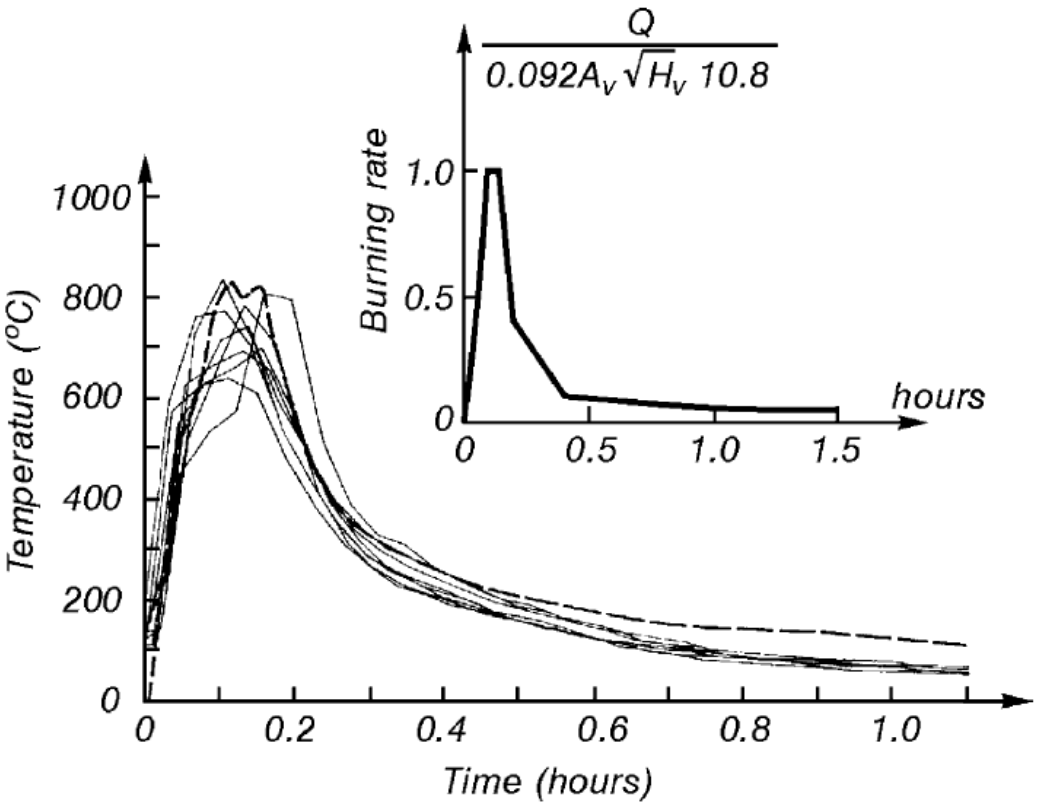

Figure 2.6: Burning rate and resulting compartment gas temperature determined from the energy balance that lead to the development of the Swedish curves (Feasey 2002).

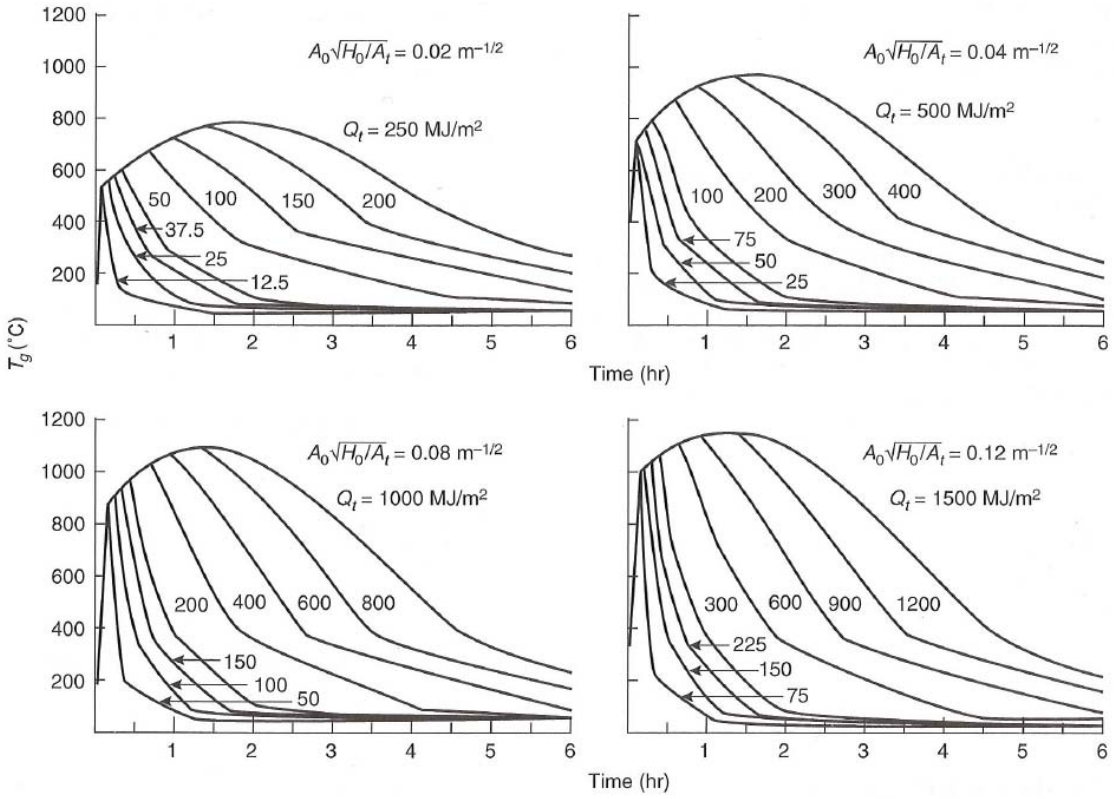

Figure 2.7: Swedish compartment gas temperature-time curves for post-flashover compartment fires (Drysdale 1998).

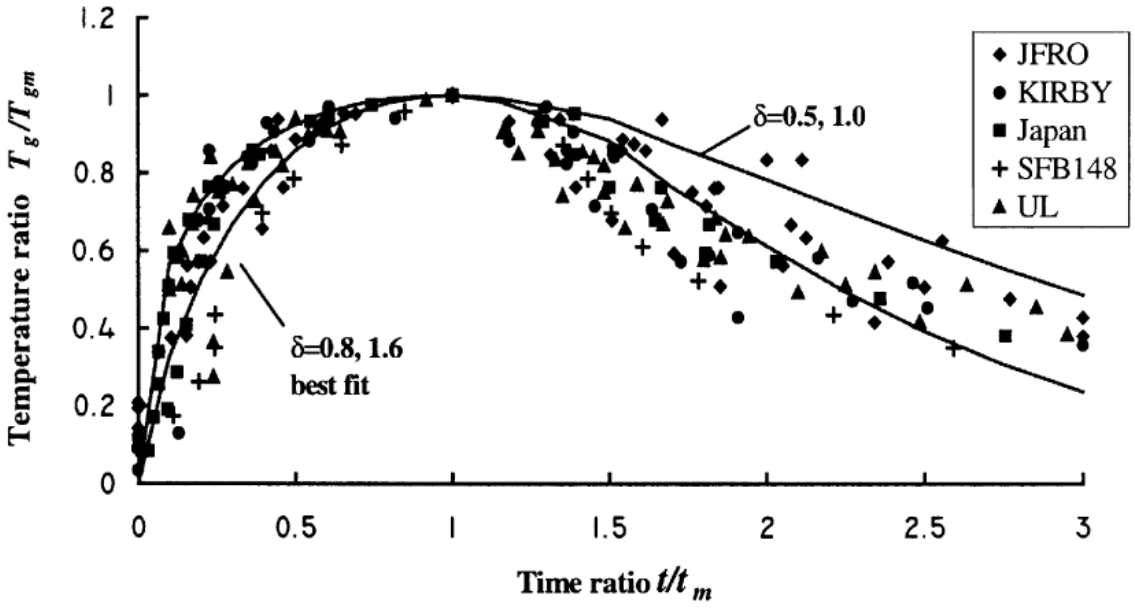

Figure 2.8: Curve-fitting Eq. (2.15) with different values of growth/decay shape factor δ (Ma 2000).

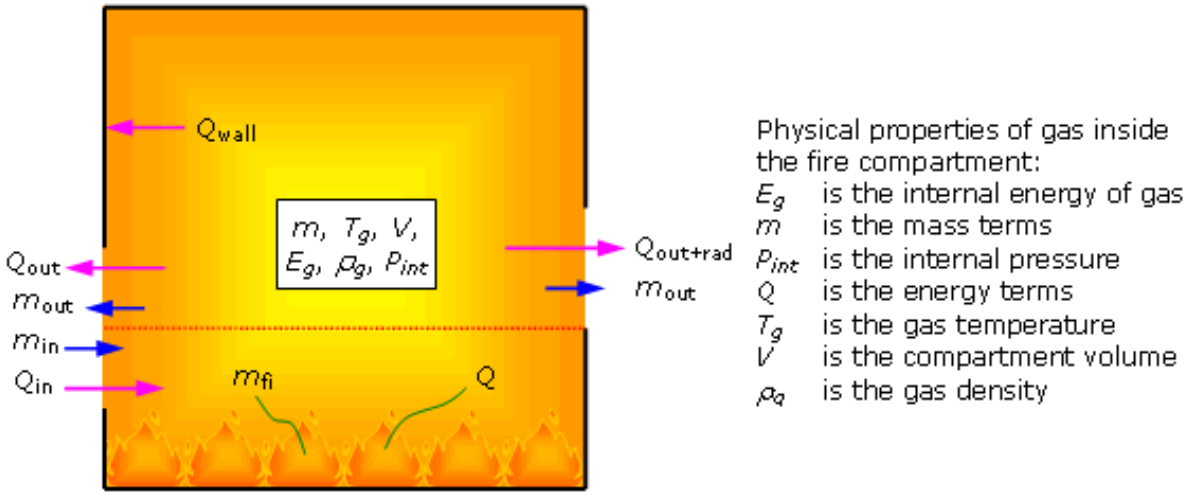

Figure 2.9: Schematic illustration of one-zone fire modelling (Bailey 2009).

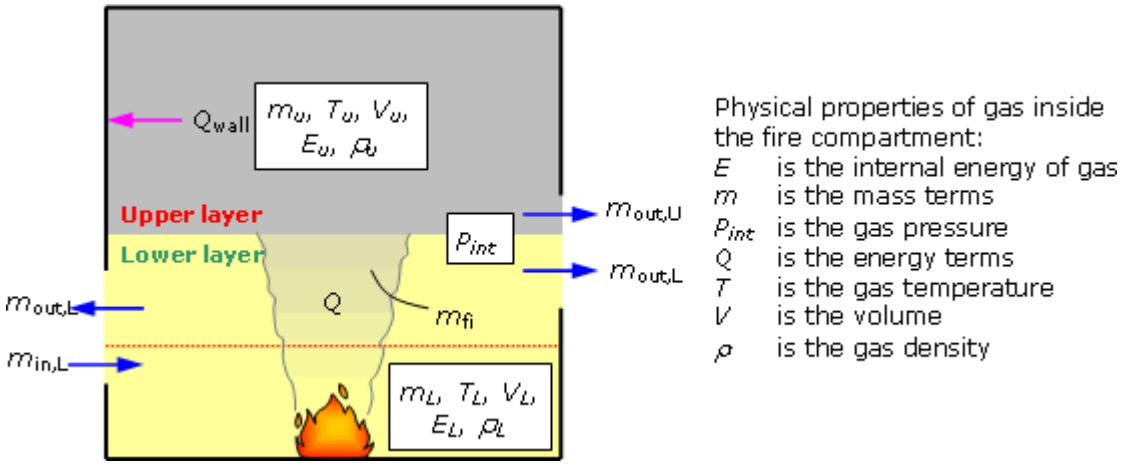

Figure 2.10: Schematic illustration of two-zone fire modelling (Bailey 2009).

Chapter 3
Analysis of Structures Subject to Fire

As discussed in Chapter 2, the design of structures subject to fire is at a point in time where objective- and performance-based fire safety regulations are providing practitioners in Canada, the US and Europe an avenue to directly design structures for the effects of fire. However, because of a lack of scientific research and experience, as well as the entrenchment of the long-established method of standard fire testing and the associated practice of applying fire protection via thermal insulation and evaluating structural performance on a component-by-component basis, a true performance-based structural fire engineering design methodology has not yet been widely adopted. Detailed analyses of structures subject to fire do exist. For instance, case studies such as the Cardington Fire Test (BS 1998) and the World Trade Centre Collapse (NIST 2005) have been published concerning the behavior of structures at elevated temperatures. However, these studies represent significant undertakings, demanding enormous amounts of time and resources that are impractical for general engineering practice. For day-to-day structural fire engineering practice, a new design approach is needed to allow ease of integration of the thermal effects due to fire into the design of structures without the need for sophisticated and computationally intensive analytical tools. With the view to advance the science of performance-based structural fire engineering, this thesis proposes to incorporate the thermal effects of fire into existing software for structural analysis. This software, called SODA (Structural Optimization Design & Analysis), was developed at the University of Waterloo and, since the 1980's, has been used in professional engineering practice for the analysis and design of full-scale structural steel building frameworks. The scope of this study is limited to adapting SODA for the analysis of planar (two-dimensional) steel building frames subject to fire. Although the study uses SODA as the computational platform, the fundamental concepts presented are universal and should be readily implementable into any other frame analysis software.

This Chapter presents the concepts and theory behind the structural analysis employed by this study to take into account the thermal effects of fire on structural behaviour. Section 3.1 presents the SODA model of the post-elastic response of steel member sections. Section 3.2 explains the nonlinear analysis techniques used in the SODA software. Section 3.3 discusses steel behaviour at elevated temperatures, and the corresponding changes to the moment-rotation response of steel

connections. Section 3.4 describes how the SODA software utilizes the moment-rotation data for connections to determine overall structural behaviour at elevated temperatures.

3.1 Post-Elastic Response

Steel members experience nonlinear material behaviour when subjected to increasing loads beyond the limit of elastic response. This behaviour can be characterized by a force-deformation (*F*-*D*) curve of the form in Figure 3.1, where: F is axial (P) or shear (V) or bending (M) force and, correspondingly, D is axial (δ) or transverse (γ) or rotation (θ) deformation; D_p is the known magnitude of plastic deformation; F_y is the initial yield capacity of the section, before which the section exhibits elastic behaviour; F_p is the plastic capacity of the fully yielded section. Between initial yielding at F_y and full plasticity at F_p, the section exhibits post-elastic behaviour. Within this range for force $F = M$, V, or P, the gradient value $dF/dD = R$, T or N is the post-elastic (bending, shearing or axial) stiffness of the section, respectively. For most section shapes commonly used in steel structures, the continuous nonlinear post-elastic regime of the *F*-*D* curve can be reasonably described by the following function (Liu 2007):

$$F = F_y + \left(F_p - F_y\right)\left[1 - \left(1 - \frac{D}{D_p}\right)^{e_0}\right]^{1/e_0} \qquad 0 \le \frac{D}{D_p} < 1, \qquad \frac{F_y}{F_p} \le \frac{F}{F_p} \le 1 \tag{3.1}$$

where the exponent $e_0 > 1$ has different values, depending on whether the force is bending, shear or axial: $F = M$, V or P. If $F \le F_y$, the post-elastic deformation $D = 0$; that is, the section is within the elastic response range. If $F_y \le F \le F_p$ then the section is within the post-elastic response range and the corresponding deformation D can be derived from Eq. (3.1) as:

$$D = D_p - D_p\left[1 - \left(\frac{F - F_y}{F_p - F_y}\right)^{e_0}\right]^{1/e_0} \qquad 0 \le \frac{D}{D_p} < 1, \qquad \frac{F_y}{F_p} \le \frac{F}{F_p} \le 1 \tag{3.2}$$

By differentiating Eq. (3.1) with respect to post-elastic deformation D, the post-elastic (bending, shearing or axial) stiffness is found as:

$$\frac{dF}{dD} = \frac{F_p - F_y}{D_p}\left(1 - \frac{D}{D_p}\right)^{e_0 - 1}\left[1 - \left(1 - \frac{D}{D_p}\right)^{e_0}\right]^{\frac{1 - e_0}{e_0}} \qquad 0 \le \frac{D}{D_p} < 1, \qquad \frac{F_y}{F_p} \le \frac{F}{F_p} \le 1 \tag{3.3}$$

where, as shown in Figure 3.1, $dF/dD = \infty$ if deformation $D = 0$ and $dF/dD = 0$ if $D \geq D_p$.

Stiffness degradation factors, defined by the ratio of the elastic deformation to the elastic-plus-plastic deformation at a member section, are employed to model the extent of plastic behaviour. As indicated in Figure 3.1, for a beam-column member with post-elastic bending, shearing or axial stiffness R, T or N, respectively, the corresponding stiffness degradation factor is r, t, or n. If post-elastic stiffness $dF/dD = \infty$, the stiffness degradation factor = 1 (i.e., fully elastic behaviour), whereas if post-elastic stiffness $dF/dD = 0$, the stiffness degradation factor = 0 (i.e., fully plastic behaviour). The stiffness degradation factors are given by (Liu 2007):

$$r = \frac{\theta_e}{\theta_e + \theta} = \frac{1}{1 + 3EI / RL} \tag{3.4}$$

$$t = \frac{\gamma_e}{\gamma_e + \gamma} = \frac{1}{1 + 3EI / TL^3} \tag{3.5}$$

$$n = \frac{\delta_e}{\delta_e + \delta} = \frac{1}{1 + AE / NL} \tag{3.6}$$

where E is the material modulus of elasticity, A is the member cross-section area, I is the cross-section moment of inertia, and L is the member length.

3.2 Nonlinear Analysis of Steel Frameworks

To conduct an analysis using SODA, the structural framework is discretized into an assemblage of beam-column members, such as the planar-frame member shown in Figure 3.2 (where G = material shear modulus). Spring elements are employed to model member end-section stiffness at various stages of the force-deformation (F-D) response curve in Figure 3.1. The member has six local end-forces f_i (i = 1 to 6) consisting of axial forces, shear forces and bending moments. The member also has six corresponding local end-deformations d_i (i = 1 to 6) consisting of axial deformations, shear deformations and flexural rotations. As shown in Figure 3.2, springs model the axial, shear and bending stiffness of the member-end sections, where the springs in the horizontal direction, designated by N_i (i = 1 to 2), represent post-elastic axial stiffness; the springs in the vertical direction, designated by T_i (i = 1 to 2), represent post-elastic shear stiffness, while the rotational springs, designated by R_i (i = 1 to 2), represent post-elastic bending stiffness. The bending, shearing and axial

stiffness have associated stiffness degradation factors, r_i, t_i, n_i (i = 1 to 2), respectively, defined as in Section 3.1.

The analysis program is based on the, so-called, Displacement Method (McGuire et al., 2000) whereby member-end forces are related to member-end deformations by a stiffness matrix. This relation is expressed as:

$$\boldsymbol{f} = \boldsymbol{k}\,\boldsymbol{d} \tag{3.7}$$

where for six local degrees of freedom (Figure 3.2), $\boldsymbol{f} = [f_1 \ldots f_6]^{\mathrm{T}}$ is the vector of member-end forces, $\boldsymbol{d} = [d_1 \ldots d_6]^{\mathrm{T}}$ is the vector of member-end displacements, and $\boldsymbol{k}$ is the element stiffness matrix given by,

$$\boldsymbol{k} = \begin{bmatrix} k_{11} & 0 & 0 & k_{14} & 0 & 0 \\ & k_{22} & k_{23} & 0 & k_{25} & k_{26} \\ & & k_{33} & 0 & k_{35} & k_{36} \\ & & & k_{44} & 0 & 0 \\ & Sym & & & k_{55} & k_{56} \\ & & & & & k_{66} \end{bmatrix} \tag{3.8}$$

The coefficients k_{ij} in Eq. (3.8) characterize axial, shear and flexural stiffness, and can be expressed as functions of material and member properties and corresponding degradation factors n, t and r, as follows (Liu 2007):

$$k_{11} = k_{11}^{a}\chi_0 = k_{44} = -k_{14} = -k_{41} \tag{3.9a}$$

$$k_{22} = k_{22}^{r}\chi_1 = k_{55} = -k_{25} = -k_{52} \tag{3.9b}$$

$$k_{23} = k_{23}^{r}\chi_1 = k_{32} = -k_{35} = -k_{53} \tag{3.9c}$$

$$k_{26} = k_{26}^{r}\chi_1 = k_{62} = -k_{56} = -k_{65} \tag{3.9d}$$

$$k_{33} = k_{33}^{r}\chi_2 \tag{3.9e}$$

$$k_{36} = k_{36}^{r}\chi_3 = k_{63} \tag{3.9f}$$

$$k_{66} = k_{66}^{r}\chi_4 \tag{3.9g}$$

where in Eq. 3.9(a), k_{11}^{a} = AE/L is the elastic axial stiffness, and the factor,

$$\chi_0 = \frac{n_1 n_2}{n_1 + n_2 - n_1 n_2} \tag{3.10}$$

accounts for post-elastic axial stiffness degradation through the axial stiffness degradation factors n_i (i=1,2).

In Eqs. 3.9(b)-(g), the stiffness coefficients are given by,

$$k_{22}^{r} = \frac{EI}{L^3\Omega}\left[3b\eta_1(1+c\eta_2)[6r_1r_2 + b\eta_1(1-c\eta_2)(r_1+r_2-2r_1r_2)] + P\frac{L^2\Omega}{EI}\right] \tag{3.11}$$

$$k_{23}^{r} = \frac{3b\eta_1 EIr_1(1+c\eta_2)}{L^2\Omega}\left[b\eta_1(1-r_2)(1-c\eta_2)+3r_2\right] \tag{3.12}$$

$$k_{26}^{r} = \frac{3b\eta_1 EIr_2(1+c\eta_2)}{L^2\Omega}\left[b\eta_2(1-r_1)(1-c\eta_2)+3r_1\right] \tag{3.13}$$

$$k_{33}^{r} = \frac{3r_1 b\eta_1 EI[b\eta_1(1-r_2)(1-b^2\eta_2^2)+3r_2]}{L\Omega} \tag{3.14}$$

$$k_{36}^{r} = \frac{9bc\eta_1\eta_2 EIr_1r_2}{L\Omega} \tag{3.15}$$

$$k_{66}^{r} = \frac{3r_2 b\eta_1 EI[b\eta_1(1-r_1)(1-c^2\eta_2^2)+3r_1}{L\Omega} \tag{3.16}$$

to account for elastic bending stiffness and, as well, for post-elastic bending stiffness degradation through the bending stiffness degradation factors r_i (i=1,2), while the factors,

$$\chi_1 = \frac{t_1 t_2}{t_1 t_2 + 4\beta(t_1+t_2-2t_1t_2)} \tag{3.17}$$

$$\chi_2 = 1 - \left(\frac{b\eta_1 r_1}{4\Omega\beta}\right)\left(\frac{(1+c\eta_2)^2[b\eta_1(1-r_2)(1-c\eta_2)+3r_2]^2}{b\eta_1(1-r_2)(1-c^2\eta_2^2)+3r_2}\right)(1-\chi_1) \tag{3.18}$$

$$\chi_3 = 1 - \left(\frac{b\eta_1(1+c\eta_2)^2}{12c\eta_2\Omega\beta}\right)[b\eta_1(1-r_1)(1-c\eta_2)+3r_1][b\eta_1(1-r_2)(1-c\eta_2)+3r_2]$$

$$\times(1-\chi_1) \tag{3.19}$$

$$\chi_4 = 1-\left(\frac{b\eta_1 r_2}{4\Omega\beta}\right)\left(\frac{(1+c\eta_2)^2[b\eta_1(1-r_1)(1-c\eta_2)+3r_1]^2}{b\eta_1(1-r_1)(1-c^2\eta_2^2)+3r_1}\right)(1-\chi_1) \tag{3.20}$$

account for post-elastic shear stiffness degradation through the shear stiffness degradation factors t_i (i=1,2).

The parameter P = axial force in Eq. (3.11). In Eqs. (3.11) - (3.16) and Eqs. (3.18) - (3.20), the parameters,

$$b = \begin{cases} \dfrac{1-\psi/\tan\psi}{\tan(\psi/2)/(\psi/2)-1} & P \le 0 \\ \dfrac{1-\psi/\tanh\psi}{\tanh(\psi/2)/(\psi/2)-1} & P > 0 \end{cases} \tag{3.21}$$

$$c = \begin{cases} \dfrac{\psi-\sin\psi}{\sin\psi-\psi\cos\psi} & P \le 0 \\ \dfrac{\psi-\sinh\psi}{\sinh\psi-\psi\cosh\psi} & P > 0 \end{cases} \tag{3.22}$$

in which,

$$\psi = \begin{cases} L\sqrt{\dfrac{-P/EI}{1+P/GA}} & P \le 0 \\ L\sqrt{\dfrac{P/EI}{1+P/GA}} & P > 0 \end{cases} \tag{3.23}$$

are geometrical stiffness coefficients used in both stability and geometrical nonlinear analysis, while the factors,

$$\eta_1 = \left(1+\frac{P}{GA}\right)\left(\frac{1+\xi f_1}{1+\xi f_2}\right) \tag{3.24}$$

$$\eta_2 = \frac{1+\xi f_3}{1+\xi f_1} \tag{3.25}$$

in which,

$$\xi = \frac{EI(1+P/GA)}{GAL^2} \tag{3.26}$$

$$f_1 = \begin{cases} \psi^2/(1-\psi/\tan\psi) & P \le 0 \\ -\psi^2/(1-\psi/\tanh\psi) & P > 0 \end{cases} \tag{3.27}$$

$$f_2 = \begin{cases} \psi^3 \tan(\psi/2)/[\tan(\psi/2)-\psi/2] & P \le 0 \\ -\psi^3 \tanh(\psi/2)/[\tanh(\psi/2)-\psi/2] & P > 0 \end{cases} \tag{3.28}$$

$$f_3 = \begin{cases} \psi^2/(1-\psi/\sin\psi) & P \le 0 \\ -\psi^2/(1-\psi/\sinh\psi) & P > 0 \end{cases} \tag{3.29}$$

account for the influence of shear deformation on elastic bending stiffness.

Lastly, in Eqs. (3.11) - (3.16) and Eqs. (3.18) - (3.20), the parameter

$$\Omega = 9r_1r_2 + 3r_2b\eta_1(1-r_1) + 3r_1b\eta_1(1-r_2) + b^2\eta_1^2(1-r_1)(1-r_2)(1-c^2\eta_2^2) \tag{3.30}$$

while in Eqs. (3.17) - (3.20), the parameter

$$\beta = \frac{L^3}{12EI}k_{22}^r \tag{3.31}$$

Upon formulating the local member stiffness matrix, ***k***, in Eq. (3.7) for each member of the frame structure, as in the foregoing, the corresponding global member stiffness matrix is readily obtained using conventional matrix transformation techniques (McGuire et al., 2000). Then, the global stiffness matrix ***K*** for the entire assembled structure is formulated by direct summation of the global member stiffness matrices. Then, for the prevailing loads ***F***, the deformations ***D*** experienced by the assembled frame are computed by solving:

$$\boldsymbol{F = KD} \tag{3.26}$$

3.3 Steel Behaviour at Elevated Temperatures

In order to implement the thermal effects of fire into the frame analysis outlined above, account must be made for the behaviour of steel at elevated temperatures. In order to achieve this, the corresponding force-deformation behaviour of steel connections at elevated temperatures must be determined, either analytically or directly from experiments.

At elevated temperatures, the elastic modulus E and shear modulus G of steel decrease, which in turn affects the member force-deformation curves (for axial, shear and bending behaviour). The reduction in section stiffness can be attributed to changes in both geometric and material properties. In some structures such as wood, fire charring of wood members will affect the geometric properties. However, for steel at elevated temperatures, such geometric changes are considered to be negligible compared to the much greater changes of material properties. Figure 3.3 is a plot of steel modulus of elasticity E as a function of temperature, where the elastic modulus as a function of temperature is expressed as (SFPE 2002):

$$E_T = \begin{cases} 1 + \dfrac{T}{2000 \ln\left(T / 1100\right)} E_0 & 0 \le T \le 600°\text{C} \\ \dfrac{690 - 0.69T}{T - 53.5} E_0 & \text{T} > 600°\text{C} \end{cases} \tag{3.27}$$

With known geometric properties and modulus of elasticity at elevated temperatures, member stiffness can theoretically be calculated from a sectional analysis. For example, a public domain program entitled *Response-2000* created at the University of Toronto (Bentz 2000) calculates sectional behavior of reinforced concrete members based on known geometric and mechanical properties. However, a companion program has not yet been developed for steel due to lack of empirical data. Therefore, stiffness values must be obtained directly from force-deformation curves, which are obtained from experiments.

A literature review indicates that data defining force-deformation curves for steel members/connections at elevated temperatures is scarce. There has only been one extensive study conducted by Al-Jabri (Al-Jabri et al 2004) in the United Kingdom, where a series of moment-rotation curves were established for flush end-plate steel connections. In the study, Al-Jabri subjected the basic beam-column assemblage schematically shown in Figure 3.4 to elevated temperatures in a fire test furnace, while applying loads at the ends of the beam to produce bending moments in the connections. For each temperature level, loads were increased from the elastic range up into the post-elastic range and corresponding connection rotations were recorded to find the set of moment-rotation curves shown in Figure 3.5.

Although this study focused on establishing moment-rotation response curves for semi-rigid steel connections, it can be expected that steel member sections in general will exhibit similar behaviour at

elevated temperatures. The curves confirm that at elevated temperatures, steel exhibits the same form of force-deformation response curve as that shown in Figure 3.1 for steel at ambient temperature (20°C), except that due to a reduction in material properties, sections enter the post-elastic range sooner at elevated temperatures, as characterized by the flatter curves in Figure 3.5. For example, the moment level M required to cause a deformation D is higher at 200°C than the moment required at 600°C. Knowledge of the force-deformation response curves in Fig. 3.5 can be utilized to calculate section stiffness at elevated temperatures, which in turn can be used to determine stiffness degradation factors and thereby allow the member stiffness matrices, $\boldsymbol{k}$, and thus the structure stiffness matrix, $\boldsymbol{K}$, to be formulated with account for the effect of elevated temperatures.

Thereafter, the effect of fire loading on the deformation response $\boldsymbol{D}$ of the assembled frame can be determined by solving $\boldsymbol{F} = \boldsymbol{KD}$ where, now, the stiffness matrix $\boldsymbol{K}$ takes into account the reduction in member stiffness through mechanical properties that are degraded at elevated temperatures. To illustrate this, consider Figure 3.5. A moment level of 110 kN-m corresponds to an elastic rotation of 15 milliradians at 20°C but to a much larger elastic + plastic rotation of 80 milliradians at 500°C; using Eq. (3.4), the rotational stiffness degradation factor is $r = \theta_e / (\theta_e + \theta) = 15 / 80 = 0.19$. That is, without any increase in external bending forces, the steel connection loses more than 80% of its flexural stiffness due to the thermal effects of fire alone. Examining the same figure and considering the curve for 20°C only, the moment level that would produce a rotation of 80 milliradians is 170 kN-m. This suggests that the effect on the connection due an increase in temperature from 20°C to 500°C is equivalent to a moment level increase from 110kN-m to 170kN-m at ambient temperature of 20°C.

3.4 Frameworks with Semi-rigid Connections at Elevated Temperatures

For this study, and as illustrated in the foregoing, fire loading is assumed to affect only the rotational stiffness of the connection and member, while any effect on their shear and axial stiffness is neglected. From this perspective, note that the beam-column member model shown in Figure 3.2 employs but one rotational spring at each end to represent the combined rotational stiffness of both a rigid connection and the member framing into it. In reality, however, steel connections are never perfectly rigid but are actually semi-rigid to some degree. Accordingly, the beam-column model is here extended to include an additional rotational spring, where one spring represents the rotational stiffness of a semi-rigid connection while the other spring represents that for the member, as shown in

Figure 3.6. This model is not only closer to reality but, for the purposes of this study, also allows the influence of fire on connection behaviour to be studied separately (see Chapter 4).

As shown in Figure 3.7(a), the beam-column element model has been extended to involve a series of two sets of springs at each end, where one spring set represents the rotational, shear and axial stiffness of the semi-rigid connection while the other spring set represents that for the connected member. In Figure 3.7(b), it is shown that the element with two series-connected spring sets at each end can be replaced by a compound element having only one set of springs at each end.

With concern only for rotational stiffness degradation under elevated temperatures, the compound rotational stiffness R in Figure 3.7(b) can be expressed as (Liu 2007):

$$R = \frac{1}{1/R_c + 1/R_p} = \frac{R_c R_p}{R_c + R_p} \tag{3.28}$$

where R_c and R_p are the rotational stiffness of the semi-rigid connection and the connected member, respectively. The corresponding compound rotational stiffness degradation factor is given by:

$$r = \frac{1}{1+\dfrac{3EI}{RL}} = \frac{1}{1+\dfrac{3EI}{L}\dfrac{R_c+R_p}{R_c R_p}} = \frac{1}{1+\dfrac{3EI}{LR_c}+\dfrac{3EI}{R_p}} = \frac{r_c r_p}{r_c + r_p - r_c r_p} \tag{3.29}$$

This study adopts the following four-parameter model relating bending moment M to rotational stiffness (Liu 2007):

$$M = \frac{\left(R_{ce} - R_{cp}\right)\theta_c}{\left\{1+\left[\left(R_{ce}-R_{cp}\right)\theta_c / M_0\right]^{\gamma}\right\}^{1/\gamma}} + R_{cp}\theta_c \tag{3.30}$$

where R_{ce} is the elastic rotational stiffness when rotation $\theta_c = 0$; R_{cp} is the post-elastic stiffness when rotation θ_c approaches infinity in the limit; M_0 is a reference moment; and γ is the shape parameter for the connection. The rotational stiffness of the connection is determined by differentiating Eq. (3.30) with respect to θ_c:

$$R_c = \frac{dM}{d\theta_c} = R_{cp} + \frac{R_{ce} - R_{cp}}{\left\{1+\left[\left(R_{ce}-R_{cp}\right)/\theta_c / M_0\right]^{\gamma}\right\}^{1+1/\gamma}} \tag{3.31}$$

As experimental moment-rotation curves at elevated temperatures are only available for semi-rigid connections, this study assumes that connected steel members are not affected by fire and remain elastic. Hence $r_p = 1$ in Eq.(3.29) and the compound rotational stiffness degradation factor becomes:

$$r = \frac{r_c(1)}{r_c + 1 - r_c} = r_c = \frac{1}{1 + \dfrac{3EI}{R_c L}} \tag{3.32}$$

The foregoing discussion has presented the basis of the beam-column analysis performed by SODA, which determines the state of the structural assemblage based on stiffness degradation factors that represent the nonlinear post-elastic behaviour of steel due to the actions of axial, bending and shear forces for each and every member within the framework. The post-elastic behaviour of the individual steel members may be attributed to increases in mechanical load or increases in thermal effects of fire (fire load), or both. By solving for the displacements ***D*** in Eq. (3.26), the post-elastic behaviour of all individual members within the context of the assembled framework is determined. Using SODA, the time for the overall framework to reach a specified 'failure' state as a result of attaining a certain temperature can be determined using one of the fire models discussed in Chapter 2, thereby producing a 'performance-based fire-resistance rating'. This type of analysis would allow practitioners to analyze and design structures for fire without the use of sophisticated structural analysis tools, provided data for the structural elements at elevated temperatures are available and integrated in the analysis. The process of implementing data in SODA that represents the physical behaviour of structural elements at elevated temperature is presented in Chapter 4, along with an illustrative example case study.

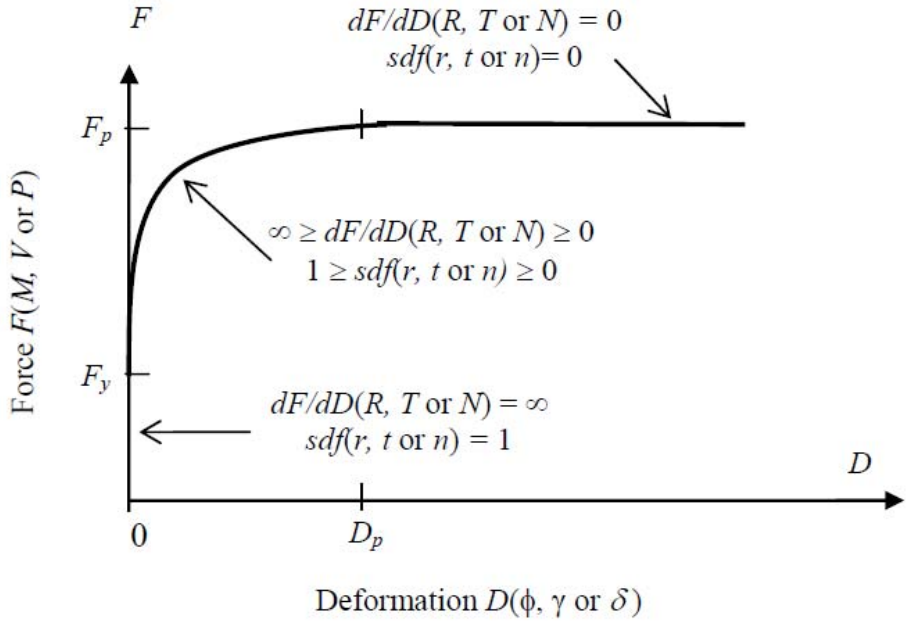

Figure 3.1: Typical post-elastic force-deformation response of a steel member section (Liu 2007)

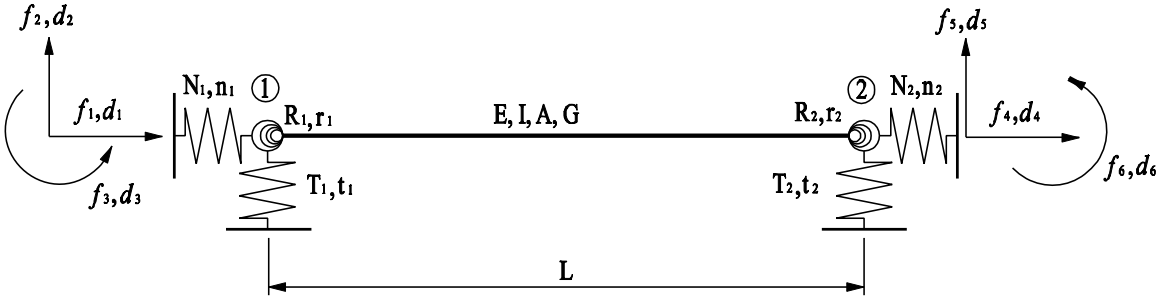

Figure 3.2: Beam-column analysis model (Xu *et al*, 2005)

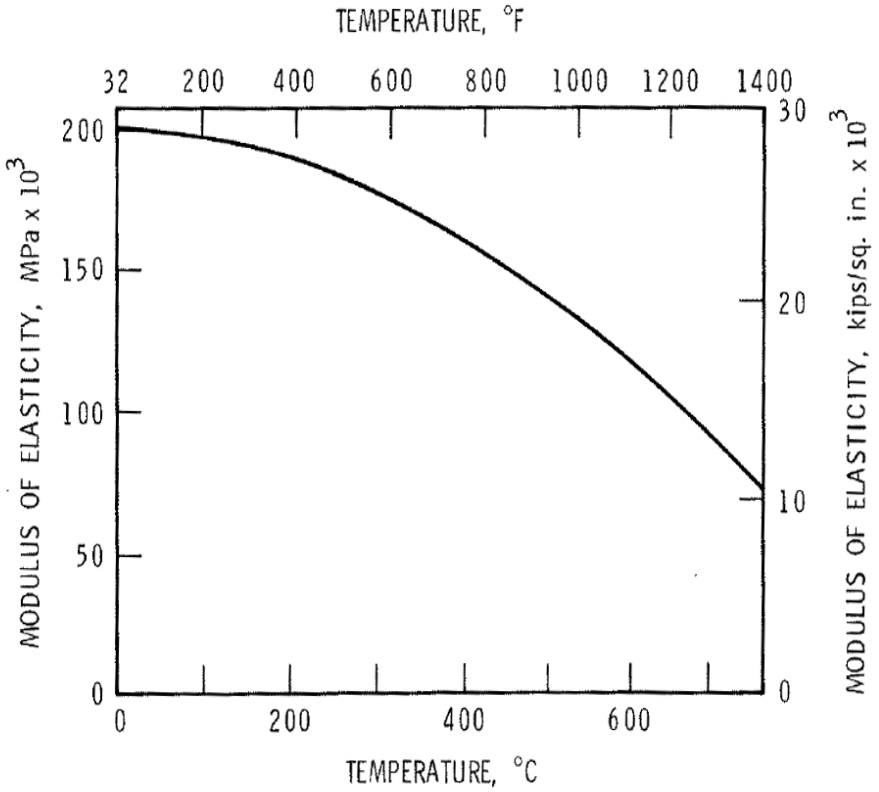

Figure 3.3: Modulus of elasticity for steel as a function of temperature (Lie 1974)

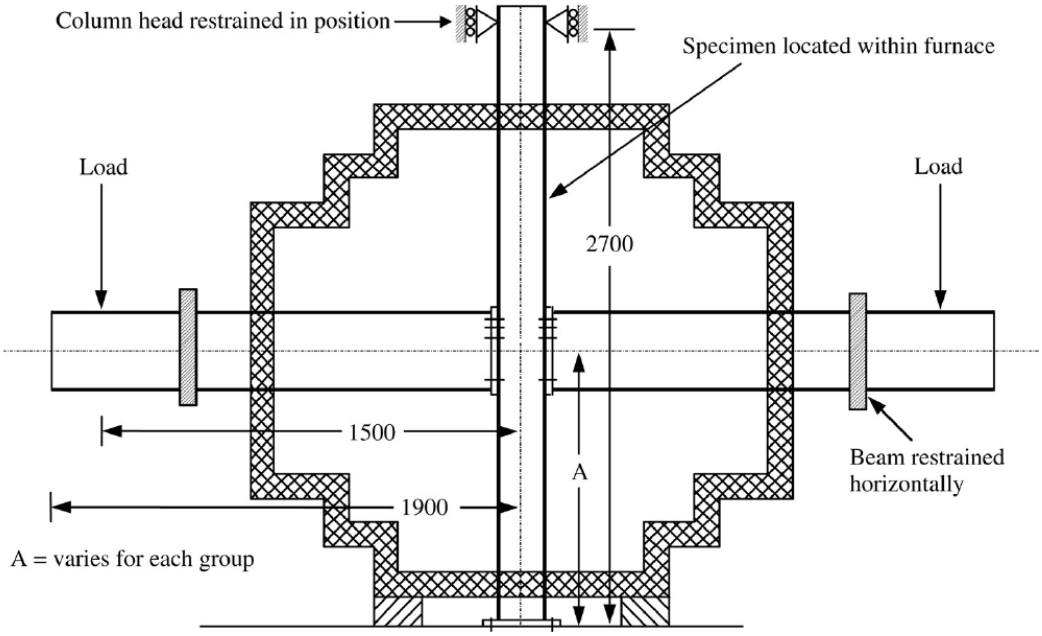

Figure 3.4: Schematic of the connection fire-test configuration (Al-Jabri et al 2004)

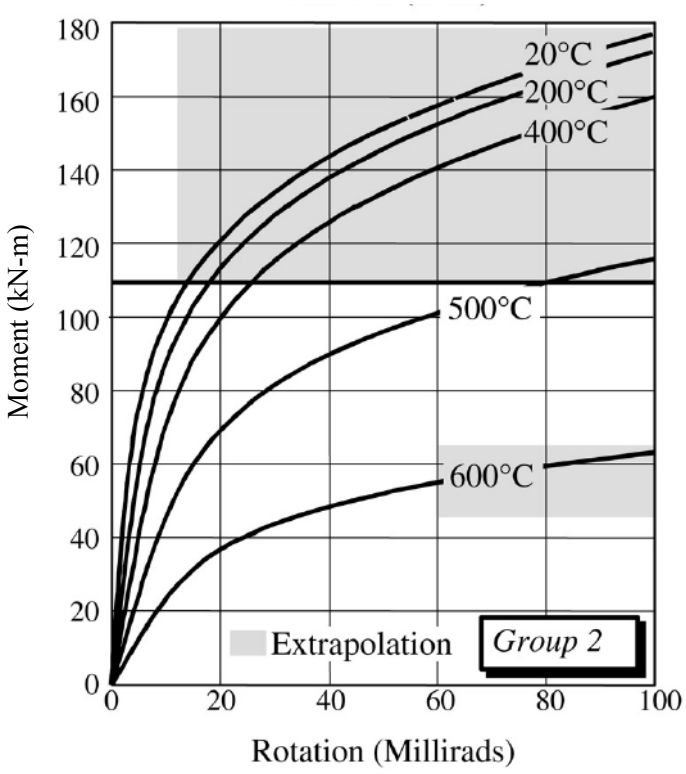

Figure 3.5: Semi-rigid connection moment-rotation curves at elevated temperatures (Al-Jabri et al 2004)

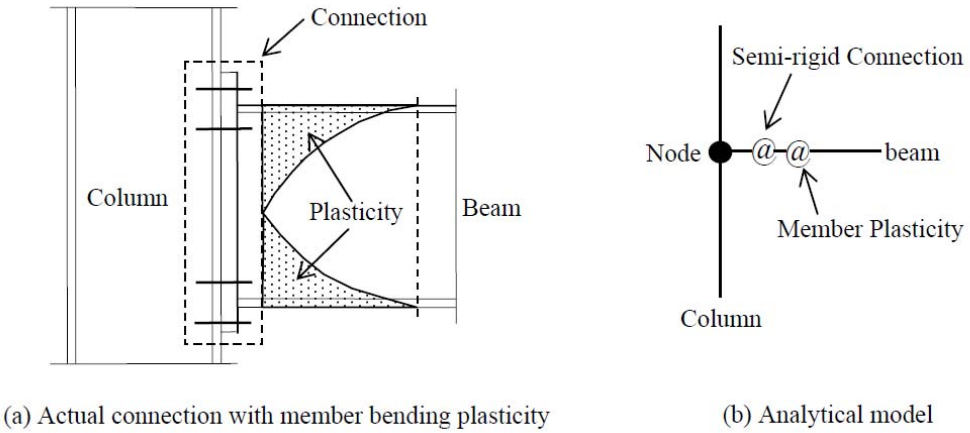

Figure 3.6: Semi-rigid connection and member flexural model (Liu 2007)

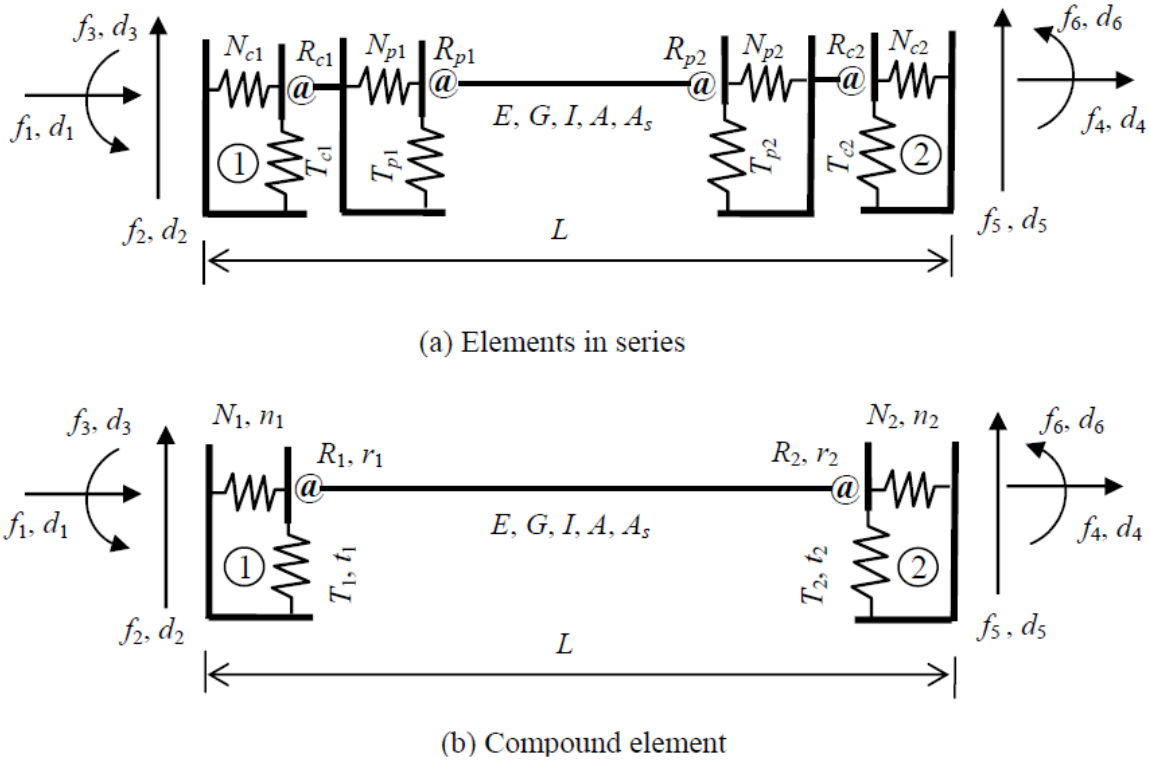

(b) Compound element

Figure 3.7: Series and compound beam-column elements (Liu 2007)

Chapter 4
Analysis Procedure and Example Case Study

This Chapter presents an example analysis of a 2-bay by 2-storey steel planar structure having one of its beam-column connections subjected to fire loading. The example is used to demonstrate the way in which the fire and structural models discussed in Chapters 2 and 3 are applied to estimate the behaviour of a structure subjected to fire loading. The objective of the analysis is to illustrate the method for, and assess the results obtained through, incorporation of moment-rotation data at elevated temperatures into the SODA structural analysis software. Such analysis facilitates determination of the response of a structure when one or more of the connections are affected by a compartment fire.

Fire and structural calculations have most often been conducted as separate, independent analyses. This is because existing structural analysis software, including that used in this study, does not allow the integration of time-temperature information or temperature dependent material properties relationships concurrently in the computation. This is primarily due to the complexity in the models required to represent the physics associated with each of the fire and structural phenomena as presented in Chapters 2 and 3. As such, a full study of a structure exposed to a fire that is progressing from the pre-flashover to post-flashover stage and even to the decay phase, usually entails the use of a discrete number of structural analyses conducted for different compartment temperature conditions, each corresponding to those typical for different stages of the fire development and each using material properties valid in the range of temperatures considered. Thus each structural analysis yields results that are intended to represent the state of the structure at the temperature studied. A time temperature curve for a given fire scenario is then determined through an appropriate fire analysis and used to approximate how the various structural response data relates to the progression of the fire. Because the structural and fire analyses have separate independent inputs, they are often conducted separately and the results are combined into a complete structural fire analysis; however, unless care is exercised, accumulated 'history' effects inherent in the progression of real structural fires over time may be lost.

Conventional structural design is generally concerned with an *ultimate limit state*, that is, design of a structure to resist the maximum possible expected loads. In the case of fire loading, however, this notion has been found to be less valid. Recent studies have suggested that the 'history' of fire loading, which varies with respect to time and space due to the *progression* of a fire, can have significant

impact on the structure. Such effects may be particularly pronounced during pre-flashover stages where the compartment is not uniformly heated. Therefore, a structural fire analysis should consider the accumulated effects on the structure of both pre- and post-flashover fires. In the present study, due to limitations of the analysis program, as well as of the available data for moment-rotation behaviour of the connections at elevated temperatures, the structural analysis provides results for a set of discrete temperatures, in the range attained during pre-flashover fires.

The key focus of this Chapter, then, is to demonstrate a method by which to integrate into the SODA software the force-deformation data for a steel beam-column connection at elevated temperatures, for the analysis of a planar steel framework. Outlined in Section 4.1 is the procedure for using the SODA (Structural Optimization, Design and Analysis) software developed at the University of Waterloo (Liu 2007) to conduct a structural analysis that considers temperature (fire) loading. Discussed in Section 4.2 is the regression procedure employed to translate available moment-rotation data for steel connections at elevated temperatures into the corresponding four-parameter connection model required as input to SODA. Section 4.3 presents an example case study that verifies the translation and use of the high temperature moment-rotation data through an analysis of a 2-storey by 2-bay steel framework for which one connection is subjected to elevated temperatures. Finally, in Section 4.4, the BFD parametric fire model is used to demonstrate the correlation of the discrete temperatures used in the example structural response calculations with the theoretical progression of a fire over time.

4.1 Structural Analysis Procedure

The structural analysis using SODA is based on solving the force-displacement equations $\boldsymbol{F} = \boldsymbol{KD}$ (see Eq. 3.26) governing equilibrium of the assembly of connected beam and column elements comprising a framework structure. For the structure, $\boldsymbol{F}$ = the applied loads and $\boldsymbol{K}$ = the stiffness matrix expressed in terms of material, geometric and stiffness degradation parameters for each of the elements. For a given state of structural stiffness, the solution of the equations determines the deformation response $\boldsymbol{D}$ at all connected nodes of the structure.

In the present study, the interest is in understanding the behavior of the structure when a connection of the structure is subjected to *thermal loads* due to fire. As discussed in Chapter 3, when a steel structure is exposed to fire, it exhibits nonlinear force-deformation behaviour caused by degradation in the stiffness properties of the steel as a result of the molecules being excited by thermal energy. At

any given temperature level, this study considers the steel to be yet an elastic material (albeit degraded) and conducts a linear analysis to find the corresponding force-deformation behaviour of the structure. The result of a sequence of such analyses for increasing temperatures gives evidence of the nonlinear force-deformation behaviour of the structure over the range of temperatures. The present research investigates a modified SODA analysis of steel framework structures that explicitly accounts for material nonlinearity due to thermal effects of fire. In fact, the SODA procedure used here is essentially the same as that for an elastic structural analysis performed at ambient temperature conditions. The main modification to the procedure involves instructing the software to reference a separate database containing experimentally determined force-deformation-temperature data (including degraded elastic modulus values) for the exposed structural elements at elevated temperatures.

The starting point of a SODA analysis involves the preparation of an input file that specifies geometric, topological, connectivity, foundation, member, material and loading data for the structure. Appendix A lists the input data file for the steel framework structure investigated in this study. It includes: 1) geometric information pertaining to the number of members, nodes, supports, etcetera; 2) topologic information defining nodal coordinates and the start and end nodes at which the individual members are connected together; 3) nodal support conditions specified as one of four types: free, fixed, pinned or roller; 4) member-end restraints assigned as one of three kinds: fully-fixed, partially-fixed, or pinned; 5) material and cross-section properties specified as member-group data: Young's modulus of elasticity, shear modulus, cross-sectional area and moment of inertia; and 6) applied external loading specified as any combination of nodal and/or member loads.

The present study considers the effects of fire on the performance of semi-rigid beam-column connections in a steel structure. It is focused on the thermal loading of semi-rigid connections because the experimental data necessary for inclusion in the SODA analysis software is available in the archival literature; specifically, the moment-rotation data for semi-rigid steel connections at elevated temperatures obtained from experiments conducted at the University of Sheffield in the UK (Al-Jabri et al 2004). The reformulation and incorporation of the Sheffield data into the SODA calculations is discussed in the following.

4.2 Four-Parameter Moment-Rotation Model

The Sheffield experiments produced moment-rotation-temperature data that the authors (Al-Jabri et al 2004) described using a three-parameter model:

$$\phi = \frac{M}{A} + 0.01\left(\frac{M}{B}\right)^n \tag{4.1}$$

where: ϕ = connection rotation, M = the moment, and A, B and n are temperature-dependent parameters used to correlate across the experimental data. The particular values of the parameters A, B and n considered in this study are those pertaining to connections categorized as 'Group 2' in the Sheffield experiments (Al-Jabri et al 2004). For reference here, Group 2 connections are semi-rigid connections consisting of two beams connected to a column using flush end-plates and eight bolts.

On the other hand, SODA calculates the bending stiffness degradation factor for connections using the four-parameter moment-rotation model presented in Chapter 3 as Eq.(3.30):

$$M = \frac{\left(R_{ce} - R_{cp}\right)\theta_c}{\left\{1 + \left[\left(R_{ce} - R_{cp}\right)\theta_c / M_0\right]^{\gamma}\right\}^{1/\gamma}} + R_{cp}\theta_c \tag{3.30}$$

where the parameters R_{ce}, R_{cp}, M_0 and γ are as defined in Chapter 3. To convert the moment-rotation experimental data represented by the three-parameter model into a format consistent with the four-parameter model, paired data points (ϕ, M) are first extracted from the three-parameter model Eq.(4.1) using the values of parameters A, B and n for Group 2 connections given in Table 4.1 at temperatures of 20°C, 200°C, 400°C and 600°C. Then, a regression analysis is performed using Liu's method (Liu 2009) to convert the data into the four parameter model format, Eq.(3.30), required by SODA.

Figure 4.1: Comparison of moment-rotation curves obtained from the 3-parameter model Eq.(4.1) and the 4-parameter model Eq.(3.30) at 20°C. to Figure 4.4 are plots of the moment-rotation curves produced by the two models described by Eqs. (4.1) and (3.30) for the Group 2 connections in the Sheffield experiments. The plots demonstrate that the data points produced by the two models correlate to within less than 5%, except for a temperature of 20°C at moment levels below 20 kN-m, where the difference is about 15%. These results indicate that the 3-parameter data reported in the literature (Al-Jabri et al 2004) has been faithfully transformed into 4-parameter data appropriate for use in the SODA analyses discussed in the next section.

4.3 Example Calculations

Some examples are presented in this Section that demonstrate structural analysis calculations accounting for thermal effects due to fire using the moment-rotation relationships for semi-rigid steel connections at elevated temperatures obtained from the Sheffield experiments (Al-Jabri et al 2004). The example calculations are based on the 2-bay by 2-storey steel frame structure shown in Figure 4.5. The frame has bay widths of 4m and 6m, first-storey height of 4m and second-storey height of 3.5m. All beams and columns have W360 × 51 and W250 × 89 sections, respectively (as SODA only references North American steel section databases, these beams and columns were chosen to best match the UK sections that were used in the Sheffield experiments). Table 4.2 presents a comparison of the dimensions and mass of different steel members, which indicates that the North American W-sections selected in the present study are effectively identical to the Universal Beam and Universal Column sections used in the Sheffield Group 2 experiments.

Two analysis examples are presented. In the first example, the frame shown in Figure 4.5 is initially analyzed when all connections are referenced to the Sheffield moment-rotation data at ambient temperature. The purpose of this analysis is to verify the integrity of the four-parameter model of the data developed for use in the SODA software. Following this, the second analysis uses SODA with the Sheffield moment-rotation data from tests conducted at a set of elevated temperatures to analyze the response of the frame when one of the connections in the frame is considered to be subjected to fire. In both examples, 64 N/mm and 32 N/mm uniformly distributed gravity load are applied on the first and second storeys, respectively. This loading is selected so as to generate moment levels at connections that are consistent with the applied moments used to generate the moment-rotation data in the Sheffield experiments.

4.3.1 Example 1: All Connections at 20ºC

For Example 1, the 2-bay by 2-storey steel frame structure shown in Figure 4.5 is subjected to a uniformly distributed gravity loading of 64 N/mm and 32 N/mm on the first and second storeys, respectively. All elements remain at ambient temperature throughout the analysis. The applied loading causes a moment of 103.6 kN/m and a corresponding rotation of 11.0 milliradian at connection #7 of the structure (this is the connection of interest in subsequent analyses performed at elevated temperature in Section 4.3.2, see Fig. 4.5). Application of the Sheffield three-parameter

model in Eq. (4.1) with parameters A = 21.5, B = 27.5 and n = 4.9 for a Group 2 connection at 20ºC (Table 4.1), and moment M = 103.6 kN/m, predicts the rotation to be,

$$\phi = \frac{M}{A} + 0.01\left(\frac{M}{B}\right)^n = \frac{103.6}{21.5} + 0.01\left(\frac{103.6}{27.5}\right)^{4.9} = 11.5 \text{ milliradian} \quad (4.2)$$

which is in reasonable agreement with the 11.0 milliradian calculated using SODA and the four-parameter model. To verify the conversions and further assess the validity of the approach, similar analyses were performed for the cases where the response of connection #7 is simulated at three additional temperatures: 200C, 400 C, and 600 C. The Sheffield three-parameter model for a Group 2 connection, Eq. (4.1), was used with appropriate values of the parameters A, B and n at each temperature as listed in Table 4.1 and with the applied moment calculated from the SODA analysis of the frame. The results for rotation of the connection are summarized in Table 4.3, which all show less than 5% difference between the two models. Therefore, these analyses confirm that the Sheffield moment-rotation data has been reasonably converted for use in SODA.

The moment levels at all the connections for the analysis conducted at ambient temperature conditions are presented in Figure 4.6. These show the 'baseline' behaviour of the structure at ambient temperature before a fire begins. Because the Sheffield experiments were conducted using semi-rigid (bolted) connections, they naturally exhibit some non-linear behaviour, even at 20°C. This is evident from the calculated rotational stiffness degradation factors presented in Figure 4.7, where the values smaller than 1 (unity) for all connections reflect the less-than-rigid moment-rotation behaviour of the connections.

The combined results from this example analysis confirm that the Sheffield moment-rotation data has been reasonably and consistently converted for use in SODA. In addition, the ambient temperature results can be used as a basis of comparison with the results of the next example, in which experimentally determined moment-rotation data at three different elevated temperatures is applied for connection #7, and the resulting response of the structure is investigated.

4.3.2 Example 2: Connection #7 at 200ºC, 400ºC, and 600ºC,

In this example, the 2-bay by 2-storey framework is analyzed considering connection #7 instantaneously heated to temperatures of 200ºC, 400ºC and 600ºC. This is accomplished for the SODA analysis by taking the experimentally determined moment-rotation data for each temperature

and using it to modify the behaviour of connection #7. The behaviour of all other parts of the frame is modeled based on moment-rotation data taken at ambient temperature (20ºC). Connection #7 in the structure was chosen for analysis at elevated temperatures in order to mimic the topology of the Group 2 connections studied in the Sheffield fire tests. In these, the moment-rotation-curves are derived for the connection schematically depicted in Figure 3.4. By applying load levels consistent with those applied in the experiments, using similar steel sections, and isolating thermal exposure to connection #7 alone in the SODA analysis, it was considered that the experimentally determined Sheffield moment-rotation-temperature data are consistent with those needed in the SODA analysis. This consideration is critical since any 'nonlinearity' in the behaviour of the connection due to thermal loading must be incorporated into the simplified SODA planar frame analysis via application of experimental moment-rotation data, since SODA includes no provisions by which to model the detailed physical processes governing the behaviour of the connection or the frame. Stated otherwise, the physical behaviour of the connection under fire loading as measured from the Sheffield experiment is directly integrated into the SODA analysis, with no modeling of the connection behaviour done by SODA; the role of the software is purely to model the behaviour of the planar structure as an assembled frame with integration of the connection behaviour data determined from the Sheffield experiment. Upon further study to determine the integrity of the model predictions for available force-deformation-temperature data for beam and column members, the present analysis procedure can be extended to examine the response of an entire structure exposed to a variety of realistic fire-induced temperature distributions.

Table 4.4 presents calculated moments and corresponding rotations at connection #7 for temperatures of 20ºC, 200ºC, 400ºC and 600ºC. The results indicate that as the temperature of connection #7 increases the rotation increases, while the moment-carrying capacity of the connection decreases. Temperature increases from 20ºC to 200ºC and from 200ºC to 400ºC produce 9.64% and 12.6% increases in rotation at connection #7, respectively. In contrast, a temperature increase from 400ºC to 600ºC produces a much more significant increase in rotation, 45.3%, at connection #7. As evident from the plot of connection rotation versus temperature shown in Figure 4.8, thermal loading on the connection caused nonlinear behavior of the connection. Changes in the slope of the curve with increasing temperature indicate that as the steel connection is heated, it gradually begins to deform as manifested by increasing rotation, with the most significant increase in deformation occurring between 400ºC and 600ºC. Physically, this means that as the connection is heated the material properties of the steel components forming the connection change, and the connection itself

becomes *less* stiff, reducing its ability to resist the stresses imposed by the gravity loads. The data in Figure 4.8 is plotted again in Figure 4.9 against the temperature-rotation curves plotted in the Sheffield study (Al-Jabri et al 2004) for Group 2 connections. These indicate a linear response of the connection until the onset of yielding in one or more components in the connection, followed by yielding and then a sharp increase in rotation with temperature. As the load level increases, the failure temperature decreases; the present study most closely relates to the loads used for tests FB2-4. The trend observed in the present results for the rotation-temperature behaviour of connection #7 (Figure 4.8, re-plotted in Figure 4.9) is consistent in that it suggests approximately linear behaviour of the connection up to a temperature of 400ºC, after which there is a change of slope corresponding to decreased stiffness at the onset of yielding in the Sheffield data. However, while the Sheffield data clearly indicate yielding of the connection, at higher temperatures the SODA results do not appear to indicate full yielding of the connection, even at a temperature of 600ºC; though there is a change of slope of the rotation-temperature relation consistent with decreasing stiffness. This difference in results occurs because the heated semi-rigid connection in the present study is modeled as one component of a larger assembled framework, whereas the experimental curves are results from a test on an isolated connection in a test chamber. In an assembled framework, the behavior of a heated semi-rigid connection, such as connection #7, is influenced by the combined effects of temperature-induced changes in material properties and connection design, which are a local phenomena, as well as by moment-level changes due to moment redistribution, which is a global phenomenon dependent on the detailed configuration of the structural frame housing the connection. This assembled-structure behaviour is explained in the following by considering the stiffness degradation factors and moment levels at all connections of the assembled framework.

The calculated stiffness reduction factors (r_c) for connection #7 are listed in Table 4.4. The slightly increasing values of these factors over the range from 20ºC to 400ºC suggest that, contrary to the understanding that increases in temperature continuously degrade the stiffness of steel elements, the present connection appears to exhibit slightly increased stiffness over this temperature range. This can be explained by studying the moment levels throughout the framework in conjunction with the stiffness reduction factors, $r_{c,}$ calculated for all the connections. Figure 4.10, Figure 4.12 and Figure 4.14 present the moment levels and Figure 4.11, Figure 4.13 and Figure 4.15 present the stiffness degradation factors for all the connections in the frame at 200ºC, 400ºC and 600ºC, respectively. By comparing these figures to Figure 4.6 and Figure 4.7 (moment levels and r_c at 20ºC from Example 1), it is seen that as connection #7 is subjected to higher temperatures, it experiences smaller bending

moments while other connections (connections 4, 9, 10, 12 and 13; refer to Figure 4.5 for location of the connections) simultaneously experience larger moments. This occurs because in actual fact connection #7 does continuously becomes less stiff as it is heated up, thereby giving rise to redistribution of moment away from connection #7 to adjacent connections that are at ambient temperature. That is, the SODA-calculated value of the stiffness degradation factor at connection #7 is determined not only by the bending stiffness of the connection, which decreases due to the thermal loading according to the experimentally determined behaviour of the connection (a combination of connection design and changes in the material modulus of elasticity of the steel), but also by the moment level at the connection, which itself decreases through moment redistribution to other connections in the framework. Stated otherwise, the exposure of connection #7 to temperatures typical of those that might be encountered in a pre-flashover fire decreases the flexural stiffness of the connection; however, the associated redistribution of moment away from the connection essentially increases its capacity to resist flexural failure. This observation is consistent with a general understanding that the ability to redistribute loads elsewhere within an assembled structural framework during a fire often affords members and connections a level of fire-resistance beyond that which would be anticipated by the prescriptive practice of testing the fire resistance of structural elements in isolation from the assembled structure (Burgess 2002; Ellingwood 2005; Al-Jabri 2007).

Although the present analysis takes into account only the limited moment-rotation data at elevated temperatures for the Group 2 connections studied by Al-Jabri (Al-Jabri et al 2004), it nonetheless demonstrates that it may take significant thermal loads to cause fully plastic behaviour of the connections of an assembled framework. This is evident in Figure 4.9 which contrasts the almost linear temperature-rotation curve found for connection #7 in the assembled-frame analysis with those for the isolated connections measured at Sheffield. Examination of the stiffness reduction factors (r_c) listed in Table 4.4 further indicates that the moment redistribution effect positively influences the behaviour of connection #7 at temperatures from 200ºC through 600ºC. Even as the stiffness of connection #7 decreases, the counterbalancing effect of moment-redistribution to other elements in the frame tempers the impact of that decrease on the overall behaviour of the connection. Therefore, the load-redistribution effect in a structural steel frame during a fire event can be significant and can lead to a higher level of fire-resistance than what would be recognized by standard fire tests used in prescriptive building codes.

Although the foregoing has exemplified the use of moment-rotation data of semi-rigid connections in the analysis of an assembled structure and unveiled potentially greater fire-resistance of a particular connection in an assembled framework, fire safety design of structures has an important third dimension to consider as well: the time evolution of the fire-exposure and fire-resistance of a structure. The results presented in this Section provided information regarding the state of the structure when connection #7 reaches an elevated temperature; however, it provided no information on *when* the connection would reach that temperature. This information is often critical as it has important impact on occupant evacuation, firefighting, and search and rescue operations. To associate the structural response with a fire loading over time, it is necessary to conduct an analysis to determine the progression of a specified fire, and hence the temperatures in a given compartment in the structure over time, and, when required, to conduct an additional energy balance and heat transfer analysis between the compartment gases and structure to predict the temperatures that would occur in the exposed structural elements over time. These additional aspects of the analysis are discussed in the next section.

4.4 Calculation of Steel Temperature

Section 4.3 presented example calculations illustrating the use of SODA to analyze a 2-bay by 2-storey structure under ambient and discrete temperature conditions representative of those that might be encountered during a fire. Because each analysis is associated with a pre-defined temperature for a connection (i.e., 20ºC, 200ºC, 400ºC and 600ºC), the results of each analysis represent the state of the structure when the connection is at the specified temperatures. To associate the structural response with the progression of the fire, a separate, independent fire analysis using one of the models presented in Chapter 2 is required to acquire the time-temperature history of the fire compartment and the associated connection. Amongst the various fire models that are available, the fire behaviour model coined the 'BFD curve' (Barnett 2002) is selected for the present analysis based on its ability to predict compartment temperatures during both pre-flashover and post-flashover stages of a fire, as well as because it has been validated against some experimental work. An example calculation for obtaining the temperature of a steel connection using compartment temperatures estimated by the BFD fire model (Barnett 2002) is presented in the following Section. This is intended to demonstrate the fire-progression analysis calculations required to be coupled with the fire-related predictions of the structural analysis presented in Section 4.3.

4.4.1 Calculation of Compartment Temperature based on the BFD Fire Model

In order to achieve consistency with the requirements for a fire-progression calculation using the BFD model, the structural geometry from the SODA analysis is used with the following assumptions to determine the temperature time curve for a fire in Compartment A where connection #7 is located (see Figure 4.16). The assumptions include:

- each bay in each storey of the structure is a single fire compartment;
- the structure for the purpose of compartment temperature calculation has a 3rd dimension; a depth of 4m as shown in Figure 4.16;
- the fire compartment, Compartment A, has a 1 m wide by 2 m high ventilation opening (the size of a standard door);
- the fire compartment, Compartment A, has a fuel content of 10,000 MJ, which gives a fuel load density of 10,000 MJ / (4 m depth × 6 m width) = 417 MJ/m^2; as a comparison, a typical home has a fuel load density of 500 MJ/m^2 while a car repair shop has a fuel load density of 300 MJ/m^2 (ABCB 2005).
- ambient temperature is 20°C
- the heating and cooling rate of the compartment fire assumes that of a 'fast' t-square fire, which is reasonable for the type of combustibles generally seen in residential and light industrial occupancies (NFPA 2008).

Based on the above assumptions, the shape constant s_c for the BFD model can be calculated using Eq. (2.24), where:

$$A_w = 2\,\mathrm{m}^2$$
$$A_t = (4\times 6)\times 4 + (4\times 4)\times 2 = 128\,\mathrm{m}^2$$
$$s_c = \frac{1}{4A_w\sqrt{H}/A_t + 0.1} = \frac{1}{4(2)\sqrt{2}/128 + 0.1} = 5.3$$

The maximum temperature in compartment A is calculated using the method of Law, which is given by (Barnett 2002; SFPE 2002):

$$T_{\max} = 6000\frac{1-e^{-0.1\eta}}{\sqrt{\eta}} \tag{4.1}$$

where η is the inverse ventilation factor given by:

$$\eta = \frac{A_t - A_w}{A_w\sqrt{H}} \tag{4.2}$$

Using the compartment characteristics, it follows that:

$$\eta = \frac{128 - 2}{2\sqrt{1}} = 63 \tag{4.3}$$

and

$$T_{\max} = 6000\frac{1 - e^{-0.1(63)}}{\sqrt{63}} = 754\ ^{\circ}\text{C} \tag{4.4}$$

The compartment temperature is assumed to be uniform throughout the compartment since this is the basis of the BFD model assumption. The time to maximum compartment temperature (minutes), $t_{\max}$, is calculated using the following expression (Barnett 2002):

$$t_{\max} = \frac{E}{Q} - \left(\frac{1}{3}t_d - \frac{2}{3}t_g\right)Q^{0.5} \tag{4.5}$$

where E is the total fuel content in the fire compartment (kJ), t_d and t_g are, respectively, fire decay and growth coefficients based on the t-square fire definition and Q is the fire heat release rate, determined by:

$$Q = k_p\, F\, \Delta h_c \tag{4.6}$$

where F is the ventilation factor = $A_w\sqrt{H}$ ($m^{2.5}$), Δh_c is the effective heat of combustion (kJ/kg) and k_p is the pyrolysis coefficient (kg/s.$m^{2.5}$), which is given by Law's method (SFPE 2002):

$$k_p = 0.18\left(1 - \exp\left(-0.036\eta\right)\right) \tag{4.7}$$

From Eq. (4.3) with η = 63, applying Eq. (4.7) gives k_p = 0.161 kg/s.$m^{2.5}$. Assuming the heat of combustion of wood of 20MJ/kg, which is a reasonable calorific value for wood and paper-based materials (SFPE 2002), Eq. (4.6) gives the heat release rate of fire as:

$$Q = \left(0.161\right)\left(2\sqrt{2}\right)\left(20\right) = 9\ \text{MW} \tag{4.8}$$

Substituting the values into Eq. (4.5), the time to reach maximum compartment temperature is calculated:

$$t_{\max} = \frac{E}{Q} - \left(\frac{1}{3}t_d - \frac{2}{3}t_g\right)Q^{0.5} = \frac{10000}{9}\left(\frac{1}{3}150 - \frac{2}{3}150\right)9^{0.5} = 1261 \text{ s} = 21.00 \text{ min} \quad (4.9)$$

With the shape constant s_c, the maximum compartment temperature $T_{\max}$, and the time to maximum temperature $t_{\max}$, Eq. (2.22) can be used to calculate the time-temperature history based on the BFD fire model using Excel (Microsoft 2007). Figure 4.17 is a plot of the calculated compartment time-temperature history for Compartment A based on the BFD fire model for the assumptions noted above.

The BFD time-temperature curve in Figure 4.17 represents the development of the fire in Compartment A. During the first 10 minutes, the compartment temperature rapidly increases to 600°C, which is generally regarded as a point near flashover (beginning of the transition from a pre-flashover to a post-flashover fire), and continues to steadily increase to the maximum temperature of 754°C. This rapid increase in compartment temperature represents a well-ventilated compartment where the burning rate is governed by the available fuel. The compartment temperature then remains in the neighborhood of 750°C for about 5 minutes, a short steady-state burning period during which the maximum burning rate is normally reached. After this point, the temperature in the compartment again gradually decreases over time. During this period, there is sufficient ventilation to supply the oxygen needed for combustion; however, the burning rate decreases as the fuel is consumed by the fire.

4.4.2 Comments on Calculation of Steel Temperature

Section 4.4.1 presented BFD fire model predictions of the time evolution of the bulk gas temperature in the fire compartment where connection #7 is located. The actual temperature of the steel connection will be determined by conduction, convection and radiation heat transfer between the connection and the hot gases in the fire compartment and conduction heat transfer within the connection itself.

Generally, the transport of thermal energy from a fire to the exposed structure is dominated by convection of the hot gases past the structural element, and, even more profoundly at high

temperature, by radiation heat transfer processes (Kodur 2009). The change in steel temperature can be derived based on the conservation of energy (Incropera 2002):

$$q_{con} = q_{rad} + q_{conv} \tag{4.10}$$

where q_{con} is the heat flux dissipated into the steel due to conduction, and q_{rad} and q_{conv} are the heat transferred from the bulk heated fire gases in the compartment to the exposed steel due to radiation and convection processes, respectively. For steel, which is a thermally thin material where the resistance to conduction within the solid is relatively small compared to resistance to convection and radiation transfer from the bulk heated gas (Incropera 2002), a quasi-steady-state temperature can be calculated by solving a simplified form of the heat equation given by (SFPE 2002):

$$\frac{\Delta T_s}{\Delta t} c_s (W / D) = \sigma \varepsilon_f \left({T_f}^4 - {T_s}^4 \right) + h\left(T_f - T_s \right) \tag{4.11}$$

where ΔT_s is the change in steel temperature (°C); Δt is the time from ignition (s); T_f is the compartment gas temperature after ignition, determined from the fire model (°C); T_s is the steel temperature (°C); W is the weight of the steel per unit length (kg/m); D is the surface of the steel member exposed to fire per unit length (m); c_s is specific heat of steel; h is the convection heat transfer coefficient (W/m^2.K); σ = Stefan-Boltzmann constant = 5.67×10^{-8} W/m^2.K^4; and ε_f = emissivity of the fire gas. Eq. (4.11) is generally used to calculate the temperature of large steel sections.

Equation (4.11) can be used to obtain a time-temperature history for each element in the steel structure that abuts a fire compartment. The temperature in the steel will lag the compartment gas temperature due to the thermal inertia of the solid structure. In Eq. (4.11), this physical phenomenon is described by the term on the left-hand side of the equation, where the W/D ratio is an indirect measure of how fast the steel will heat up. While Eq. (4.11) can be applied to calculate a more precise temperature history, for small steel elements such as the steel connection in the present study, it is generally reasonable to assume that the steel temperature is the same as the compartment gas temperature because the W/D ratio of each element is small. This assumption is confirmed by studying Eq. (4.11); as W/D approaches zero, the steel temperature, T_s, approaches the fire temperature T_f in the equation. Therefore, as W/D decreases, the thermal lag between T_s and T_f becomes negligible. Based on the assumption of equal compartment gas and steel temperature, a pseudo-time domain with respect to the development of a typical compartment fire can be imposed on

the structural response for the example presented in Section 4.3.2. Table 4.4 presents the moment level, rotation and stiffness degradation factors for connection #7 with representative times from start of fire as determined using the BFD fire model depicted in Figure 4.17.

4.4.3 Discussions on the Model Result

The results contained in the five columns of Table 4.4 represent a set of output from a simplified, yet combined, fire-structural analysis intended to simulate a representative thermal loading due to fire on one connection within a larger structural framework. The behaviour of the structure is summarized for discrete temperature loadings on the connection and then related back to a simulation of fire development within the compartment containing the connection. The results are therefore based on simplification of both the time evolution of the fire conditions as well as the true structural exposure and response under thermal loads. Some of the implications are discussed here.

First, while the analysis using the BFD model provided a full compartment temperature history, the structural analysis only considered temperatures up to 600°C due to the availability of experimental moment-rotation data for the connection of interest. Although the moment-rotation data for temperatures between 600°C and 750°C, the maximum temperature predicted by the BFD model, is lacking, based on the results in Table 4.4 it can be seen that the decrease in stiffness degradation factor r_c is most significant towards 600°C, often considered to be a temperature characterizing the transition point between a pre- and post-flashover fire. Therefore, as expected, structural failure is most likely to occur under exposure to post-flashover fire temperatures. At the same time, based on the results shown in Figure 4.9, which contrasts the temperature-rotation curve of connection #7 found from the assembled-frame analysis with the isolated-connection measurements from the Sheffield experimental testing, significant thermal loads can sometimes be required to cause fully plastic behaviour of a connection in an assembled framework.

Secondly, the present analysis assumed idealized insulation of all structural elements other than connection #7. In reality, as the compartment fire develops, a temperature gradient will also develop within the fire compartment, particularly for pre-flashover fires. Therefore, as a fire near connection #7 heats up the connection, adjacent structural members will also be exposed to elevated temperatures, and will respond according to their individual force-deformation relationships. In the present analysis, this has not been considered due to the lack of force-deformation data for beams and columns subjected to the temperatures of interest; however, it is anticipated that such pre-flashover

exposure and the resulting temperature gradients within different parts of the structural framework will also have a significant impact on the overall fire-resistance of the structure.

4.4.4 Summary

This Chapter presented example calculations for the thermal loading of a semi-rigid connection within a 2-bay by 2-storey steel framework. The Sheffield experimental data (Al-Jabri 2004) was incorporated into the structural analysis software SODA to determine the overall structural response to thermal loading of one interior connection at three elevated temperatures, and the BFD fire model (Barnett 2002) was used to correlate an example compartment time-temperature history with the structural response. The example calculation illustrated that experimental force-deformation data obtained for steel elements at elevated temperatures can be reasonably used in SODA to determine the behavior of an assembled steel framework under various discrete thermal loadings due to fire. It is seen from the example calculation that the effective stiffness of a connection subject to thermal loading is determined by a combination of local (connection) and global (framework) effects. Locally, the behaviour depends on the force deformation characteristics of the element which is heated. These include both the design of the connection and any changes in material properties with temperature. Globally, the response depends on load redistribution which occurs throughout the entire framework. Load redistribution effects can play a significant role in determining the overall fire-resistance of the steel framework; however, these are not accounted for under current prescriptive-based fire testing programs. With additional force-deformation-temperature data, such as could be obtained from further experimental work or via finite element analysis, an entire framework can theoretically be analyzed with different elements exposed to different temperatures, as might be determined through predictions obtained via an appropriate fire model. The overall behavior of a structure subject to fire loading could then be determined, and fire protection measures optimized as dictated by the fire safety designer.

Table 4.1: Parameter values for the three-parameter and four-parameter models describing the moment-rotation-temperature data from the Sheffield experiment (Al-Jabri et al 2004).

Temperature	Three-Parameter Model Eq. (4.1)			Four-Parameter Model Eq. (3.30)			
ºC	A	B	n	R_{ce}	R_{cp}	M_0	γ
20	21.500	27.500	4.900	27083	479.44	134.59	1.120
200	13.000	27.000	4.900	15188	428.44	133.24	1.325
400	8.325	25.500	4.900	8885.5	468.88	116.53	1.722
600	2.500	10.200	4.900	2626.8	190.48	45.250	1.971

Table 4.2: Comparison of the beam and column steel sections used in the Sheffield experiment and the present study.

	Beam	Column
Sheffield		
Section Designation	356 × 171UB51	254 × 254UC89
Mass (kg/m)	51.0	89.0
Section Depth (mm)	356.6	260.4
Flange Width (mm)	171.5	255.9
Web thickness (mm)	7.3	10.5
Present Study		
Section Designation	W360 × 51	W250 × 89
Mass (kg/m)	51.0	89.0
Section Depth (mm)	355	260.0
Flange Width (mm)	171	256.0
Web thickness (mm)	7.2	10.7

Table 4.3: Comparison of moments and corresponding rotations calculated by SODA versus using Eq. (4.1). The check confirms that the conversion from the three-parameter model to the four-parameter model is appropriate and that SODA correctly references the fire connection in the calculation.

Temperature Level (ºC)	Moment (kN-m)	Rotation Computed by SODA (radian × 10^3)	Rotation Computed by Eq (4.1) (radian × 10^3)	Difference (%)
20	103.60	11.00	11.5	-4.35
200	95.17	12.06	12.12	-0.495
400	83.49	13.58	13.37	1.57
600	36.53	19.73	19.80	-0.354

Table 4.4: Moments and corresponding rotations and stiffness reduction factors at connection #7 due to the fire.

Time from Start of Fire (minute)	Temperature Level (ºC)	Moment (kN-m)	Rotation computed by SODA (radian × 10^3)	Stiffness Reduction Factor (r_c)
0.0	20ºC	103.60	11.00	0.100
1.9	200ºC	95.17	12.06	0.109
3.6	400ºC	83.49	13.58	0.106
6.4	600ºC	36.53	19.73	0.033

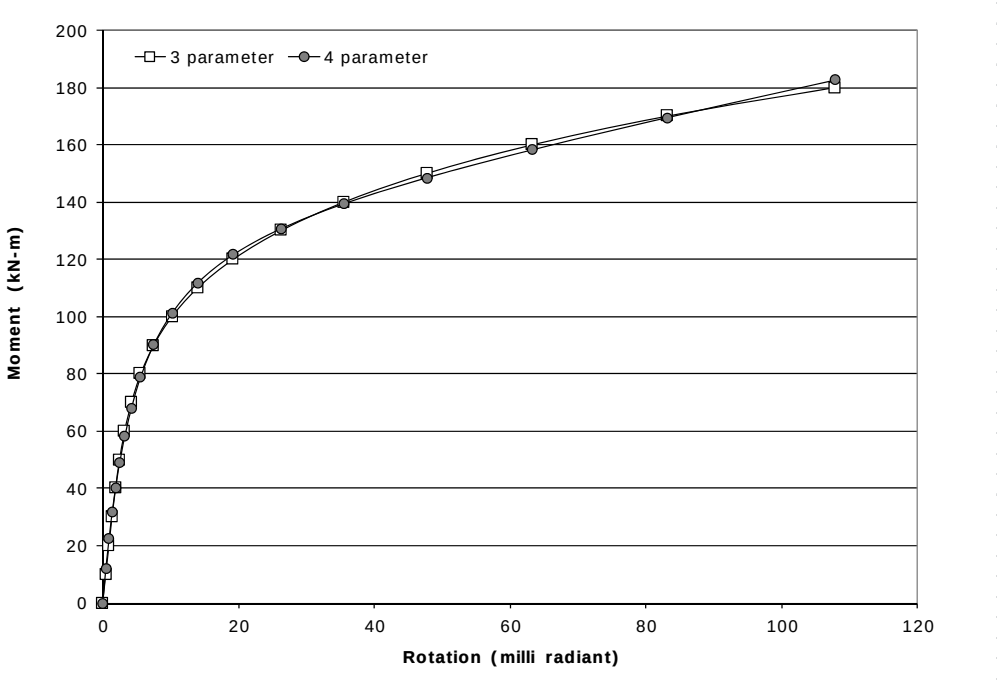

Figure 4.1: Comparison of moment-rotation curves obtained from the 3-parameter model Eq.(4.1) and the 4-parameter model Eq.(3.30) at 20°C.

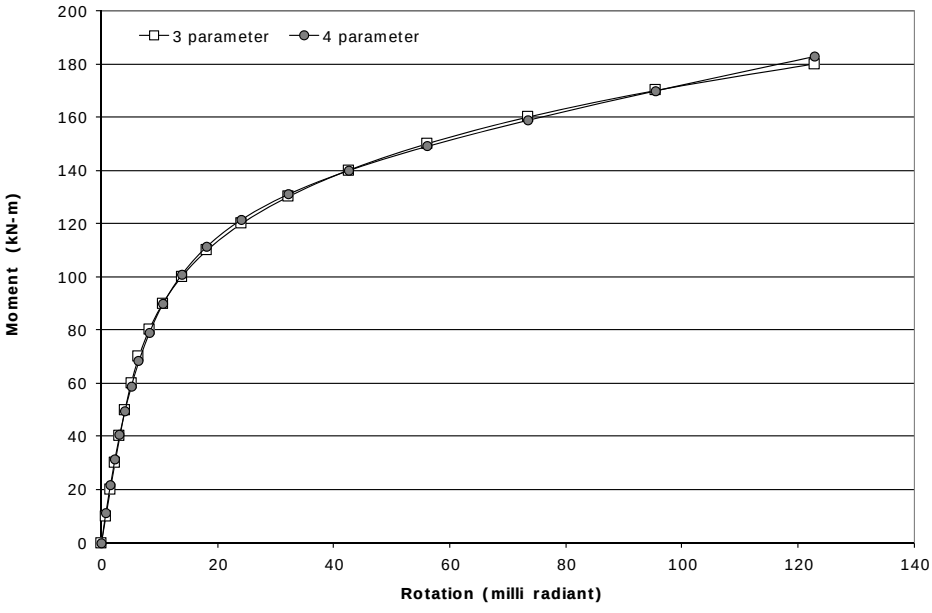

Figure 4.2: Comparison of the moment-rotation curves obtained from the 3-parameter model Eq.(4.1) and the 4-parameter model Eq.(3.30) at 200°C.

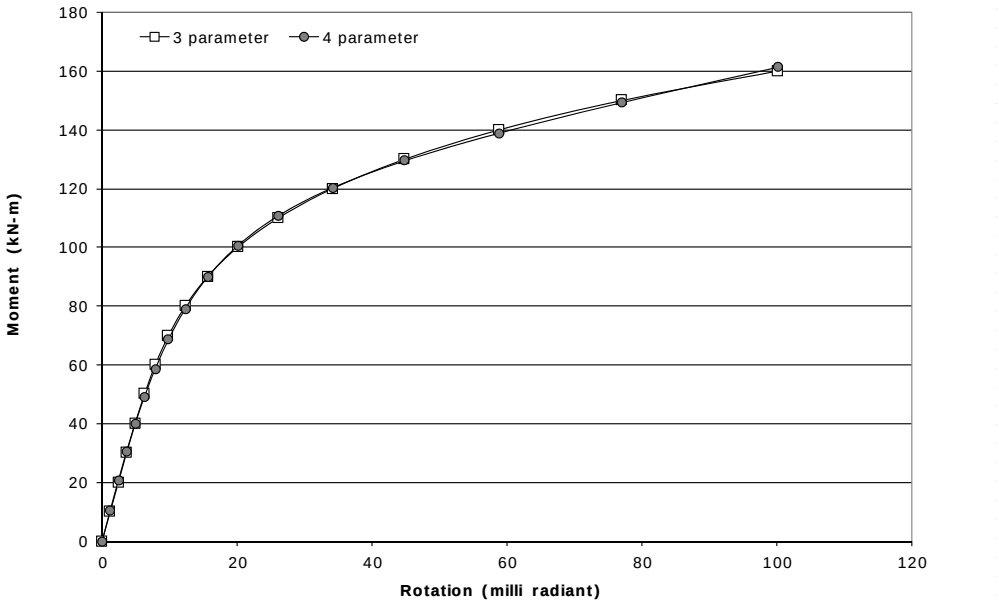

Figure 4.3: Comparison of the moment-rotation curves obtained from the 3-parameter model Eq.(4.1) and the 4-parameter model Eq.(3.30) at 400°C.

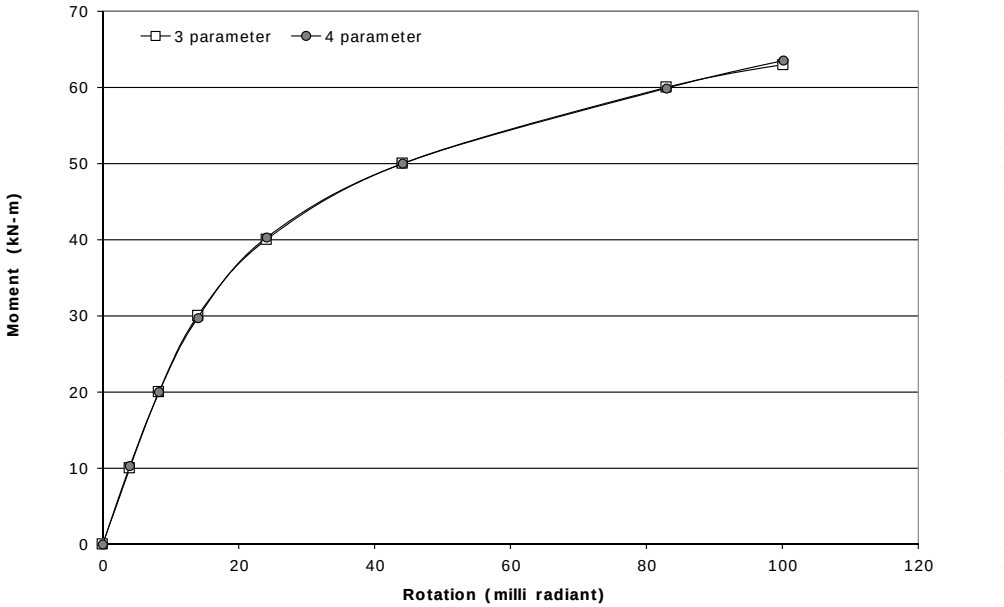

Figure 4.4: Comparison of the moment-rotation curves obtained from the 3-parameter model Eq.(4.1) and the 4-parameter model Eq.(3.30) at 600°C.

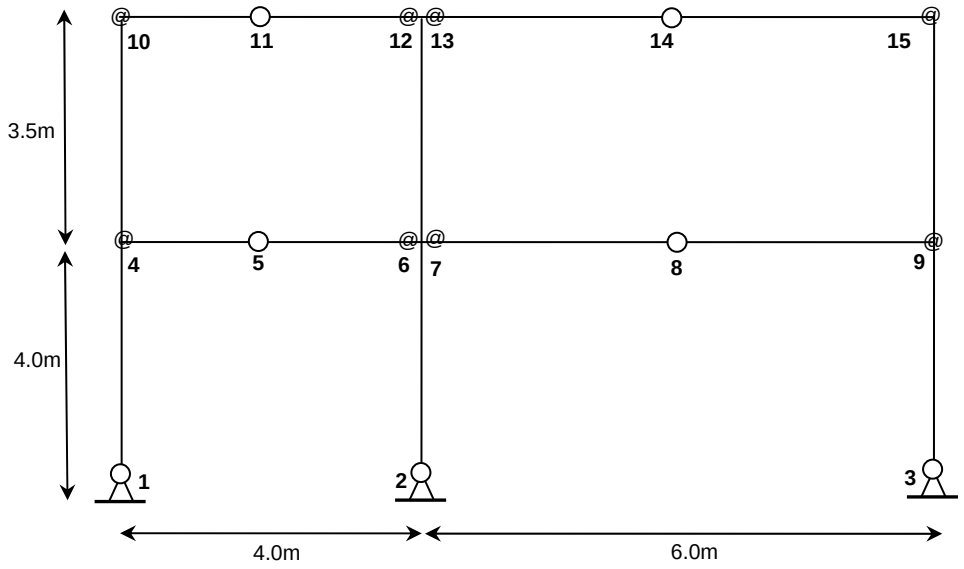

Figure 4.5: Example 2-bay by 2-storey steel frame.

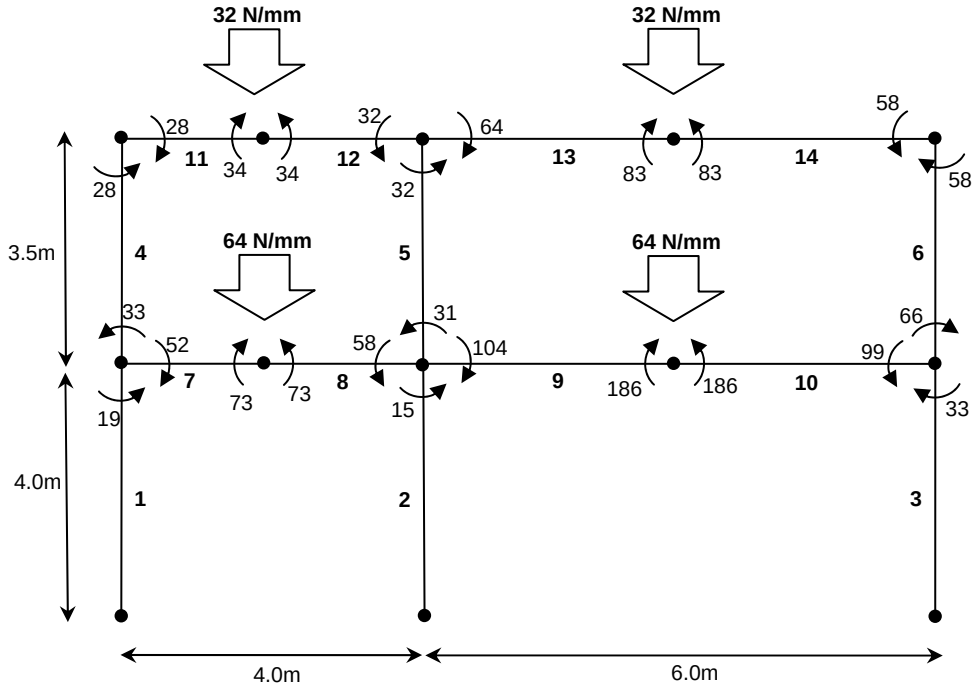

Figure 4.6: Example 1-Moment levels for all connections at 20°C.

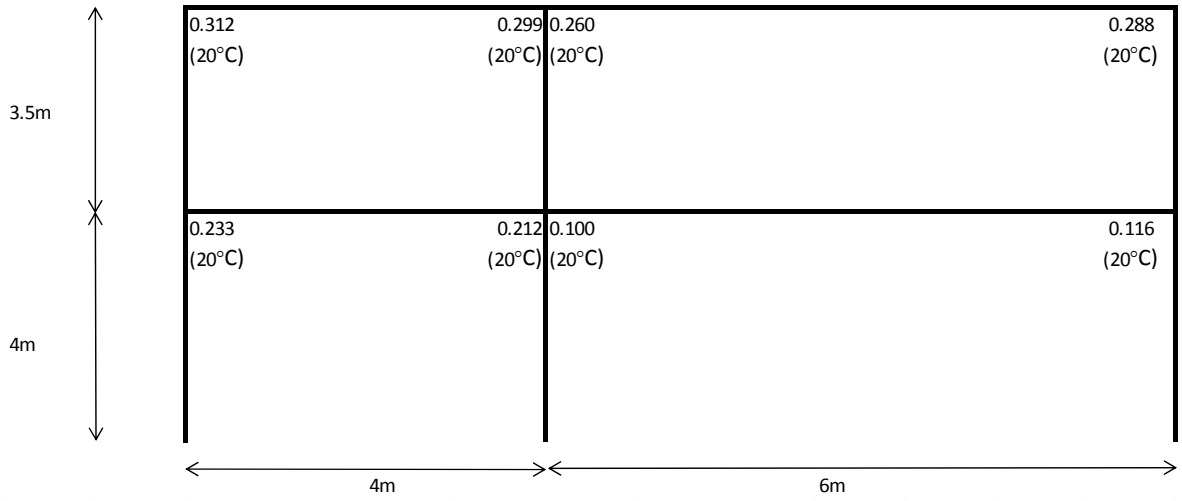

Figure 4.7: Example 1-Stiffness degradation factors r_c for semi-rigid connections at 20°C

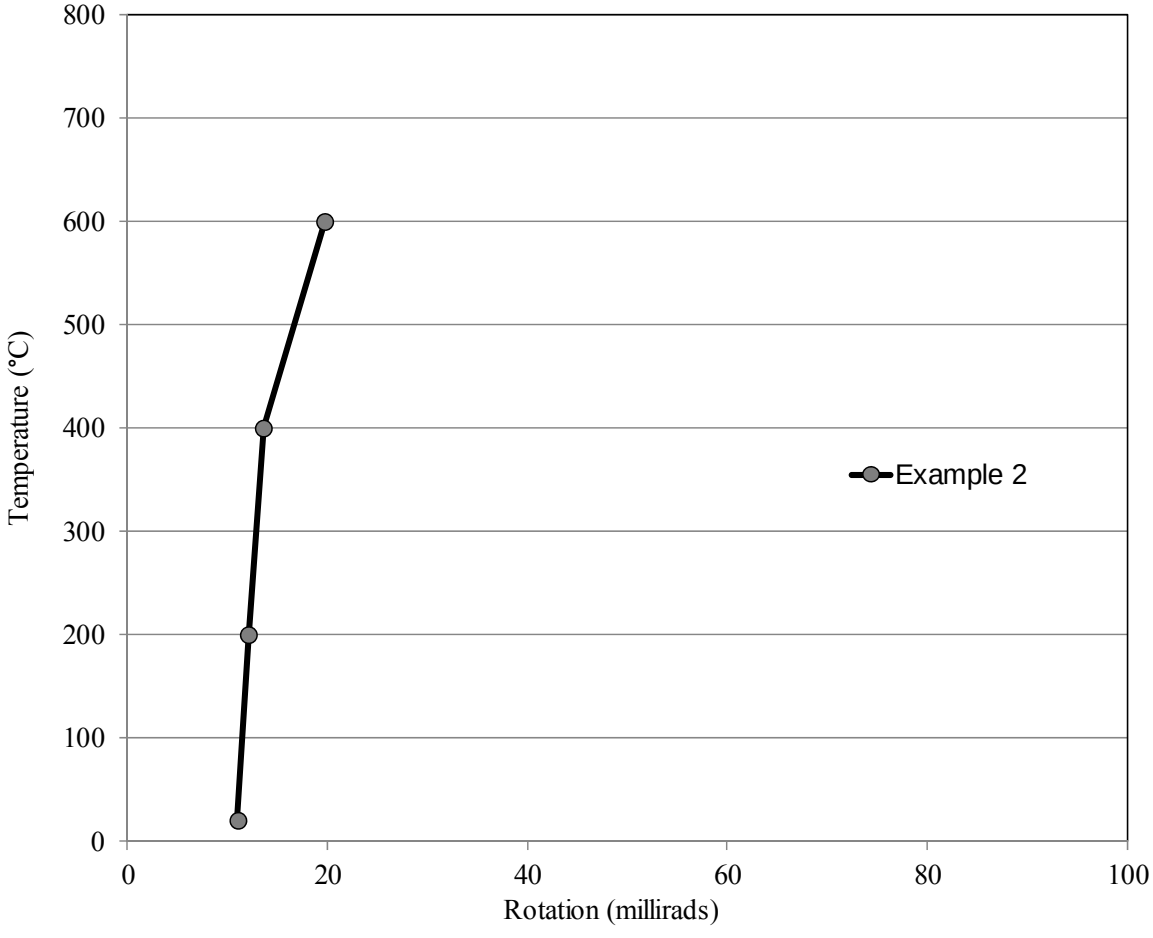

Figure 4.8: Example 2- Rotation versus temperature for connection #7

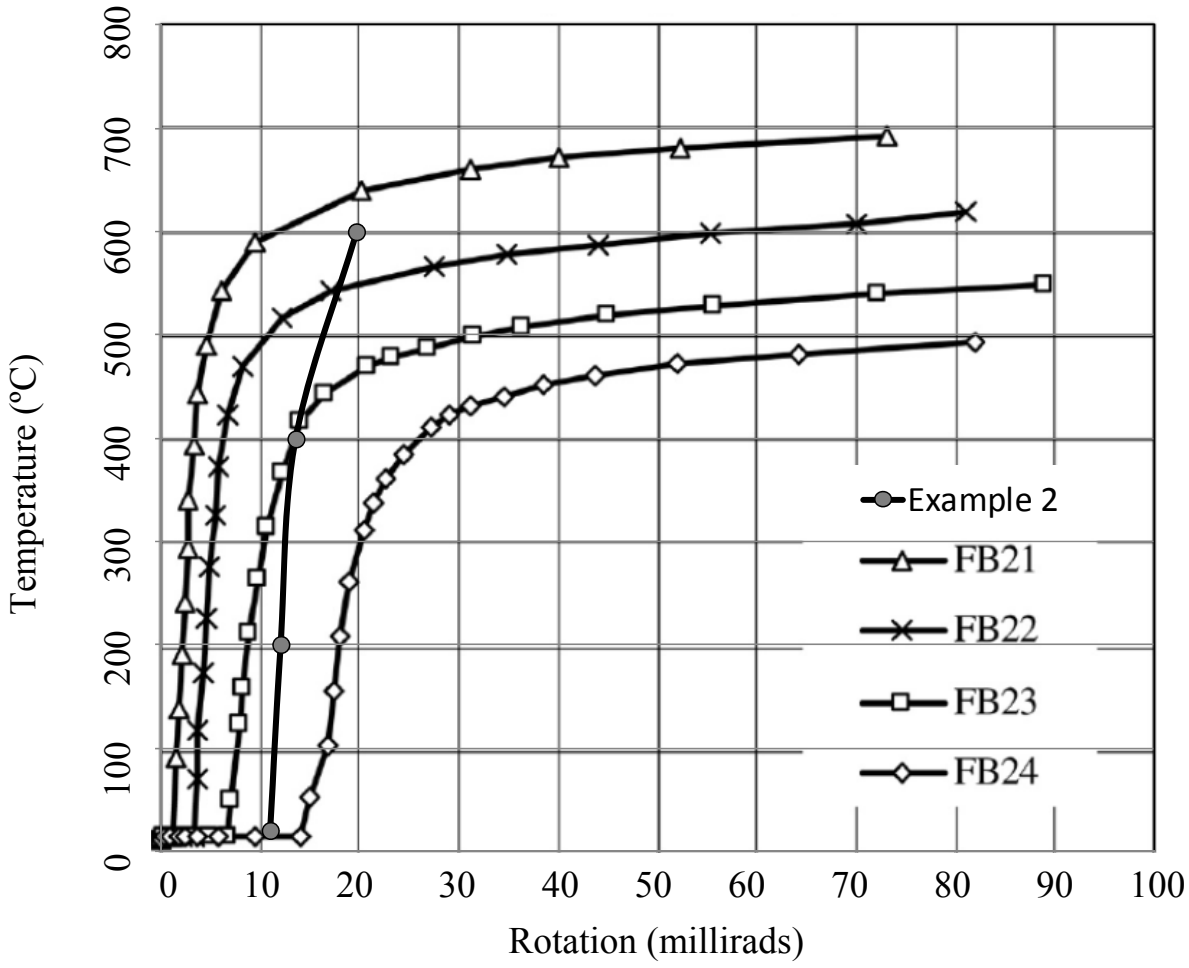

Figure 4.9: Example 2-Rotation vs temperature plot for connection #7 (Fig. 4.14) superimposed onto temperature vs rotation plots for Group 2 connections from Sheffield experiments (Al-Jabri et al 2004).

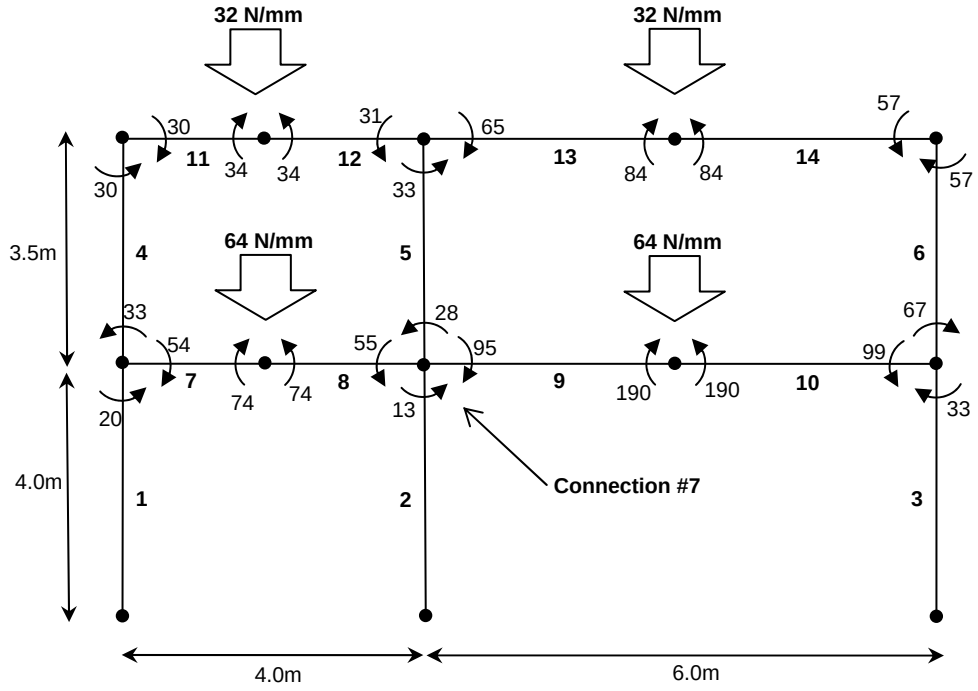

Figure 4.10: Example 2-Moment levels for connection #7 at 200°C and other connections at 20°C

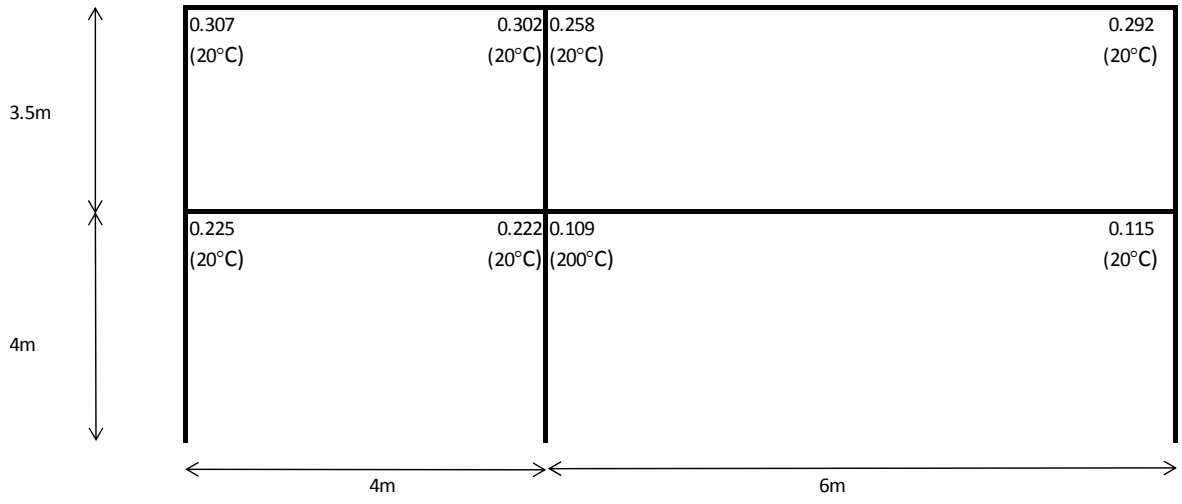

Figure 4.11: Example 2-Stiffness degradation factors r_c for connection #7 at 200°C and other connections at 20°C

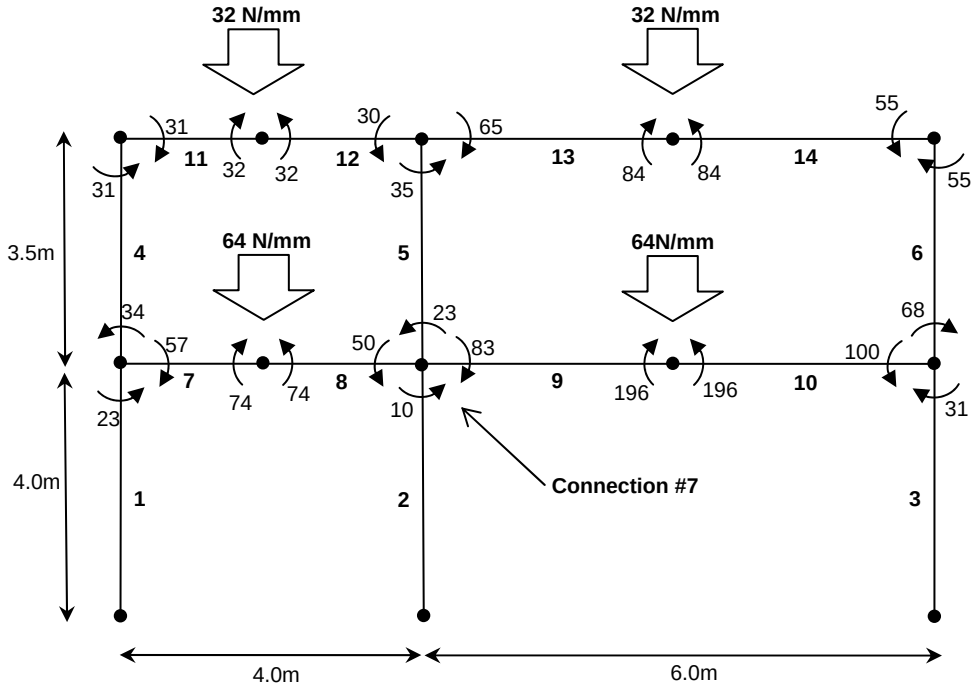

Figure 4.12: Example 2-Moment levels for connection #7 at 400°C and all other connections at 20°C

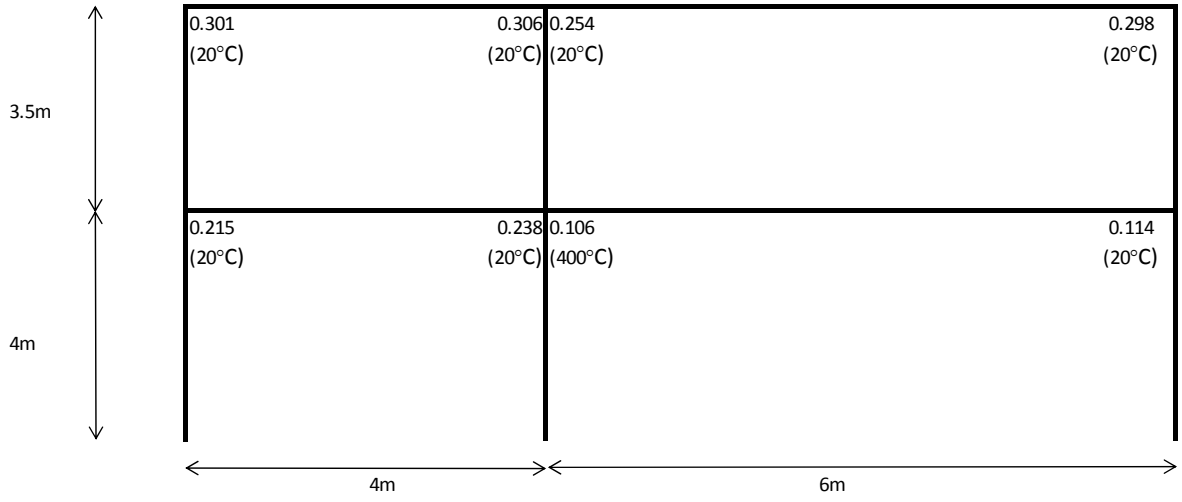

Figure 4.13: Example 2-Stiffness degradation factors r_c for connection #7 at 400°C and all other connections at 20°C

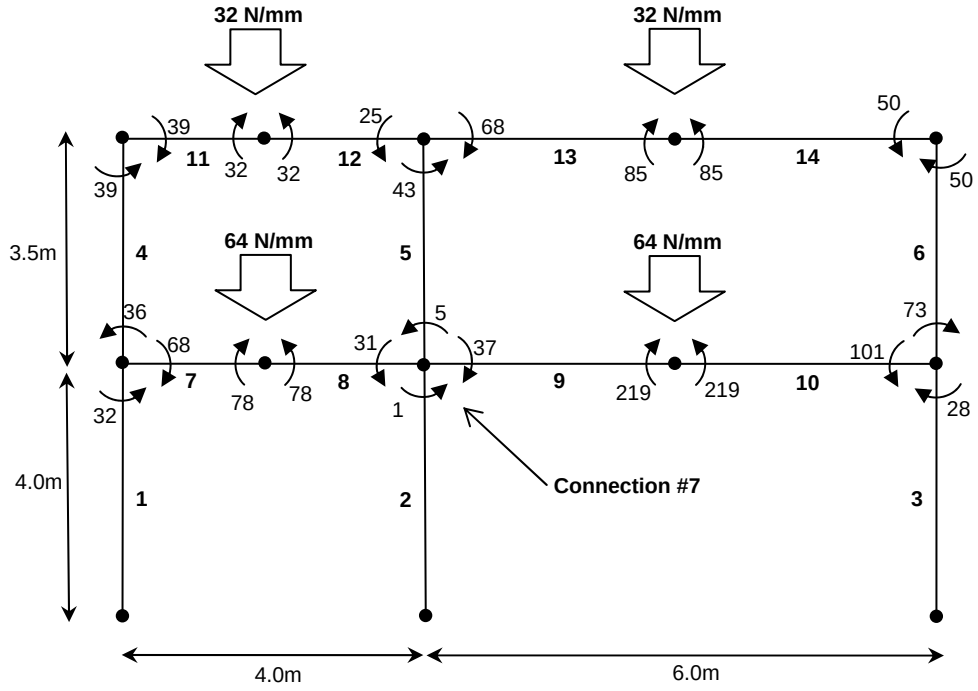

Figure 4.14: Example 2-Moment levels for connection #7 at 600°C and all other connections at 20°C

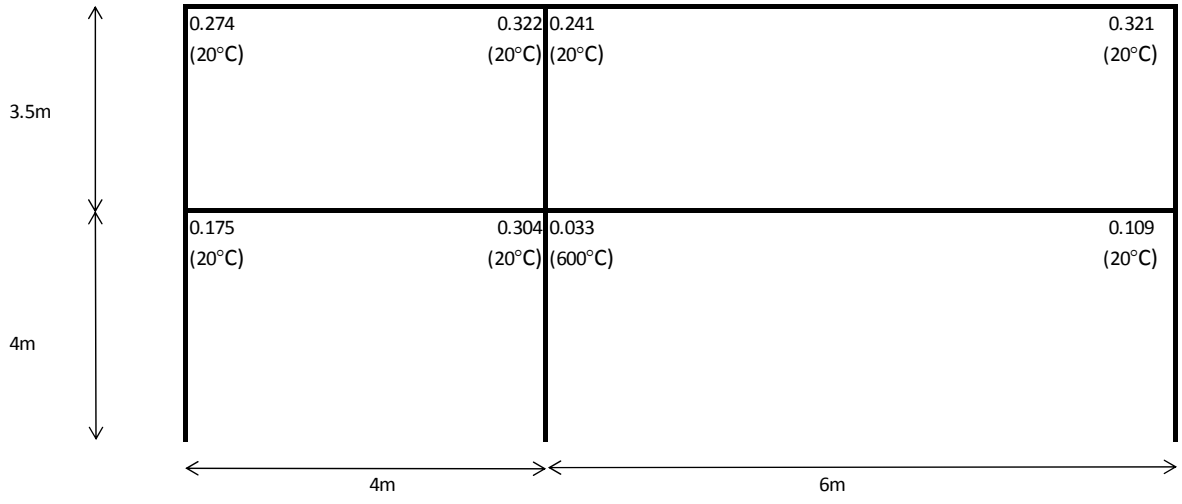

Figure 4.15: Example2-Stiffness degradation factors r_c for connection #7 at 600°C and all other connections at 20°C

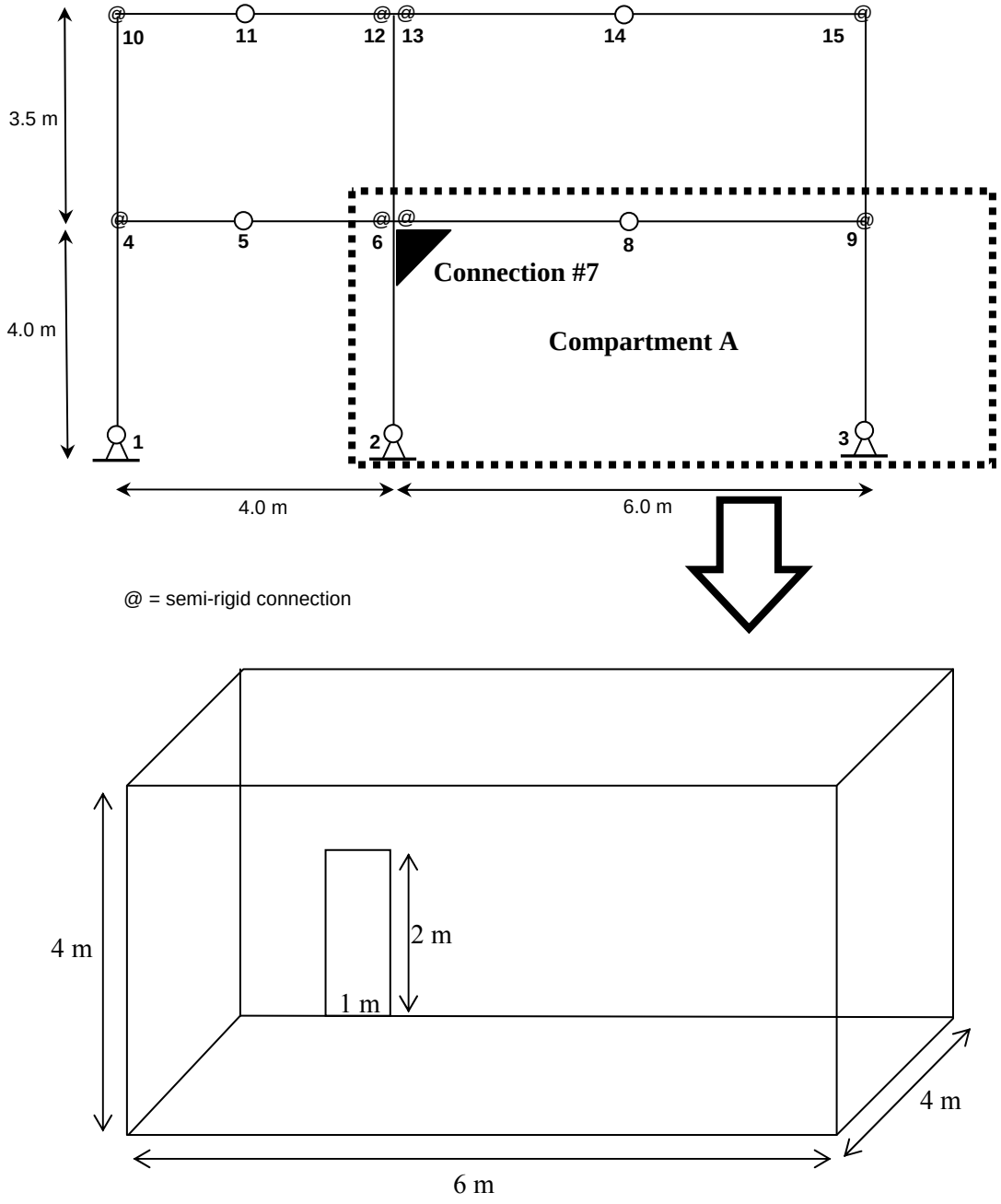

Figure 4.16: Geometry of Compartment A where Connection #7 is located.

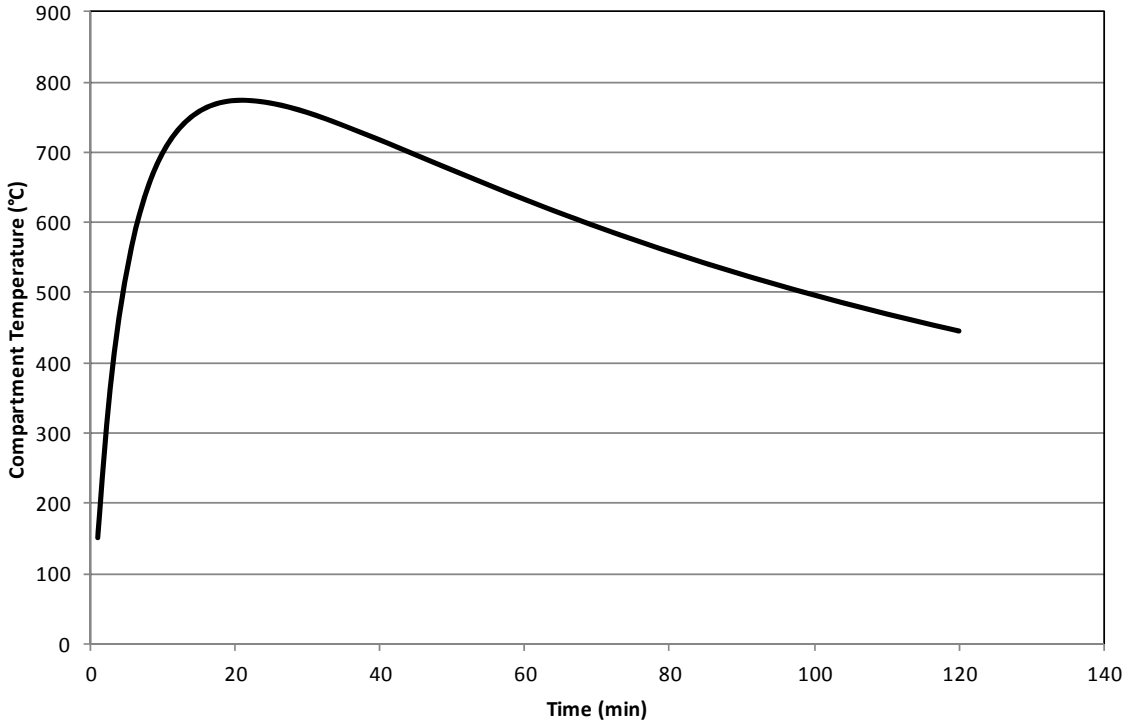

Figure 4.17: Compartment temperature history from the start of the fire as calculated using the BFD fire model (Barnett 2002) for the hypothetical Compartment A (6m by 4m by 4m) containing connection #7.

Chapter 5
Summary, Conclusions and Future Work

The demand for greater flexibility in the design of buildings has driven acceptance of performance-based fire protection practice. Yet, there has been limited basic research and development to support full performance-based design of structures for fire, specifically in areas relating to the inclusion of realistic fire loads in design of building structures. As a result, while engineers are able to use fire modeling tools to provide a performance-based analysis of the thermal loads in compartments due to different fire scenarios, thermal insulation continues to be used as the main method for structural fire protection.

In response to these much needed tools, this thesis develops an approach to predict the behaviour of a 2-bay by 2-storey steel framework when a semi-rigid connection is exposed to thermal loads defined as discrete values of constant elevated temperature. The approach is principally based on incorporating moment-rotation-temperature data for the connection, as found in archival literature, into the structural analysis software SODA, developed at the University of Waterloo. This Chapter presents a summary and concluding comments concerning the work completed, and recommends research directions for future study.

5.1 Summary

Chapter 1 provided an introduction to the current regulatory framework for the practice of structural fire protection engineering and contrasted the difference between prescriptive-based and performance-based approaches. It is established that a true performance-based design for structures for fire must account for *both* the physics of compartment fire and the structural response through the use of appropriate models. To this end, Chapter 2 provided a literature review on compartment fire behaviour, as well as outlining the models available to predict that behaviour for different stages of fire development. Models developed from parametric studies to more sophisticated zone and computational fluid dynamics models were presented. Following that, Chapter 3 introduced the SODA (structural optimization, design and analysis) software used in the present study and provided an overview of the theory behind the beam-column element model central to that software. A discussion on the post-elastic range response of steel structures when subjected to abnormal / extreme loads was presented and similarities in behaviour when steel structures are subjected to thermal loads

from fire was illustrated. From this, the link between the analysis procedure and the available experimental moment-rotation-temperature data for semi-rigid connections was drawn. Chapter 4 then presented the procedure for incorporating the moment-rotation response data of semi-rigid connections at elevated temperatures into the full analysis of a 2-bay by 2-storey planer steel framework using SODA. The structural response was presented, and the significance of the observed moment redistribution phenomenon was discussed. A parametric fire model was then presented to demonstrate the link between the different stages of the structural response and the development of a compartment fire.

5.2 Conclusions

Based on the example study presented in this thesis, the following specific conclusions can be made:

- The beam-column element model employed by the SODA software can utilize moment-rotation data derived from experiment or finite element analysis, provided the experimental data can be cast into the form required by the 4-parameter model used by the software. Where the data is reported in a different form, a regression exercise can be carried out to convert the data into the 4-parameter form recognized by the software.
- The example analysis of the 2-bay by 2-storey steel planar framework with one connection, connection #7, at elevated temperatures demonstrated that, as expected, the stiffness of the connection changes as the temperature increases from ambient temperature. The effective stiffness of the connection was determined by combined local and global effects, including connection design, changes in material properties with temperature, specifically the modulus elasticity, and load redistribution within the members of the framework.
- Because of the load redistribution effect, the connection subjected to elevated temperatures affords additional fire-resistance as indicated by the *increase* in effective stiffness degradation from 20°C to 400°C, even though the modulus elasticity of the connection is decreasing. This inherent fire-resistance is not measurable via current prescriptive fire testing, which only tests the performance of each individual structural element in isolation.
- With additional force-deformation data obtained from experiment or via finite element analyses, it would be possible to study the response of a framework when other structural elements such as beams and columns are also at elevated temperatures. This study can be

carried out with SODA or other similar structural analysis methods provided it is possible to incorporate the force-deformation data into the computational algorithm.

- The ability to study the fire performance of an assembled structural framework will allow practitioners to conduct a true performance-based structural fire safety design. Although significant research is still required in this area, a design tool of this kind should allow the fire protection measures in a building to be optimized, and applied only where they are truly needed.

5.3 Future Work

The following areas of research are recommended as future work concerning structural fire engineering of steel frameworks:

- **Gathering of Force-Deformation Data at Elevated Temperatures**

  The analysis presented in this study is predicated upon the use of moment-rotation data at elevated temperatures from the Sheffield experiments. To extend the present analysis to study other connections and other structural elements such as beams and columns, it is necessary to utilize additional force-deformation data. Areas where additional work can be carried out include conducting additional experiments similar to those of the Sheffield experiments but using North American steel sections, and/or performing finite element analyses targeted towards obtaining additional force-deformation data for a variety of structural elements.

- **Computation of Force-Deformation Relationship at Elevated Temperatures**

  As mentioned in Chapter 3, for concrete structures it is possible to obtain the force-deformation relationship of beams and columns by performing a sectional analysis using the *Reponse-2000* software. Such an analysis would require known geometric properties and modulus of elasticity as the input. A similar research and development effort aimed at producing the same procedure for *steel* structures would add to the ability to calculate appropriate force-deformation relationships at elevated temperatures, given that geometric properties of the steel sections remain relatively unchanged and the modulus of elasticity for steel at elevated temperatures is well known. This would allow the analysis of the kind

presented in this study to be extended to include other types of structural elements without the need to gather significant force-deformation data from experiments or finite element analysis.

Appendix A

Input File for the SODA Analysis

The following is the SODA input file `strusys.in`. Reference to the semi-rigid connection is under the heading 'C Group' where `EEP_95` = semi-rigid connection at 20°C and `EEP_97` = semi-rigid connection at 200°C. The reference 'EEP_#' is changed in different analysis runs to reference different moment-rotation curves for the semi-rigid connection at different temperatures.

```
OUTPUT FILE NAME: New_2b2s frame
DERSION 2.04
PROJECT TITLE: Inelastic Analysis for light loading frame
SODA DIRECTORY: C:\abnormal\2dc\database\soda\
DATABASE DIRECTORY: C:\abnormal\2dc\database\soda\cdndbase\
SECTION DATABASE: cisc.SDC
DATABASE DIRECTORY: C:\abnormal\2dc\database\cbank.01\
FOREIGN SECTIONS: ON
PDELTA:           ON
COMBINED:         ON
LOAD INCREMENT:   ON
SWAY:             ON
CONNECTION BANK:  ON
NONLINEAR CURVE:  ON
SHEAR DEFORMED:   ON
Mechanism  :      OFF

     Structure   Action      Design Code Output      Units
     Frame       Dsign       86LRFLD     Detail      N;mm
     balfa     pcst      resp      rmaxi     wtol      toll
     1.0       1.2       0.6       0.8       0.01      0.001
     imax      iprint    noconv    narea     nlds      nphs1
     20        9         2         2         0         90
     Displace  Stress    allowed   HSS Section
     constrnt  Constrnt  Value     Yes or No
     Yes       No        1.0       No
     Members    M-Groups     C-Groups    Nodes      Load Cases   Supports
     14         10           2           13         1            3
NODE NAMES
1    101 1
2    102 1
3    103 1
4    104 1
5    105 1
6    106 1
7    107 1
8    108 1
9    109 1
10   110 1
11   111 1
12   112 1
13   113 1
     Member    Start     End       Memb. End Length Factors       Group
     Name      Node      Node      Retraints Kx     Ky     Kb     Name
1    c11       101       104       o---+     1      1      1      col1
        1.0, 1.0
2    c12       102       106       o---+     1      1      1      col2
```

```
        1.0, 1.0

3    c13       103       108       o---+     1      1      1      col3
        1.0, 1.0
4    c21       104       109       +---+     1      1      1      col4
        1.0, 1.0
5    c22       106       111       +---+     1      1      1      col5
        1.0, 1.0
6    c23       108       113       +---+     1      1      1      col6
        1.0, 1.0
7    b11       104       105       @---+     1      1      1      bea1
        1.0, 1.0
8    b12       105       106       +---@     1      1      1      bea1
        1.0, 1.0
9    b13       106       107       @---+     1      1      1      bea2
        2.0, 1.0
10   b14       107       108       +---@     1      1      1      bea2
        1.0, 1.0
11   b21       109       110       @---+     1      1      1      bea3
        1.0, 1.0
12   b22       110       111       +---@     1      1      1      bea3
        1.0, 1.0
13   b23       111       112       @---+     1      1      1      bea4
        1.0, 1.0
14   b24       112       113       +---@     1      1      1      bea4
        1.0, 1.0
         Group     Shape X-Section     Weak  Young's  Shear    X-Sect'n Moment
     Name      File  Designation   Axis  Modulus  Modulus  Area     Inertia
1    col1      W     250X89        NO    200000.  77000.   0        0
2    col2      W     250X89        NO    200000.  77000.   0        0
3    col3      W     250X89        NO    200000.  77000.   0        0
4    col4      W     250X89        NO    200000.  77000.   0        0
5    col5      W     250X89        NO    200000.  77000.   0        0
6    col6      W     250X89        NO    200000.  77000.   0        0
7    bea1      W     360X51        NO    200000.  77000.   0        0
8    bea2      W     360X51        NO    200000.  77000.   0        0
9    bea3      W     360X51        NO    200000.  77000.   0        0
10   bea4      W     360X51        NO    200000.  77000.   0        0
     Group     Yield     Ultimate  Maximum Allow KL/r  X-Section Depth
     Name      Stress    Stress    Comp'n    Tension   Minimum   Maximum
1    col1      248       380       200       300       8         500
2    col2      248       380       200       300       8         500
3    col3      248       380       200       300       8         500
4    col4      248       380       200       300       8         500
5    col5      248       380       200       300       8         500
6    col6      248       380       200       300       8         500
7    bea1      248       380       200       300       8         500
8    bea2      248       380       200       300       8         500
9    bea3      248       380       200       300       8         500
10   bea4      248       380       200       300       8         500
     Group     Elastic   Plastic   Expected            Beam or
     Name      Modulus   Modulus   Yield Stress        column Control
1    col1      0         0         248                 c
2    col2      0         0         248                 c
3    col3      0         0         248                 c
4    col4      0         0         248                 c
5    col5      0         0         248                 c
```

```
6    col6      0         0         248               c
7    bea1      0         0         248               b
8    bea2      0         0         248               b
9    bea3      0         0         248               b
10   bea4      0         0         248               b
     C-Group   Type      ID-No.    Stiffness Cost      Beam      Column
1    con1      EEP_95              150000    0.0002    2         1
2    con2      EEP_97              150000    0.0002    2         1
                              Nodal_Coordinates   Nodal_Support_Condition (1=fixed)
               X         Y         X         Y         Rot'n
1              0         0         1         1         1
2              4000      0         1         1         1
3              10000     0         1         1         1
4              0         4000      0         0         0
5              2000      4000      0         0         0
6              4000      4000      0         0         0
7              7000      4000      0         0         0
8              10000     4000      0         0         0
9              0         7500      0         0         0
10             2000      7500      0         0         0
11             4000      7500      0         0         0
12             7000      7500      0         0         0
13             10000     7500      0         0         0
INPUT LOADS
No loading combination
1   Nodal LOADS
     Node      Force   Direction   Load_index
1    4         0        1         1
2    9         0        1         1
0 0 0 0 0 0 ' ' 0 ' '
2   member LOADS
     Member    w@Start   Start     w@Finish  Finish    Orient-  Load Type   INDEX
1    7         -6.4         0        -64        1        'P' 1 'FULL UNIDL'    1
2    8         -6.4         0        -64        1        'P' 1 'FULL UNIDL'    1
3    9         -6.4         0        -64        1        'P' 1 'FULL UNIDL'    1
4    10        -6.4         0        -64        1        'P' 1 'FULL UNIDL'    1
5    11        -3.2         0        -32        1        'P' 1 'FULL UNIDL'    1
6    12        -3.2         0        -32        1        'P' 1 'FULL UNIDL'    1
7    13        -3.2         0        -32        1        'P' 1 'FULL UNIDL'    1
8    14        -3.2         0        -32        1        'P' 1 'FULL UNIDL'    1
0 0 0 0 0 0 ' ' 0 ' ' 1
5   END OF LOAD INPUT
Factors of limit f_p
0.0025
Factors of loading increment
0.01
Load factor of impact, residual stress for M, V, P
1.0,0.7,0.95,0.7

Output nodal displacement with load factor
9,1
Input health information
0
```

The following is the `Eep.bnk` file, which contains the parameters of Eq. (3.30) for the Group 2 semi-rigid connection tested at Sheffield (Al-Jabri et al 2003). EEP_95 = moment rotation curve at 20°C; EEP_97 = moment rotation curve at 200°C; EEP_98 = moment rotation curve at 400°C; EEP_99 = moment rotation curve at 600°C.

```
EEP Extended End-Plate Connection

4
Type+No.   Mn          Mo/Mn      Ke/Mn      Kp/Mn      n          K.01
-------------------------------------------------------------------------------------------
EEP_95     1.191E+03  1.000E+00  2.012E+02  3.566E+00  1.120E+00  3.370E+05
EEP_97     1.179E+03  1.000E+00  1.140E+02  3.216E+00  1.325E+00  3.370E+05
EEP_98     1.031E+03  1.000E+00  7.625E+01  4.024E+00  1.722E+00  3.370E+05
EEP_99     4.004E+02  1.000E+00  5.805E+01  4.210E+00  1.971E+00  3.370E+05
```

References

AISC (American Institute of Steel Construction). 2005. *Specification for Structural Steel Buildings – Appendix 4: Structural Design for Fire Conditions*. Chicago: American Institute of Steel Construction.

Al-Jabri, K.S., Burgess, I.W., Lennnon, T., and Plank, R.J. 2004. Moment-Rotation-Temperature Curves for Semi-Rigid Joints. *Journal of Constructional Steel Research*. 61: 281-303.

Al-Jabri, K.S., Burgess, I.W., and Plank, R.J. 2005. Spring-Stiffness Model for Flexible End-Plate Bare-Steel Joints in Fire. *Journal of Constructional Steel Research.* 61: 1672-1691.

Al-Jabri, K.S. 2007. Behavior of Steel-Framed Buildings in a Fire. *Steel Structures*. 7: 227-237.

ASCE (American Society of Civil Engineers). 1992. *Structural Fire Protection*. New York: American Society of Civil Engineers.

ASTM (American Society for Testing and Materials). 2008. *ASTM E119: Standard Test Method for Fire Tests of Building Construction and Materials.* West Conshohocken: American Society for Testing and Materials.

ABCB (Australian Building Codes Board). 2005. *International Fire Engineering Guidelines*. Australia: Australian Building Codes Board.

Babrauskas, V. 1976. *Fire Endurance in Buildings*. PhD Thesis. Berkeley: University of California.

Babrauskas, V. 1996. Fire Modelling Tools for FSE: Are They Good Enough? *Journal of Fire Protection Engineering*. 8:87-96.

Bailey, C. 2009. *Zone Models – One Zone Models.* University of Manchester. http://www.mace.manchester.ac.uk/project/research/structures/strucfire/Design/performance/fireModelling/zoneModels/oneZoneModel.htm

Barnett, C.R. 2002. BFD Curve: A New Empirical Model for Fire Compartment Temperatures. *Fire Safety Journal*. 37:437-463.

BS (British Steel). 1998. *The Behaviour of a Multi-Storey Steel Framed Building Subjected to Fire Attack*. http://www.mace.manchester.ac.uk/project/research/structures/strucfire/DataBase/TestData/BRETest/BehaviourMultiStoreySteelBuilding.pdf

Buchanan, A. 2001. *Structural Design for Fire Safety*. West Sussex: John Wiley & Sons Ltd.

Bukowski, R.W. 2001. Fire as a Building Design Load. *Interflam 2001 9th Proceedings*. Interscience Communications. 1:341-350.

Burgess, I. 2002. Fire Resistance of Framed Buildings. *Physics Education*. 37: 390-399.

Chen, X., Yang, L., Deng, Z., and Fan, W. 2005. A Multi-Layer Zone Model for Predicting Fire Behaviour in a Fire Room. *Fire Safety Journal*. 40:267-281.

Chen, K. M. Gary and Harmsworth, Andrew. 2008. *Building Code Provisions for Residential Buildings and Identification of Technical and Process Risks – Stage 1 Report*. Vancouver: Building Safety and Policy Branch. http://www.housing.gov.bc.ca/building/wood_frame/reports.htm

Dembsey, N.A., Pagni, P.J., and Williamson, R.B. 1995. Compartment Fire Experiments: Comparison with Models. *Fire Safety Journal.* 25: 187-227.

Drysdale, D. 1998. *An introduction to fire dynamics, 2nd edition*. West Sussex: John Wiley & Sons Ltd.

Ellingwood, B.R. and Corotis, R.B. 1991. Load Combinations for Buildings Exposed to Fires. *AISC Engineering Journal*. 28:37-44.

Ellingwood, B. R. 2005. Load Combination Requirements for Fire-resistant Structural Design. *Journal of Fire Protection Engineering.* 15: 43-61.

Feasey, R. and Buchanan, A. 2002. Post-Flashover Fires for Structural Design. *Fire Safety Journal*. 37:83-105.

Fike, R.S. and Kodur, V.K.R. 2009. An Approach for Evaluating the Fire Resistance of CFHSS Columns under Design Fire Scenarios. *Journal of Fire Protection Engineering*. 19: 229-259.

Friedman, R. 1992. An International Survey of Computer Models for Fire and Smoke. *Journal of Fire Protection Engineering*. 4: 81-92.

Fu, Z. and Hadjisophocleous, G. 2000. A Two-Zone Fire Growth and Smoke Movement Model for Multi-Compartment Buildings. *Fire Safety Journal*. 34: 257-285.

Gewain, R.G. and Troup, E.W.J. 2001. Restrained Fire Resistance Ratings in Structural Steel Buildings. *Engineering Journal.* Second Quarterly:78-89.

Hajisophocleous, G.V. and Benito, N., 1997. *Fire Safety Design Guidelines for Federal Buildings*, National Research Council of Canada, Ottawa http://www.nrc-cnrc.gc.ca/obj/irc/doc/pubs/a4409.2/a4409.2.pdf (last accessed December 7, 2009)

Hua, J., Wang, J., and Kumar, K. 2005. Development of a Hybrid Zone Model for Fire Smoke Propagation Simulation in Buildings. *Fire Safety Journal.* 40:99-119.

Hurley, Morgan. 2005. Evaluation of Models of Fully Developed Post-flashover Compartment Fires. *Journal of Fire Protection Engineering*. 15:173-197.

Kodur, V. 2009. *ME 720: Fire Resistance Lecture Notes*. Waterloo: University of Waterloo.

Kodur, V. 2009. Guidelines for Improving the Standard Fire Resistance Test Specifications. *Journal of ASTM International.* Vol. 6, No. 7.

Lie, T.T. 1974. Characteristic Temperature Curves for Various Fire Severities. Fire Technology. 10:315-326.

Liu, T.C.H. 1999. Moment-Rotation-Temperature Characteristics of Steel/Composite Connections. *Journal of Structural Engineering*. 1188-1197.

Liu, Y. 2007. Progressive-Failure Analysis of Steel Building Structures under Abnormal Loads. *PhD Thesis*. University of Waterloo.

Ma, Z. And Mäkeläinen P. 2000. Parametric Temperature-Time Curves of Medium Compartment Fires for Structural Design. *Fire Safety Journal*. 34:361-375.

Microsoft Corporation. *Excel 2007*. 2007.

NFPA (National Fire Protection Association). 1997. *Fire Protection Handbook*. Quincy: National Fire Protection Association.

NFPA. 2008. *Standard for Smoke Management System in Malls, Atria and Large Spaces 92B*. Quincy: National Fire Protection Association.

NFPA. 2009. *NFPA 101 – Life Safety Code*. Quincy: National Fire Protection Association.

NIST (National Institute of Standards and Technology). 2005. *Final Report on the Collapse of the World Trade Center Towers*. http://wtc.nist.gov/NCSTAR1/NCSTAR1index.htm

NIST. 2009. *Fire Dynamics Simulator (Version 5) Technical Reference Guide – Volume 2: Verification*. http://fire.nist.gov/fds/documentation.html

NIST. 2009. Fire Dynamics Simulator and Smoke View Official Web Site. http://fire.nist.gov/fds/documentation.html

NRCC (National Research Council of Canada). 2005. *National Building Code of Canada*. Ottawa: National Research Council of Canada.

NRCC. 2005. *User's Guide – NBC 2005 Structural Commentaries (Part 4 of Division B)*. Ottawa: National Research Council of Canada

Olenick, S.M. 2003. An Updated International Survey of Computer Models for Fire and Smoke. *Journal of Fire Protection Engineering*. 13:87-110.

Peacock, R. D. 1993. Verification of a Model of Fire and Smoke Transport. *Fire Safety Journal*. 21: 89-129.

Quintiere, J.G. 1989. Fundamentals of Enclosure Fire "Zone" Models. *Journal of Fire Protection Engineering*. 1: 99-119.

Remesh, K. and Tan, K.H. 2006. Performance Comparison of Zone Models with Compartment Fire Tests. *Journal of Fire Sciences*. 25:321-353.

SFPE (Society of Fire Protection Engineers). 2002. *SFPE Fire Protection Engineering Handbook, 3rd Edition*. Bethesda: Society of Fire Protection Engineers.

SFPE. 2004. *Engineering Guide – Fire Exposures to Structural Elements*. Maryland: Society of Fire Protection Engineers.

SFPE. 2004. *The Code Official's Guide to Performance-Based Design Review*. Maryland: Society of Fire Protection Engineers.

Underwriters Laboratory. 2009. *UL Classification Mark on Intumescent Coatings*. http://www.ul.com/global/eng/pages/offerings/perspectives/regulator/fireandbuilding/additionalresources/intumescent/

Underwriters Laboratory of Canada (ULC). 2004. *CAN/ULC-S101 Standard Method of Fire Endurance Tests of Building Construction and Materials*. Toronto, Ontario: ULC

Versteeg, H.K. and Malalasekera, W. 2007. *An Introduction to Computational Fluid Dynamics – The Finite Volume Method, 2nd Edition*. Harlow: Pearson Education Limited.

Weckman, E.J. 2008. *ME 765: Fire Dynamics I Lecture Notes*. Waterloo: University of Waterloo.

Zou, G.W. and Chow, W.K. 2005. Evaluation of the Field Model, Fire Dynamics Simulator, for a Specific Experimental Scenario. *Journal of Fire Protection Engineering*. 15:77-92.